NASA Technical Memorandum 84387

Simulation and Evaluation of the SH-2F Helicopter in a Shipboard Environment Using the Interchangeable Cab System

Clyde H. Paulk, Jr., David L. Astill, and Shawn T. Donley

(NASA-TM-84387) SIMULATION AND EVALUATION OF THE SH-2F HELICOPTER IN A SHIPBOARD ENVIRONMENT USING THE INTERCHANGEABLE CAB SYSTEM (NASA) 87 p HC A05/MF A01 CSCL 01C

N84-11176

Unclas
G3/08 42413

August 1983

NASA
National Aeronautics and
Space Administration

NASA Technical Memorandum 84387

Simulation and Evaluation of the SH-2F Helicopter in a Shipboard Environment Using the Interchangeable Cab System

Clyde H. Paulk, Jr.,
David L. Astill, Ames Research Center, Moffett Field, California
Shawn T. Donley, Naval Air Development Center, Warminister, Pennsylvania

NASA
National Aeronautics and
Space Administration

Ames Research Center
Moffett Field, California 94035

TABLE OF CONTENTS

SIMULATION AND EVALUATION OF THE SH-2F HELICOPTER IN A SHIPBOARD ENVIRONMENT USING THE INTERCHANGEABLE CAB SYSTEM

Clyde H. Paulk, Jr., David L. Astill, and Shawn T. Donley*

Ames Research Center

SUMMARY

The operation of the SH-2F helicopter from the decks of small ships in adverse weather has been simulated using a large-amplitude vertical-motion simulator, a wide-angle computer-generated-imagery visual system, and an interchangeable cab (ICAB). This report describes the simulation facility, the mathematical programs, and the validation method used to ensure simulation fidelity. The results show the simulator to be a useful tool in simulating the ship-landing problem. Characteristics of the ICAB system and ways in which the simulation can be improved are presented.

INTRODUCTION

The effectiveness of future naval helicopters will be strongly influenced by their ability to operate from small ships in adverse weather. The present fleet capability for helicopter tactical operations is limited by low visibility, ship motion, and airwake turbulence. Operational capability is further reduced by a high pilot workload resulting from aircraft control/display deficiencies. The current operating minima are 0.5-mile visibility, obscure ceiling, and sea-state 3.

Ames Research Center has been assisting the Naval Air Systems Command in exploring solutions to this problem. The objective of this effort is to develop and demonstrate the feasibility of techniques for safe and consistent operations of Navy and Marine Corp hovering aircraft from small ships under conditions as severe as obscure ceiling, 700-ft forward visibility, and sea-state 5, as well as from austere land sites. The operations include takeoff, approach, hover, and landing with both fixed-wing, vertical and short takeoff and landing (VSTOL) and rotary-wing aircraft.

To achieve this goal, the Navy is considering the application of advances in multiple technical disciplines, including flight controls and displays, landing guidance sensors, visual landing aids, piloting techniques, and deck securing/traversing techniques. The approach includes advanced developments in each of these technical disciplines, integration and concept validation through piloted simulation, and feasibility demonstrations in dedicated helicopter and VSTOL test-bed aircraft.

To achieve the program goal for helicopter operations, a new simulator facility at Ames was used. Major characteristics of the simulation facility are a wide-angle, computer-generated-imagery visual system, an interchangeable cab system, and a large-

---

*Naval Air Development Center, Warminister, Pennsylvania.

amplitude vertical-motion system. The aircraft simulated was a Kaman SH-2F helicopter which is currently deployed from the decks of small destroyers and escort ships.

This report describes the simulation facility, the mathematical models programmed, and the validation method used to ensure simulation fidelity, and presents some of the simulation results. Emphasis was on validating and evaluating the ability of the simulator system to perform helicopter approach and landing in the shipboard environment under adverse weather conditions.

SH-2F HELICOPTER CHARACTERISTICS

SH-2F Description

The SH-2F helicopter (ref. 1) is configured to meet the U.S. Navy requirement for a Light Airborne Multi-Purpose System (LAMPS). This system extends the search and attack capabilities of destroyers and escort vessels by deploying helicopters directly from the decks of these ships. The two primary missions of the SH-2F (fig. 1) are antisubmarine warfare (ASW) and antiship surveillance and targeting (ASST). The helicopter may also be used for such missions as search and rescue, observation, reconnaissance, and transportation of internal and external cargo. It is manufactured by Kaman Aerospace Corp., Bloomfield, Conn.

The SH-2F helicopter has a single main rotor, an antitorque tail rotor, and is powered by two turboshaft engines. The rotor mast is tilted forward and to the left to provide the SH-2F with a wings-level hover capability. Because of the mast tilt, the SH-2F exhibits unconventional inherent sideslip characteristics throughout its flight envelope.

Cyclic and collective pitch control is obtained through servo-driven blade flaps attached at the outboard trailing edge of each main-rotor blade. Aerodynamic action of the flaps changes the pitch (angle of attack) of the main-rotor blades in response to the pilot's operation of the cyclic and collective controls. The major portion of the energy required to accomplish rotor-pitch changes is supplied by the aerodynamic action of the blade flaps rather than by pilot applied force. Although the control forces are light, the aircraft is equipped with irreversible hydraulic boost actuators in all axes. An in-flight blade-tracking system automatically adjusts the tip path of the main-rotor blades. The pitch of the tail-rotor blades is controlled by the directional pedals, which are mechanically linked to the tail-rotor pitch-changing mechanism.

The SH-2F is equipped with limited authority automatic stabilization equipment (ASE); has retractable main landing gear; and has a full- swivel, nonretractable tail wheel. It is powered by two General Electric Model T58 turboshaft engines which are mounted above the cabin. The engine fuel-control system automatically adjusts the gas-generator speed to maintain the power-turbine speed within the governed rpm range selected by the pilot.

Automatic Stabilization Equipment

The ASE of the SH-2F is designed to maintain automatically any airspeed, roll attitude, or heading established by the pilot. In addition, the equipment can maintain altitude or ground speed or both. While the ASE is engaged, the pilot may

maneuver the aircraft in any manner within its maneuvering capability. Upon completion of the maneuvers, the ASE will stabilize the aircraft in any airspeed, roll attitude, or heading for which it was trimmed. The equipment will operate throughout the aircraft's altitude and speed range, including hover. In turbulent air, the ASE will restore the aircraft to its preset attitude and heading with a minimum overshoot. The ASE may be engaged or disengaged at any time during level flight without objectionable disturbance, and the helicopter may be precisely trimmed while under ASE control.

An ASE system block diagram is shown in figure 2. Heading signals come from the compass system. ASE airspeed signals are furnished by two airspeed transducers. One transducer is set to low-airspeed range (22 to 122 knots) and the other is set to a high-airspeed range (92 to 182 knots). Altitude signals come from either the radar or barometric altimeter. Attitude information is provided by a vertical gyro in the ASE sensor unit, which also controls the copilot's remote attitude indicator. The pilot may, at any time, override the ASE by using the primary flight controls or the trim switches.

A collective pitch-to-lateral-cyclic coupler utilizes the lateral-cyclic ASE hydraulic servoactuator to provide the proper amount of lateral-cyclic rotor control to eliminate the lateral trim change, when collective pitch is changed by the pilot. This feature, incorporated into the SH-2F with the Model 101 rotor system, replaces a mechanical collective-to-lateral crossfeed used in the earlier SH-2D aircraft. Signals from the ASE airspeed and the collective-stick position transducer are fed into the lateral-cyclic hydraulic servo. The coupler circuitry produces proportional coupling between collective-stick position and lateral-cyclic-control input to the rotor. This is further controlled by the airspeed signals to vary smoothly from no coupling at speeds below 22 knots to a maximum coupling at a speed of 122 knots and above. The coupler continues to operate whether the ASE is engaged or disengaged.

In addition, a control actuator accelerometer (cyclic bobweight) is located on the left side of the ASE control actuator. When the helicopter is flying with the hydraulic boost actuator on, the accelerometer senses vertical acceleration and introduces a proportional corrective signal to the longitudinal boost actuator. This limits the nose-down pitching tendency associated with rapid lowering of the collective. The cyclic bobweight is inoperative below 40 knots.

The ASE operates through limited-authority series hydraulic servos in pitch, roll, and yaw, and through a full-authority, limited-rate, parallel hydraulic servo in collective. In addition there are limited-rate, full-authority, parallel electromechanical trim servos in pitch, roll, and yaw. A complete description of the ASE is given in reference 2.

SIMULATOR DESCRIPTION

Interchangeable Cab Facility

The simulation facility used for the SH-2F shipboard landing simulation was the Interchangeable Cab System (ICAB). It consists of an interchangeable cab crew station, a fixed-base laboratory area, and the vertical motion simulator (VMS). The ICAB consists of a modular cab housing the pilot, instruments, displays, force-feel control system, and a four-window computer-generated-imagery (CGI) visual display. The ICAB (fig. 3) is modular so that the simulation can be built up, checked out, and validated

in the fixed-base laboratory before being mounted on the VMS for motion experiments. The fixed-base development station (fig. 4), consists of a work station for the engineers and data recorders, and houses electronics for communication with the host computers and the ICAB. The fixed-base ICAB configuration provides the pilot with all the cues required to fly the simulated aircraft, with the exception of motion and sound.

Once the cab has been checked out in the fixed-base area, about 4 hr are required to move it and mount it on the VMS (fig. 5). The cab is then interfaced to the simulation computers used in the fixed-base area for the motion tests.

The VMS motion generator consists of a synergistic hydraulic motion system mounted on a moving platform with large vertical and lateral motion capabilities (fig. 6). Vertical motion is the primary degree of freedom. Lateral-motion capability is provided by a carriage that is driven across the vertical-drive platform. The rotational and longitudinal motion are obtained with the synergistic six-legged (hexapod) motion system.

The current operational VMS motion-generator performance envelope with the ICAB is given in table 1. These peak motion-system capabilities are with a payload that includes all hardware attached to the synergistic motion system with the weight and moments of inertia defined in table 2. The moments of inertia are referenced to the center of the top platform on the synergistic system.

A simplified block diagram showing the computer configuration for the ICAB/VMS/CGI simulator is shown in figure 7. The host computer was a Sigma series, real-time digital computer interfaced through a logic pulse unit to a PDP 11/55 (a PDP 11/34 is used in the Development Station). This computer receives data from the host computer and distributes the data to the various remote input/output units (RIOU) which drive the VMS motion system; the ICAB cockpit, including control loaders; instruments and displays; and the data-recording equipment. The four-window visual system equipment receives data directly from the Sigma computer, through a digital-to-digital interface called a computer input/output unit (CIOU). The direct digital transfer of data between computers helps to minimize time delays in the visual-system scene being presented to the pilot. The actual CGI computations are performed by a Perkin/Elmer digital computer.

Visual System

The premier feature of the simulator is the four-window CGI visual system. Designed for use with the ICAB system to perform basic studies on both helicopter and VSTOL aircraft, the system provides the pilots with a wide-angle field-of-view presentation of the outside world. The CGI visual at Ames was funded by the Navy and is a modification of the F-111 system trainer originally procured by the Air Force. To make the system compatible with NASA's requirements, the F-111 system was modified to include a (1) fourth visual channel, (2) 1000-line vertically scanned CRT displays to reduce horizontal-line stair-stepping, and (3) additional scenes in the data bases.

Some basic characteristic and capabilities of the CGI visual are

1. Real-time full-color imagery from a variety of data bases

2. Day/night takeoff and landing

3. Destroyer and carrier operations

4. Nap-of-the-Earth flight

5. Reduced visibility and weather operations

The CGI system creates the scene by storing coordinates and numbers representing the light values of the simulated world. This is referred to as the data base. These are retrieved for any viewing point in this data base and the data used to reconstruct the scene as it would be viewed from this point. The scene details are then displayed to the pilot on a cathode ray tube (CRT) and collimated with a mirror beam-splitter. Smoothing and shading techniques are used to create imagery that is convincingly realistic (ref. 3).

In a simulation, the visual-system scene represents the outside world and the field of view is the pilot's window to that world. Because certain parts of the outside scene are important to the accomplishment of the ship-landing task, the shape, orientation and size of the field of view (FOV) can greatly influence the way the pilot flies the simulated aircraft.

The FOV available to the pilot from the SH-2F is shown in figure 8 on a Hammer equal-area projection of a sphere. From this perspective in the right-hand seat, the pilot can look out the forward, quartering, and door windows and out the copilot's forward window. (Pilots often perform the actual shipboard landing with the door open.) Superimposed over the available FOV is the arrangement of the four CRTs of the CGI visual system. The three upper CRTs cover a lateral FOV from 65° left to 70° right and a vertical FOV from about 8° up to 15° down. The fourth CRT expands the lateral viewing from 43° to 90° laterally and a look-down to 45°. The fourth window represents the view the pilot would obtain when looking out his door during a ship landing. All plots assume binocular vision with the pilot's eye at the aircraft design eye-point.

Two data bases were used in the simulation. The first was the so-called F-111 data base and the second was a DD-963 data base. The F-111 data base contains land area of about 400 square miles containing both geographical and man-made features around the area of upstate New York. Most of the evaluation flying, however, was done about an airport scene representing Plattsburg AFB in New York, which includes landmarks such as a runway, hangars, control tower, water tower, and a VTOL pad. A field-of-view montage of the runway scene as viewed from the SH-2F ICAB is shown in figure 9.

The DD-963 data base contains a destroyer under way at sea. Special visual effects were included to represent sea state, bow and stern wake, and ship motion. Sea-texturing effects, such as whitecaps on waves, and details of the ship, such as ladders and seams, were not present. A field-of-view montage of the destroyer scene in the vicinity of the landing pad is shown in figure 10. Both data bases were capable of being presented under four ambient light levels, daylight, dawn, dusk, and night, and with variable weather minima conditions. Deck edge, centerline, extended centerline dropline, and hovering lights were simulated.

SH-2F Simulated Cockpit

The cockpit setup (fig. 11) for the SH-2F simulations provided the pilots with the essential controls and instruments needed to fly the aircraft effectively.

Instrument scan, control feel, manipulation, and systems functions during normal operations were realistic. The instrument panel for the simulator is shown in figure 12. The instruments, although not identical to those in the aircraft, were in most cases similar in size and location. The major exception was the attitude indicator; the aircraft has a simple 4-in. instrument and the simulator had a 6-in. instrument with flight-director capability and an expanded attitude scale.

The center console of the simulator (fig. 13) incorporated the engine control and landing-gear levers. The remaining switches on the console were for control of the simulator. The power lever and control switch in the simulator were configured to match those of the SH-2F and incorporated the same function and switches in their design. All of this attention to simulator detail was important to the evaluation of the aircraft response and flying qualities.

SH-2F Control Characteristics and Control Loaders

The simulation of control feel is as important to simulation as it is to flight. Aircraft designers have long recognized that control feel is an important part of the overall handling qualities built into the aircraft. The SH-2F/ICAB simulator uses an electro-hydraulic actuation device which provides the pilot a controller force-feel simulation. The system consists of a four-axis set of cockpit controls (cyclic stick, pedals, and collective) driven by integral rotary hydraulic actuators, valves, transducers, and associated servo-control and function-generating electronics. The loaders are interfaced to the central digital computer through an analog computer in which the SH-2F control characteristics are programmed.

A tabular summary of the SH-2F control characteristics is given in table 3 where the total travel, the breakout force, the force gradient, and the maximum deflection force are given for each control. Note that for the SH-2F, the force gradient on the cyclic stick has two levels. For example the longitudinal cyclic has a high gradient of 4.17 lb/in. for deflections up to 0.25 in. and a lower gradient of 1.60 lb/in. for deflections from 0.25 in. to 7.0 in. The lateral axis is similar. The control characteristics listed are for cyclic pedals trimmed at their center of travel. The SH-2F trim system employs trim motors which reposition the ends of the feel system spring struts. Consequently, the neutral (zero-force) position and force gradients around neutral are not modified by trim position. Average trim rates are 0.75 in./sec (longitudinal), 0.75 in./sec (lateral), and 0.5 in./sec (pedals). The collective in the SH-2F has a variable friction adjustment.

In addition to the longitudinal static-force characteristic, the SH-2F longitudinal cyclic-force changes with load factor. Negative load factor produces a force that tends to move the cyclic stick aft and vice versa. The steady-state gain is 7.3 lb/g. The load-factor component is created by hydraulic forces in the bobweight servo and is additive with the static stick force.

MATHEMATICAL MODELS

SH-2F Mathematical Model

A detailed discussion of the SF-2F mathematical model is beyond the scope of this paper. The model contains a complete nonlinear representation of the SH-2F helicopter, including all the aerodynamic characteristics of the main rotor, tail rotor, and

fuselage through a range of angles of attack and sideslip of ±180°. Also included are representations of the primary flight controls, actuators, automatic stabilization equipment, and the effects of winds and turbulence on the dynamics of the airframe.

The SH-2F mathematical model was developed by R. L. Nave (User's Manual for SH-2F Helicopter Mathematical Model. Naval Air Development Center, report in preparation) from data originally supplied by the Naval Training Equipment Center for the SH-2F Weapons System Training Simulator (ref. 4). The central element of the model is the main rotor-blade flap-feather equations which were based on a set of partial derivative algebraic equations developed by McIntyre (ref. 5). Analysis by Nave has indicated that these equations are very sensitive to the assumed aerodynamic properties of the blade, which makes their predictive capability suspect. The mathematical model incorporated into the simulation corrects this deficiency.

One of the major problems in developing the SH-2F mathematical model was the lack of flight-test data on flap and feathering angles as a function of control inputs. Since blade pitch is determined by complex aerodynamic forces arising from servo-flap deflection, and not simple swashplate angle, the rotor model was not straightforward. Lack of good flap and feather data resulted in a situation in which rotor-model improvements had to be made based on second-order (fuselage) response measurements. Additional flight tests are required to obtain the rotor-system data.

The flight-control-position equations define the rotor-head control displacements as a function of the appropriate cockpit flight-control displacements. The equations are defined for the cockpit flight-control displacements expressed in terms of normalized percentage of the full-control travel displacements for (1) the collective stick, (2) the lateral cyclic stick, (3) the longitudinal cyclic stick, and (4) the yaw pedals. Additional equations are included to define the servo-flap deflection angles. The deflections are defined for the control axis as the steady and harmonic cyclic azimuth coefficients. The total flap deflection results from the simulation of the cockpit displacements and the appropriate ASE actuator displacements. The mechanical linkage of the control rods and the rotation of those linkages producing a mechanical feedback from the blade flapping and pitching are included.

These equations define the servo-flap deflection which is the unique control scheme of the Kaman servo-flap controlled rotor. It is the aerodynamic reaction of the servo-flap that produces the blade-feathering and flapping-control angles and provides the full rotor-head control. Predominantly, it is the aerodynamic pitching moment of the servo-flap that causes the main-rotor blades to deflect torsionally.

The main-rotor simulation mathematical model defines the forces and moments resulting from the aerodynamic characteristics of the rotating rotor. The major parameters are those of rotor thrust, which maintains flight, and the power required to rotate the rotor system. The main-rotor thrust is defined according to the standard helicopter-performance-determination equations based on the assumption of the linear lift-curve slope. This assumption permits use of an analytic closed-form expression to define the radial and azimuthal integration of the incremental blade-element forces without requiring real-time integration; the latter was not practical at the high frequencies required for piloted simulation.

Mean induced-inflow velocity is defined according to momentum theory considerations. Blade airfoil characteristics are deduced from tabulations of lift and profile-drag coefficients data as functions of angle of attack. Utilization of mean lift coefficients removes the requirement to define specific blade-station angle of

attack. Wake-skew angle is developed to define the longitudinal variation of induced-inflow velocity so that the lateral flapping angles may be correctly modified.

Rotor angular velocity is defined from rectangular integration of the rotor angular acceleration, the angular acceleration being defined from the summation of torques applied to the rotor shaft. These torques include engine, rotor brake, tail-rotor requirements, accessory and transmission requirements, and the aerodynamic loading from the main rotor. The aerodynamic torque is defined from considerations of induced power losses and accelerating flight power requirements in addition to the blade-profile-drag power losses.

Retreating-blade stall, drag divergence, and power settling effects are determined and described empirically. These effects are then superimposed upon the basic model. The tail-rotor control is the standard control system. Thus, an expression for the mean tail-blade pitch angle is defined for the tail-rotor equations directly from the yaw-pedal position.

Automatic Stabilization Equipment

The basic functions of the ASE are to maintain the helicopter at any airspeed, roll attitude, and heading selected by the pilot and to do so automatically. These basic functions were included in the simulation. The additional ASE features of altitude-hold and ground-speed hold were not included.

Since a detailed ASE transfer function was not available from the manufacturer, a mathematical model of the ASE was developed through a process of reverse engineering based on data contained in reference 2. Fortunately, those data included all pertinent sensor scale factors and most time-constants. The task of developing the model consisted of calculating feedback gains, command gains, and mode-logic equations based on electronic schematic diagrams of the ASE.

Figure 14 shows the ASE pitch channel engaged in its basic airspeed-hold mode. Typical of equipment manufactured at the time, the ASE uses 400-Hz carrier signals for feedback. These signals are combined through a resistor summing bus to generate a series servo command. The procedure for calculating gains consisted of finding the linear variable differential transformer (LVDT) position output in volts rms at full ASE series authority deflection, and relating this to the known authority in equivalent inches of stick. With this number calculated (volts/inch-stick), the voltage from each sensor required to offset the LVDT feedback was computed using simple network theory to arrive at a gain relating each sensor output to equivalent inches of stick deflection. Similar calculations were performed to develop gains for the trim actuator paths.

The resulting pitching-axis simulation diagram is shown in figure 15. A track-and-hold was used in place of a model of the electromechanical synchronizer to simplify ASE model software. Also, the track-and-hold acted on only airspeed and attitude, whereas the synchronizer in the actual ASE balances all summing bus inputs prior to ASE engagement. For the usual procedure of engaging ASE only in trimmed flight, both approaches are equivalent.

The dual-speed, longitudinal-stick trim system of the pitch ASE was modeled to reflect accurately the aircraft system. For longitudinal cyclic trim inputs without simultaneous application of longitudinal stick force, the trim button serves only to slew the airspeed/attitude reference at a fixed rate. The resulting series servo

displacement causes the trim actuator to follow-up through the autotrim path. For trim inputs while holding stick force, the airspeed/attitude reference is changed at a higher rate, and the trim actuator responds through both the autotrim path and a direct path.

The normal acceleration path to the trim actuator was an attempt to model the cyclic bobweight by causing the load factor to change the zero-force (trim) position of the cockpit force loaders and thereby create a stick force during maneuvering flight. The gain AZK7 and time-constant AZTAU were not established with high confidence.

The roll-axis block diagram (fig. 16) was developed using the same technqiues employed in pitch. Once again, a simple track-and-hold was substituted for a synchronizer model and only roll attitude was referenced, not the entire summing-bus output as in the actual ASE. Series servo commands were a sum of ASE and lateral cyclic system outputs. The lateral trim system in both the aircraft and the ASE mode is straightforward, with no autotrim feature.

The yaw-axis block diagram is shown in figure 17. There is considerable mode-logic in the yaw ASE, particularly with respect to trim-actuator control, and every attempt was made to duplicate this logic in the model. A problem arose because the simulator rudder pedals did not have "feet-on-pedals" microswitches, as does the actual aircraft. These switches are used to drop heading-hold and do not require rudder-pedal deflection to activate. As a substitute, logic was established to determine if differential pedal forces were being applied by the pilot. SH-2F pilots are conditioned to expect heading-hold to drop just by resting their feet on the pedals. In the simulator, a small pedal force was required. As a consequence, small abrupt yaw ASE inputs could and did occur in turns initiated through lateral stick after coordinating pedal was applied. Thse effects were reduced to an acceptable level by modeling the heading synchronizer rather than using a track-and-hold, and by using ramped switches (ramp from gain = 0 to gain = 1) in the yaw ASE model.

The yaw ASE coordinated-turn feature, which requires the pilot to press a switch on the cyclic grip, was included in the model and did not suffer the above-mentioned transient problems. The calculated stick force and acceleration gains for this mode seem rather low, however. The yaw-trim system was modeled to include the yaw autotrim, pedal-force trim, yaw-trim switch (on collective-stick grip), and collective-stick rate inputs. With the ASE engaged, yaw trim was provided as follows:

1. When the rate of turn was less than 7°/sec and the pilot's feet were off the pedals, the yaw-trim switch functioned as a heading adjust switch to change the aircraft's heading at the rate of 4°/sec as long as the switch was depressed.

2. When the rate of turn was less than 7°/sec and a control force was applied to the pedals, the force was automatically trimmed out. In this case the yaw-trim switch was inoperative.

3. When the rate of turn was greater than 7°/sec or when the coordinated-turn button was depressed, the yaw-trim switch provided motorized pedal trim.

With ASE disengaged but with the lateral coupler on, yaw trim was provided as follows: When the rate of turn was less than 7°/sec and a control force was applied to the pedals, the force was automatically trimmed out. In this case, the yaw trim was inoperative. In all other cases the yaw switch provided motorized pedal trim.

Simulated Landing Environment

A Spruance-class destroyer (DD-963) model was used in the simulation. The ship-motion model consisted of representing the ship motion by a sum of sinusoids in each of the six degrees of freedom (roll, pitch, yaw, surge, sway, and heave) at the ship's center of gravity. Long-crested seas were assumed with the mean wind parallel to direction of propagation. Representative ship motions were obtained using the method outlined by Brown and Camaratta (ref. 6). In general, the method generates ship-motion time-histories from a power spectra by decomposing the spectra into a series of discrete sinusoids, with each component sinusoid weighted by the power in the frequency band it represents. Selection of the number of sinusoids is a trade-off between accuracy and computational time. Fortenbaugh (ref. 7) compared a 6-component and a 32-component ship-motion approximation and showed that the 6-component approximation resulted in less than a 5% error in most cases for rms position, rates, and accelerations in each degree of freedom. It was concluded that the six-component approximation will give an excellent representation of ship motions for studies that involve relatively short time exposure to the ship environment. Studies directed toward the flying-qualities and flight-control aspects of launch and recovery on small ships would fall into this category. Other types of studies, such as ship-motion forecasting and landing-gear load studies, would require further analysis of the comprehensive ship-motion program.

The model used for ship airwake turbulence was also similar to that defined by Fortenbaugh (ref. 7). This model was developed from data obtained from a 1/50 scale-model test of an FF-1052-class destroyer by Boeing-Vertol (ref. 8). The FF-1052 data were used to approximate the DD-963 by using Strouhal-number scaling techniques. Full-scale turbulence-mapping of the DD-963 has not been performed to validate either the wind-tunnel data or the Strouhal-scaling assumptions.

The airwake model generated both mean and random linear velocity components of the three-dimensional flow-field aft of the ship as a function of aircraft position and wind-over-the-deck (WOD) magnitude and direction. The rotational components were not included. The airwake velocity components were then applied to the helicopter's center of gravity in the standard way. The effect of airwake velocity gradients acting on the rotor were not included in the model. This would require a higher-order or blade-element type of model which is more complex than the quasi-steady-state model used.

Outside the airwake, a standard Dryden turbulence model was used (ref. 9). Shaping functions were used to provide a smooth transition to the airwake model.

SIMULATOR VALIDATION

The value of a flight-research simulator is its ability to duplicate actual airborne performances so as to affect the design of the aircraft or prepare the pilot for the actual aircraft experience. Thus, the fidelity requirements for validating a simulator are a combination of how well the simulator duplicates the aircraft and the ability of the simulator to allow performance of the desired task. Sinacori (ref. 10) defines fidelity in two ways: engineering fidelity, meaning the physical closeness to the real world, and perceptual fidelity, meaning the pilots perceived closeness to the real world. Good engineering fidelity is measured by the degree to which the simulator is observed to reproduce its real-life-counterpart aircraft as measured by a nonphysiological instrument system. This includes, for example, the mathematical

model, the visual system, the motion system, and the sound system. Good perceptual fidelity is the degree to which a well-trained and motivated pilot perceives the simulator to reproduce its real-life-counterpart aircraft in flight and in the operational-task situation.

Inherent uncertainties exist in theoretical mathematical modeling, wind-tunnel measurements, and flight-test instrumentation. Also, simulator-system limitations exist in terms of computer size and speed, visual-scene presentation, and motion-drive logic and response. Thus, compromises are required which reduce the engineering fidelity. When such conflicts arise between engineering and perceptual fidelity, the emphasis has to be on the perceptual (ref. 11). The engineering and perceptual fidelity with which the ICAB system simulates an SH-2F helicopter in the ship-landing environment is discussed in the following sections.

Engineering Fidelity

Sh-2F Mathematical Model.- The mathematical model was validated by comparing its characteristics with those of actual SH-2F flight-test results as given in reference 12. The simulated test conditions were adjusted to match the corresponding aircraft flight-test conditions. These included the flight airspeed, gross weight, center-of-gravity location, and atmospheric conditions. The procedure allowed a direct comparison of the ICAB simulation and the SH-2F helicopter flight-test results.

Trimmed flight comparison. Trimmed forward-flight conditions were compared with the flight-test data across the entire flight regime from an airspeed of 40 to 120 knots. Data for the engine torque, pitch attitude, and the four control positions are shown versus airspeed in figure 18 for both the simulator and the aircraft. All of the simulated trim conditions were obtained by assuming the helicopter to be in trimmed or equilibrium flight at the sideslip angle shown in figure 19.

The comparison indicates a good agreement for the pitch axes in terms of pitch attitude and longitudinal cyclic-control position. For the vertical and lateral axes, the simulator requires less engine torque than the flight-test aircraft. This results in a decrease in the collective-control position and less right-pedal position across the airspeed range. However, the curves do have the same shape. Additionally, the simulator lateral-stick deflection indicates a slow migration from more right-lateral stick to more left-lateral stick across the airspeed range.

Low-speed trimmed conditions compared with the flight-test data between forward and rearward ground speeds of ±40 knots are shown in figure 20; lateral trimmed flight conditions compared with flight-test data between a lateral ground speed of ±30 knots are shown in figure 21. The flight-test data were taken with the aircraft in ground-effect. No ground-effect model was implemented in the simulation. The comparison indicates a good agreement of all the parameters except engine torque and directional-control position. The latter discrepancy is attributed to ground effect where more power and a concomitant amount of directional-control deflection were required.

The individual effect of power on the trimmed control positions is presented in figure 22. Below 30% of torque, minor differences are evident. Above 30%, the simulator's pedal position indicates a strong and increasing requirement for left pedal with power. This difference in increased pedal input at high power settings between flight and simulator results may lead to a different piloting technique for the simulator.

Hover tests for out-of-the-wind conditions where the aircraft is required to establish hover trim conditions with respect to a relative wind at various azimuthal angles to the aircraft centerline are called critical azimuth tests. The significance of these tests is illustrated in the interrelation and phasing of the controls with changes in the relative wind direction. The comparison of the simulation and flight-test results is shown in figure 23. The results need to be considered concurrently with the previously discussed in-ground-effect control-position data. Fidelity in this area is necessary to simulate high-workload tasks such as the hover and landing. The results are satisfactory and indicate a reasonable fidelity with the aircraft performance.

Static longitudinal stability characteristics for both a 70-knot and a 110-knot airspeed trim point were compared, and the data are presented in figure 24. These data, particularly the force gradient, affect the pilots ability to fly a selected airspeed without retrimming. Around the 110-knot trim, the force position and pitch attitude data compared well. Around the 70-knot trim point, a steeper force gradient was required for the same change in pitch attitude.

As a measure of static lateral-directional stability, steady-heading sideslips were evaluated. A comparison of the results is presented in figure 25. The flight-test procedure used to collect the data was to fix the collective at the required trim condition before entry into the maneuver, and then to establish the required bank angle and control positions for various sideslip angles. The primary flight instrument was the turn rate and inclinometer indicator. The simulator procedure was to trim the aircraft at the desired sideslip angle. The unique control positions associated with a specific steady-heading sideslip verified the lateral-directional stability characteristics of the simulator.

Dynamic response comparison. The response of the simulator to step inputs in the controls was determined and compared with flight-test data. Steps in the four controls (longitudinal and lateral cyclic, pedal, and collective) at airspeeds of 10 and 70 knots with the ASE on and off were performed. Control inputs of approximately 0.5 in. were accomplished.

The flight-test data (ref. 12) were obtained by using the standard flight-test technique of maneuvering the aircraft to the desired flight condition, manually applying the desired step input, and recording the resulting vehicle response parameters with a data-acquisition system. On the other hand, the simulator data were obtained by using a software program that trims the aircraft at the desired condition and automatically applies a step input into the desired control while holding the others constant. Care was taken in the simulation to produce the data at the same environmental and vehicle condition as the flight-test data. A summary of the dynamic response tests is given in table 4 and a comparison of the time-histories in the same format is given in figures 26 through 49.

The dynamic response tests at 10 knots with the ASE off for the pitch, roll, and yaw axes are given in figures 26, 30, and 34, respectively. The responses generally indicate that when compared with the flight-test data, the model is less responsive in pitch, a reasonable match in roll, and more responsive in yaw. For the tests at 70 knots with the ASE off, the data for the pitch, roll, and yaw axes are given in figures 27, 31, and 35, respectively. The 70-knot responses indicate that the model produces similar responses to the flight-test data in the pitch and roll axes. In the yaw axis there is a similar peak yaw rate, but a quicker return to zero rate than the flight-test data.

The dynamic response tests at 10 knots with the ASE on for the pitch, roll, and yaw axes are given in figures 28, 32, and 36, respectively. The responses generally indicate that the model is similar in response, but more stable in pitch and reasonable match in roll and yaw. For the tests at 70 knots with the ASE on, the data for the pitch, roll, and yaw axes data are given in figures 29, 33, and 37, respectively. The 70-knot responses indicate that the model produces a reasonable match in pitch and a similar initial response, but is less damped in roll and has a higher peak rate with a quicker return to zero rate in yaw.

Aerodynamic coupling was concurrently evaluated with the control response by analyzing data from additional axes. Coupling data from pitch and roll axes inputs at 10 knots and 70 knots with the ASE on and with it off are determined. Pitch due to roll inputs are given in figures 42 through 45 and roll due to pitch inputs in figures 46 through 49. Pedal-induced coupling inputs were insignificant in both the simulator and the aircraft.

For the ASE off, pitch due to roll input coupling (figs. 42 and 43), the model results show a good agreement with the flight-test data at both hover and at 70 knots, where a right longitudinal step input resulted in a down-pitch attitude. For the ASE on (figs. 44 and 45), the iritial response is correct; however, the model response continues to pitch down while the aircraft response returns to the original trim value.

For the roll due to pitch input coupling, the pitch-rate data from the flight-test instrumentation was unavailable. However, for both ASE on and off at 10 and 70 knots, the model shows good agreement with the flight-test data. A longitudinal forward step produces a left-roll attitude change with ASE off and a very slight left-roll change with the ASE on.

No flight-test data were available for the aircraft in the vertical axes (Figs. 38-41) which made a check in these axes difficult. As a substitute, aircraft stability derivatives were computed from the nonlinear mathematical model at hover and at 70 knots; they are shown in table 5. Using data published by Heffley et al. (ref. 13), the SH-2F model was compared with other helicopters of similar size at hover and at 70 knots. These comparisons are shown in table 6. Comparing the sensitivity Z_{δ_c} and damping Z_w at hover, the SH-2F model appears fairly consistent with similar-sized aircraft, although the sensitivity appears a bit low. The SH-2F model, when compared with the same aircraft at 70 knots, indicates that for the model, both the sensitivity and the damping are low compared with other helicopters of about the same size.

CGI Visual System.- The inherent serial architecture of digital simulations leads to the propagation of delays. In particular, the delay between a pilot input, such as stick movement, and the perceived response as a visual scene can have a serious effect on the ability of the pilot to accomplish a task. Gum and Albery (ref. 14) among others have reported simulation problems traced to time delays in visual-system cueing. The use of a CGI system tends to aggravate this problem, for an additional delay is added by the computer generating the visual scene.

To determine this delay for the ICAB system, a simple experiment was devised to measure the total delay from the pilot input to visual-scene response. In the experiment, shown schematically in figure 50, a switch and an oscilloscope were used. The switch fulfills a dual function of providing a step input in stick position by the pilot and triggering the sweep of the oscilloscope.

The oscilloscope was used to monitor the signal to the CGI visual monitor in the cockpit. A fixed scene was displayed that resulted in a known waveform on the scope. Any change in this scene would result in a new waveform on the scope which was discernible to the observer. The step signal was fed into the computer system through an analog-to-digital converter (ADC). The Sigma 7 computer was programmed to scale this signal and send it to the CGI system as a step in pitch of the visual scene. This resulted in a new waveform on the oscilloscope. At the same time the oscilloscope was triggered by the step signal. The time taken from the step until the waveform changed can be considered to represent the delay between pilot input and perceived visual change.

The feedback signal measured was the green input drive to the CRT. The CRT was operating at a 60-Hz field rate which implies that an additional 17 msec can elapse between the drawing of the first line of the field and the last line of the field. In addition, it should be noted that no aircraft dynamics were included in the Sigma computer computations. A Polaroid camera was used to record the results of the experiment.

For the experiment, the Sigma was run at different cycle times DT and the time-delay between the pilot input and the first perceivable visual change ΔT was measured. The results shown in figure 51, indicate that a linear relationship exists between the visual time-delay and the cycle time according to the relationship

$$\Delta T = 1.53\ DT + 91.3\ \text{msec}$$

The first term can be interpreted as the 3 DT/2 delay associated with the analog-to-digital converters and the Sigma computers. The second term can be interpreted as the time required for the CGI computer hardware to perform its calculations and draw the picture.

For the SH-2F ICAB simulation, the host Sigma computer was running at a cycle time of 62 msec. Thus, the time delay between the pilot input and the first perceivable visual change was about 186 msec. The effect of the delay will be discussed later in the Perceptual Fidelity section.

VMS Motion System.- Because the ICAB has significantly different mass properties and motion system servo requirements than the original cab on the VMS, performance tests were conducted on the VMS motion system. The purpose of the tests was to measure and document the performance and frequency-response characteristics of the motion system in its new configuration.

The measured performance limits in terms of excursion, velocity, and acceleration are listed in table 1. The listed limits are considered maxima and represent the maximum operational capability of the motion generator. The limits apply only to the motion-system hardware and do not include the effects of software limits in the motion drive logic. The rotational limits are for single-degree-of-freedom motions. The limits for coupled angular motions are complex, nonlinear functions because they are provided by the synergistic motion generator.

The source of the performance limits result from different mechanisms. The translational excursions and velocities are command-limited in the servo-electronics, the rotational excursion limits result from end-of-travel limit switches on the hexapod actuators, and the remaining limits reflect physical limitations of the hardware such as hydraulic flow, current, or torque limits. The values listed in table 1 for translational accelerations are for momentary duty. These levels of acceleration

require driving the motors significantly above their rated loads, and sustained operation in this mode causes overheating and automatic shutdown. Maximum continuous-duty translational accelerations are about one fourth the tabulated values.

Frequency-response measurements of the five degrees of freedom were conducted using a commercial frequency-response analyzer. The test setup is illustrated in figure 52. In all cases, acceleration command was used as the reference signal, and acceleration feedback, measured by a cab-mounted accelerometer, was used as the response signal. Therefore, the frequency responses measured represent only the dynamics of the motion generator and do not include the effects of the digital computer used to drive the system. Figures 53 through 57 present the results of the measurements in the form of Bode plots of amplitude ratio and phase angle versus frequency for the roll, pitch, yaw, lateral, and vertical axes, respectively. These data were measured with no lead compensation provided in the motion-drive logic and with the noise suppression filters in the analog-to-digital converter cards bypassed. Also shown in these figures is an analytically determined effect, based on the results of reference 15, of digital computer delay for several values of frame time. These data are representative of operational conditions since they include the phase-lag increase caused by the simulation computer. Figure 58 presents the frequency response of the vertical degree of freedom with the inclusion of compensation provided in the motion-drive logic. Compensation of this form was used in the simulation and is illustrated in figure 59.

Perceptual Fidelity

Piloted runs were performed to evaluate the flying performance and handling characteristics of the simulator and to assess the ability of the simulator to perform approach and landings in the environment of the DD-963 destroyer.

Two test pilots participated in the evaluations. The first had over 1,500 hours in a variety of helicopters, but no SH-2F or small-deck landing experience. The second pilot had 2,500 hours of helicopter time, 1,000 in the SH-2F, and had made about 500 landings onto small ships, including ships of the DD-963, FFG-1, and FF-1052 classes. Most of the runs evaluating perceptual fidelity specific to the SH-2F were made by the second pilot. Other test pilots flew the simulator fixed-base and their comments were integrated into the discussion of the CGI visual system.

SH-2F Mathematical Model.- The pilots overall opinion was that the simulator representation of the aircraft was satisfactory over the airspeed range from hover to 90 knots with the ASE on. Above 90 knots, the simulator required excessive forward and left-lateral stick deflection. With the ASE off, the sensitivity and damping of the aircraft were satisfactory; however, precise attitude control and maneuvering appeared to be easier than in the actual aircraft. With the ASE either on or off, the effectiveness of lateral and directional attitude-control was greater than expected.

The portion of the model that was judged to be least like the aircraft was the vertical degree of freedom in hover where the pilot had difficulty maintaining altitude in a simulated landing task. Collective response seemed overly sensitive and although the onset of vertical-rate in response to a collective input appeared representative, height damping seemed low. This comment appeared to be in opposition to the stability-derivative data presented earlier where the collective sensitivity, when compared with that of other helicopters, appeared low and the damping representative. The problem may be related to the question of whether the motion and visual systems of

the simulation can present the proper dynamic perceptual characteristics to the pilot (ref. 16).

According to the pilot who had flown both the ICAB and the SH-2F Weapons System Trainer (WST) currently being used by fleet pilots in Norfolk and San Diego, the ICAB simulator was

> in spite of the fidelity of the collective control axes, much easier to hover than the WST currently being used by the fleet pilot in Norfolk and San Diego. Unlike the WST, the SH-2F ICAB could successfully perform a shipboard landing from a stabilized hover over the deck. The SH-2F ICAB simulation was satisfactory except for the collective response characteristics.

Improvements in the model are required following Navy flight testing.

Environment.- The simulator response to free-air turbulence seemed reasonable. However, the magnitude of aircraft disturbances induced by the airwake turbulence model was judged by the pilot to be excessive for the wind-over-deck (WOD) conditions simulated. With WOD velocities in excess of 25 knots along a 30° radial from port, induced disturbances while hovering over the landing circle and below the hangar roof were of such a magnitude that hover positioning became very difficult with the ASE control system. It appeared that both the standard deviation and frequency content of the airwake was excessive; however, when hovering over the aft portion of the ship (aft and to the left of the landing pad) the response of the aircraft to turbulence was reasonable. Additionally, two characteristic far-field air disturbances generated by the stacks of the DD-963 and normally encountered during a 30° to port or starboard approach were absent. Verification and modification to the airwake turbulence model in magnitude, bandwidth, and special location needs to be performed.

CGI Visual System.- Pilot ratings of vehicle dynamics and control/display contributions are strongly influenced by the available out-the-window visual-cue levels. Often the simulation pilot is unaware that the source of a control problem is in the visual-scene content or scene processing of the display. With this in mind, five evaluation test pilots, four of whom had ship-landing experience, were asked to complete questionnaires about the CGI visual system. The major topics on the questionnaire were general comments, visual-cueing comparison with other visual systems, geometrical characteristics, and dynamic characteristics. The visual scene or real-time data bases evaluated were the DD-963 destroyer and the runway/airport scene in the F-111 data base discussed in the Visual System section.

The ship landing-approach procedures used called for acquisition of landing guidance signals at or beyond 2 miles from the ship at an altitude of 450 ft. The reference trajectory was a constant-bearing approach from the aft starboard quarter at an indicated airspeed of 70 knots. Following intercept of the 3° glide slope, the pilot performed a decelerating approach to a station-keeping point aft of the touchdown point. From there a hover and vertical descent to the deck were accomplished.

In general, the overall ratings of the CGI were very good. Most of the positive comments had to do with the use of color, the wide-angle field of view, and the inclusion of the ship scene with ship-motion dynamics. The major negative comments had to do with the inability of the pilots to determine their closure rate, altitude rate, and depth of field. As a general comment, one pilot responded that "the simulation is a good responsive system with which I could actually perform a visual hover around the ship without reference to cockpit gages." All of the pilots felt that in general, the position and attitude cues obtained from the visual system were good and that the range-rate and altitude cues were fair. Specifically, during the approach,

cues to determine range and range-rate were lacking, because of the lack of depth of field of the scene. During hover runs over the runway, the pilots had difficulty estimating altitude and the size of objects in the field of view. This was also true for hover runs over the destroyer flight deck where it was difficult to estimate the altitude above the deck. The addition of texturing to the scene, including white caps and waves to the ocean and more detailing to the hangar face, may improve the lack of depth of field of the scene.

Limited visibility conditions (e.g., fog and ceiling) were simulated in which the pilot flew a decelerating, constant glide slope approach, breaking out visually at or before 700 ft of range prior to the ship-landing. The pilots found the CGI visual mechanization to be realistic, in terms of the breakout and the occulting of the horizon after the ship is visible. This realism is not present with model-terrain boards.

Most of the pilots had experience with either the SH-2F Weapons System Trainer (WST) (ref. 12), which has a CGI visual, or with other simulators, in which model-terrain boards are used. According to the pilots who had flown both the SH-2F ICAB and the WST, "The CGI/ICAB was superior to the WST because of FOV layout, day color instead of night/dusk presentation, better definition of the DD-963 destroyer with ship motion and no apparent time delays." One pilot commented that he preferred the model-terrain board because of the texture and resulting depth of field cues.

The geometrical characteristics of the CGI/ICAB provided a wide-angle field of view which was a definite asset in hovering. The two forward windows provided such a large FOV that the side windows tended to be left out of the pilot's scan pattern. Also contributing to this scan situation was the large angular viewing discontinuity between the front window and the upper and lower right window. Because extra effort was required to use the side windows, they were used less in the simulator than in the actual aircraft.

The other geometrical characteristic deserving pilot comment was related to the pilots seat position. The SH-2/ICAB simulator was designed such that the pilot would be seated at the aircraft design eye-point. For ship-landing operations, however, the pilot will raise his seat to the maximum height to maximize his over-the-nose viewing angle. Since this was not possible in the simulator because of the ICAB frame and glare shield, the pilots were required to fly the simulator from an unfamiliar position with less look-down capability than in the actual aircraft.

The pilots found the dynamical characteristics of the CGI good, but did have some reservations. No time delays between control inputs and the response of the visual system were perceived, and no pilot indicated a pilot-induced oscillation during any simulation run. Some pilots did, however, comment on the breakup of picture edges across the vertical scan line of the 1,000-line CRT. This occurred when using runway line markings or when the sides of buildings were used as lateral and azimuthal cues during precise tracking tasks; the result was a "fuzzy" picture and loss of visual cueing. Finally, several pilots were mildly distracted by the CGI characteristic of building the far-field scene in real time. This characteristic should be reduced in the CGI software by adjusting the range-sorting algorithm.

CONCLUSIONS

The following conclusions derive from the SH-2F helicopter simulation using the ICAB simulator system.

1. The ICAB/CGI/VMS simulator has been demonstrated to be a useful tool in the simulation of helicopter ship-landing problems.

2. Based on the engineering and perceptual validation tests, the simulator was judged to be satisfactory except for the vertical-response characteristics. Overall, the simulator accurately represented the helicopter to an airspeed of 90 knots with the ASE on and was more stable and more easily maneuvered than the actual aircraft with ASE off. With ASE on or off, lateral directional attitude-control was more effective than in the actual helicopter.

3. The field of view attainable with the four-window CGI visual allows valid low-speed maneuvering to be simulated. The CGI scene is presented with no perceived time delay.

4. Attitude cueing with the CGI is good but the range and range-rate cueing is only fair because of a lack of depth-of-field cues.

5. Additional SH-2F flight-test data are needed to validate the model in the vertical axis.

6. Improvements and validation of the ship airwake turbulence model are required.

REFERENCES

1. NATOPS Flight Manual, Navy Models SH-3D/SH-2F/HH-2D Aircraft. NAVAIR 01-260HCD-1, Mar. 1978.

2. Automatic Stabilization Equipment, Navy Models SH-2D/SH-2F. NAVAIR 01-2LOHCD-2-5,

3. Characteristics of Flight Simulator Visual Systems. AGARD Advisory Report 164, May 1981.

4. Mathematical Model Report (Final Report), Trainer LAMPS: SH-2F Helicopter Weapon System, Device 2F106. NATRADEVCEN 73-C-0130-15/50, Contract N61139-73-C-0130, Sept. 7, 1977.

5. McIntyre, H. H.: Longitudinal Dynamic Stability of a Helicopter with Torsionally Flexible Blades and Servo-Flap Control. 13th Annual National Forum of the American Helicopter Society, Washington, D.C., May 2-4, 1962, pp. 46-70.

6. Brown, R. G.; and Camaratta, F. A.: NAVAIRENGCEN Ship Motion Computer Program. NAEC MISC-903-8, 1978.

7. Fortenbaugh, R. L.: Progress in Mathematical Modeling of the Aircraft Operational Environment of DD-963 Class Ships. AIAA Paper 79-1677, Boulder, Colo., 1979.

8. Garnett, T. S., Jr.: Investigation to Study the Aerodynamic Ship Wake Turbulence Generated by an FF-1052 Frigate. Boeing Vertol Report D210-11140-1, Boeing Aircraft Co., Seattle, Wash., Dec. 1976.

9. Chalk, C. R. et al.: Background Information and User Guide for MIL-F-8785B (ASG) Military Specification Flying Qualities for Piloted Airplanes. AFFDL-TR-69-72, Aug. 1969.

10. Sinacori, John B.: Piloted Aircraft Simulation Concepts and Overview. T.R. 1074-2, Systems Technology, Inc., Hawthorne, Calif., Mar. 1978.

11. Fidelity of Simulation for Pilot Training. AGARD Advisory Report 159, Oct. 1980.

12. Woomer, C.; and Carico, G.: Flight Fidelity Evaluation of thw SH-2F Weapons System Trainer (DEVICE 2F-106). Report No. RW-11R-77, Naval Air Test Center, Patuxent River, Md., Mar. 1978.

13. Heffley, R. K. et al.: A Compilation and Analysis of Helicopter Handling Qualities Data. Vol. 1. NASA CR-3144, 1979.

14. Gum, D. R.; and Albery, W. B.: Time-Delay Problems Encountered in Integrating the Advanced Simulator for Undergraduate Pilot Training. J. Aircraft, vol. 14, 1977, pp. 327-332.

15. Cleveland, W. B.: A Time Lag Study of the Vertical Motion Simulator Computer System. NASA TM-81306, 1981.

16. Bray, R. S.: Helicopter Simulator Technology: An Ames Research Center Perspective. NASA CP-2219, Apr. 1982, pp. 199-208.

TABLE 1.- VMX MOTION GENERATOR PERFORMANCE LIMITS

Motion	Displacement	Velocity	Acceleration	Frequency at 30° phase lag, Hz
Lateral	±17 ft	±8 ft/sec	±15 ft/sec	1.6
Vertical	±25 ft	±16 ft/sec	±24 ft/sec	1.1
Roll	±19.5°	±19.5°/sec	±57.3°/sec	1.2
Pitch	+20.0°, -24.5°	±19.5°/sec	±57.3°/sec	1.1
Yaw	±34.0°	±19.5°/sec	±57.3°/sec	1.1

TABLE 2.- ICAB MASS PROPERTIES

Weight	= 7,600 lb
I_x	= 35,000 in.·lb·sec^2
I_y	= 61,000 in.·lb·sec^2
I_z	= 46,000 in.·lb·sec^2

TABLE 3.- SH-2F LOADER CHARACTERISTICS

Parameter	Longitudinal	Lateral	Rudder	Collective
Travel, in.	±7.0	±5.6	±3.04	5.75
Breakout force, lb	±1.8	±1.5	±3.1	
Force gradient (range), lb/in. (in.)	4.17 (0 - 0.25) 1.60 (0.25 - 7.0)	4.67 (0 - 0.25) 1.66 (0.25 - 5.6)	±6.13	
Maximum deflection force, lb	±12.7	±10.4	21.5	

TABLE 4.- DYNAMIC RESPONSE TESTS SUMMARY

Figure	Dynamic step response	Initial flight conditions					
		Airspeed, knots	ASE	Weight, lb	c.g., in.	Altitude, m	OAT, °C
26	Pitch axis	10	Off	10921	169.8	244	8
27	Pitch axis	70	Off	12120	171.0	610	16
28	Pitch axis	10	On	11588	170.5	244	7
29	Pitch axis	70	On	11632	170.1	610	10
30	Roll axis	10	Off	10721	170.1	244	8
31	Roll axis	70	Off	12012	170.9	610	16
32	Roll axis	10	On	11471	170.4	244	7
33	Roll axis	70	On	11320	170.2	610	10
34	Yaw axis	10	Off	10021	167.3	61	9
35	Yaw axis	70	Off	11852	170.4	610	14
36	Yaw axis	10	On	10138	167.0	61	9
37	Yaw axis	70	On	10972	170.1	610	10
38	Height axis	10	Off	12120	170.1	610	10
39	Height axis	70	Off	12120	170.1	610	10
40	Height axis	10	On	12120	170.1	610	10
41	Height axis	70	On	12120	170.1	610	10
42	Pitch/roll coupling	10	Off	10562	167.3	305	19
43	Pitch/roll coupling	70	Off	11932	170.6	610	14
44	Pitch/roll coupling	10	On	10792	167.6	305	19
45	Pitch/roll coupling	70	On	11222	170.1	610	10
46	Roll/pitch coupling	10	Off	10871	169.7	244	8
47	Roll/pitch coupling	70	Off	12032	170.9	610	16
48	Roll/pitch coupling	10	On	11521	170.4	244	7
49	Roll/pitch coupling	70	On	11540	170.4	610	10

TABLE 5.- SH-2F STABILITY AND CONTROL DERIVATIVES
[Level flight, 11,250 lb, 170.1 c.g.]

	x, ft/sec^2	y, ft/sec^2	z, ft/sec^2	L, rad/sec^2	M, rad/sec^2	N, rad/sec^2
			0.1 knots			
/U ft/sec	-0.30212E-01	0.78004E-02	-0.33442E-01	-0.18563E-02	0.14839E-01	-0.20770E-02
/V ft/sec	-.40905E 00	-.19812E 00	-.25837E-01	-.70769E-01	.51059E-01	.52415E-01
/W ft/sec	.63484E-01	-.16239E-01	-.32087E-00	-.56596E-02	-.19971E-02	.49740E-02
/P rad/sec	-.32910E-01	-.41385E 01	.14764E 01	-.37907E 01	-.21210E 00	.17570E 00
/Q rad/sec	.49880E 01	-.20590E 01	-.51197E 00	.23473E 01	-.38989E 01	.32355E-01
/R rad/sec	-.84088E 00	.25844E 01	.19050E 00	.45359E 00	.25771E 00	-.17963E 01
/COL %	.34614E 01	-.23549E 01	-.31996E 02	-.86534E 00	.91904E-01	.20055E 01
/LON %	-.49676E 01	.39797E 00	-.44381E-01	.93521E-01	.27358E 01	.64187E-02
/LAT %	.54512E-01	.42790E 01	-.29170E-02	.40782E 01	.26705E-01	.61158E-01
/PED %	.00000E 00	-.69551E 01	.00000E 00	-.24432E 01	.93047E-01	.42560E 01
			70 knots			
/U ft/sec	-0.38800E-01	0.97143E-02	-0.20107E-01	0.77248E-02	0.38913E-02	-0.35785E-02
/V ft/sec	.44927E-03	-.12874E 00	-.46256E-01	-.30080E-01	.18871E-02	.59505E-01
/W ft/sec	.24691E-01	-.49625E 01	-.57465E 00	-.19800E-01	.51237E-02	-.74288E-02
/P rad/sec	-.42825E 00	-.43715E 01	-.61793E 01	-.39513E 01	-.15974E 01	.49635E 00
/Q rad/sec	.60406E 01	-.57071E 00	.64294E 01	.49452E 01	-.40703E 01	-.17338E 00
/R rad/sec	-.47476E 00	.84051E 00	-.42267E 00	-.27575E 00	.82791E-01	-.71761E 00
/COL %	.64361E 00	-.72573E 00	-.37907E 02	.67111E 00	.18532E 01	.10051E 01
/LON %	-.43563E 01	-.67466E 00	-.99985E 01	-.22659E 00	.29857E 01	.28111E 00
/LAT %	-.39380E-01	.44310E 01	.20378E 00	.41222E 01	.33292E-01	-.33740E 00
/PED %	.00000E 00	-.67291E 01	.00000E 00	-.23638F 01	.31344E-01	.41177E 01

TABLE 6.- COMPARISON OF HELICOPTER VERTICAL CHARACTERISTICS

Parameter	SH-2F	OH-6A	BO-105	AH-1G	UH-1H	CH-53D
			Hover			
Z_{δ_c}, (ft/sec^2)/in.	-5.75	-7.34	-9.68	-12.76	-9.77	-6.38
Z_w, 1/sec	-.32	-.34	-.33	-.37	-.39	-.30
			70 knots			
Z_{δ_c}, (ft/sec^2)/in.	-6.6	-8.62	-12.07	-15.07	-12.0	-8.10
Z_w, 1/sec	-.57	-.74	-.83	-.88	-.91	-.70

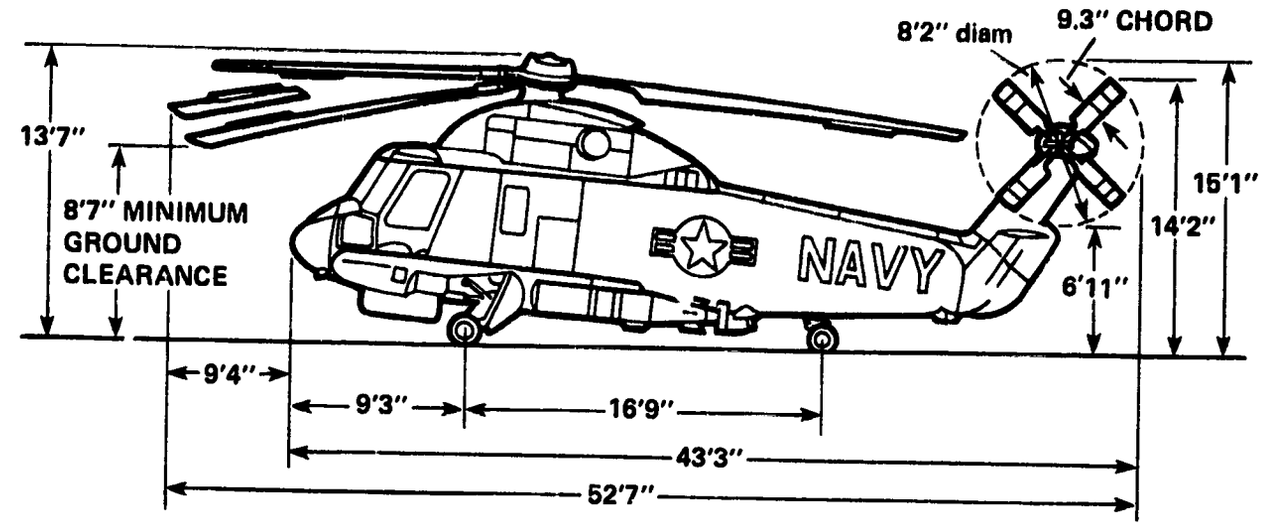

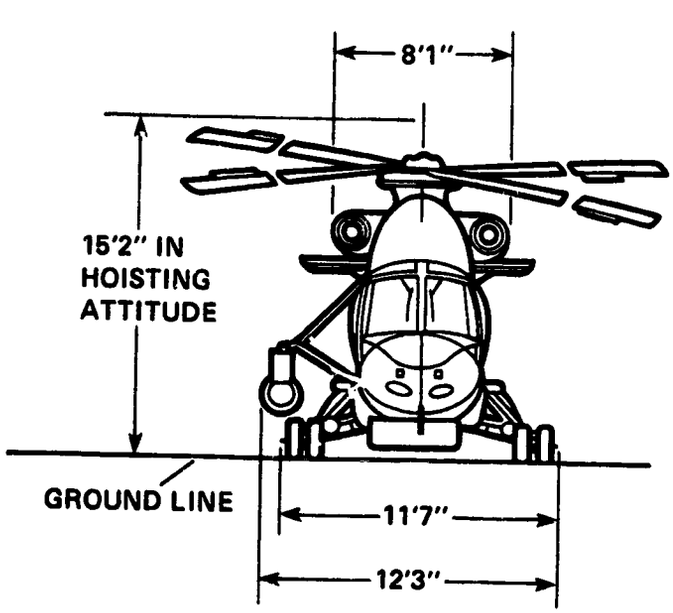

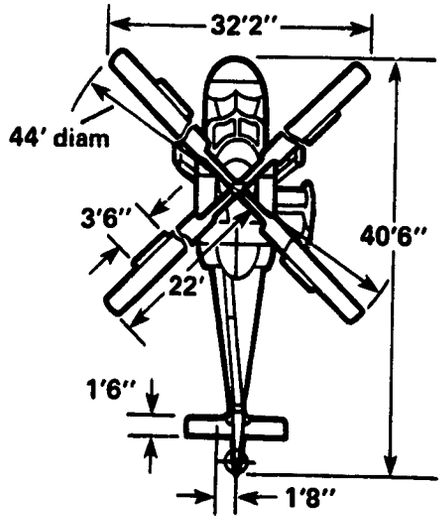

DIMENSIONS ARE AT NORMAL STATIC CONDITION AND 12,800 lb, EXCEPT AS NOTED

Figure 1.- Kaman SH-2F helicopter.

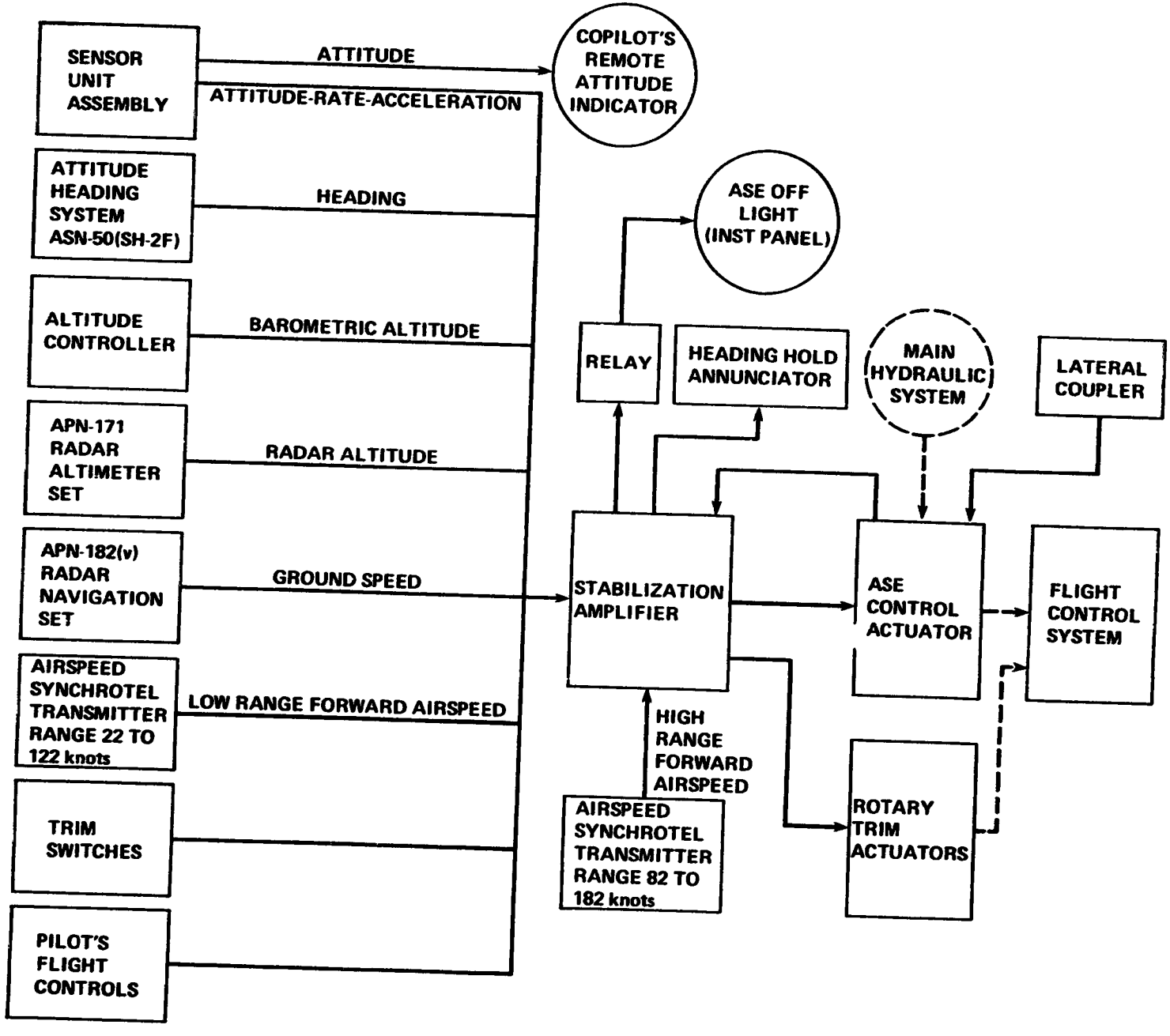

Figure 2.- Automatic Stabilization Equipment block diagram.

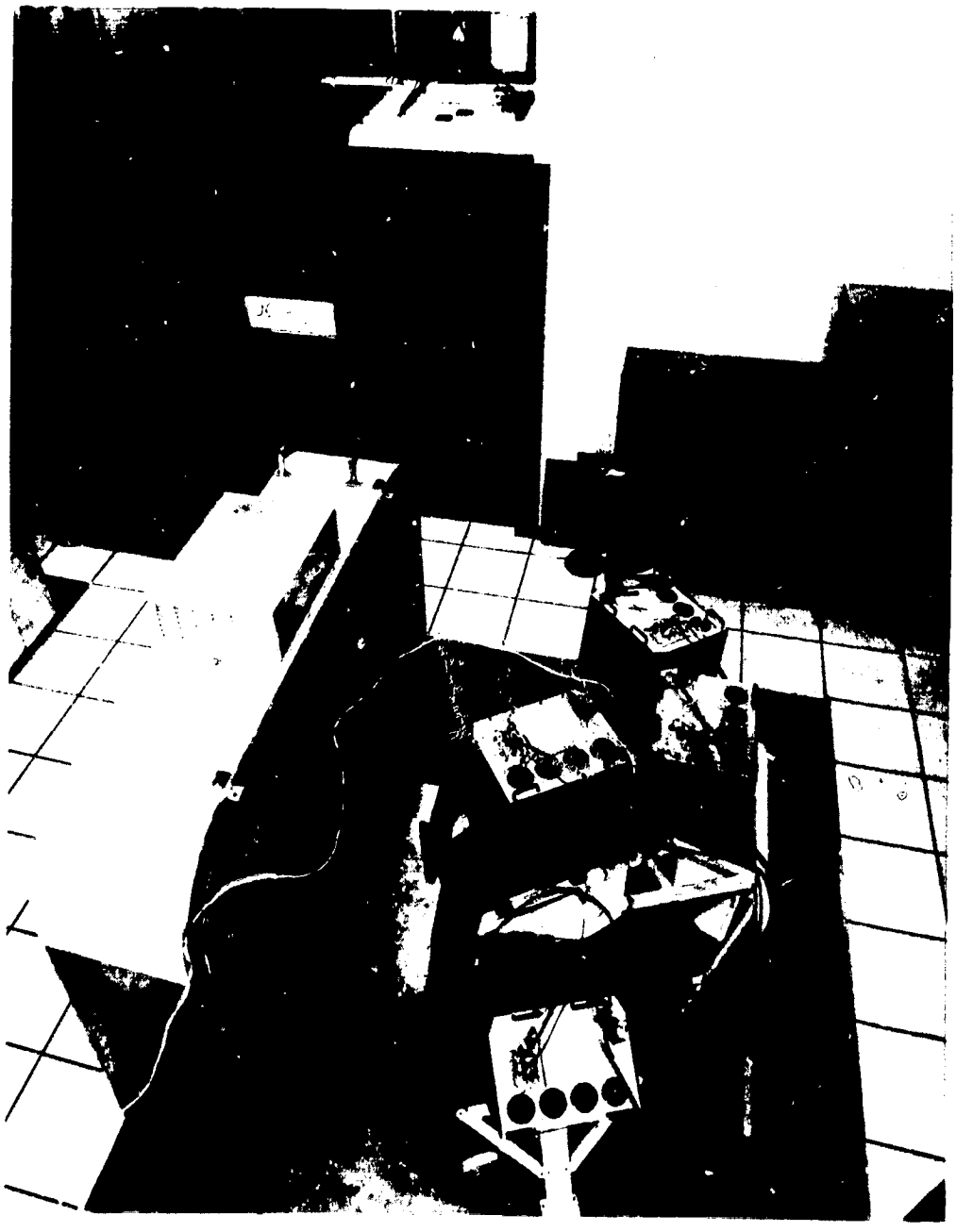

Figure 3.- ICAB in fixed base area (shown with canopy removed).

Figure 4.- ICAB development station.

Figure 5.- ICAB being mounted on Vertical Motion Simulator.

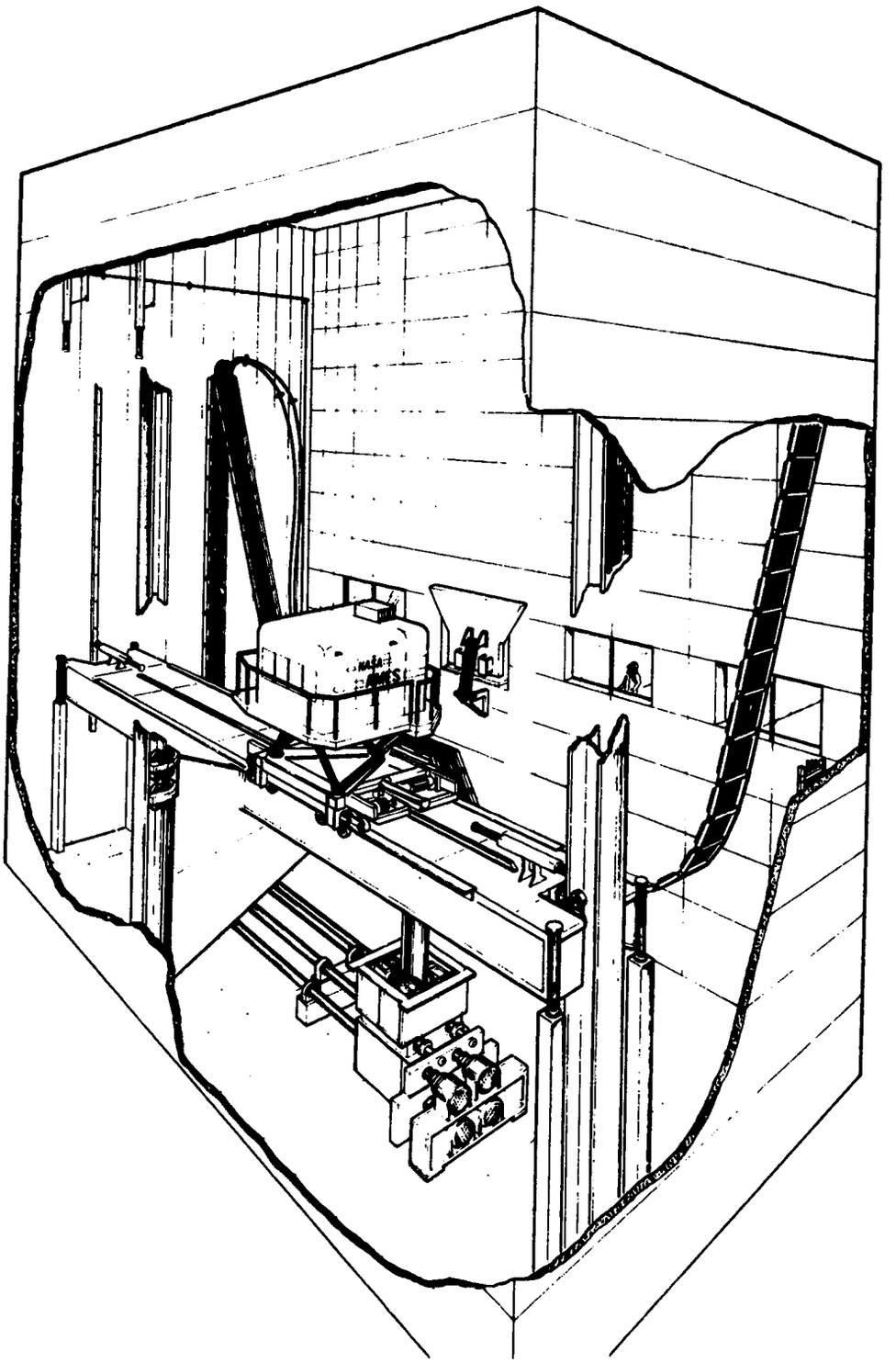

Figure 6.- Vertical Motion Simulator with ICAB.

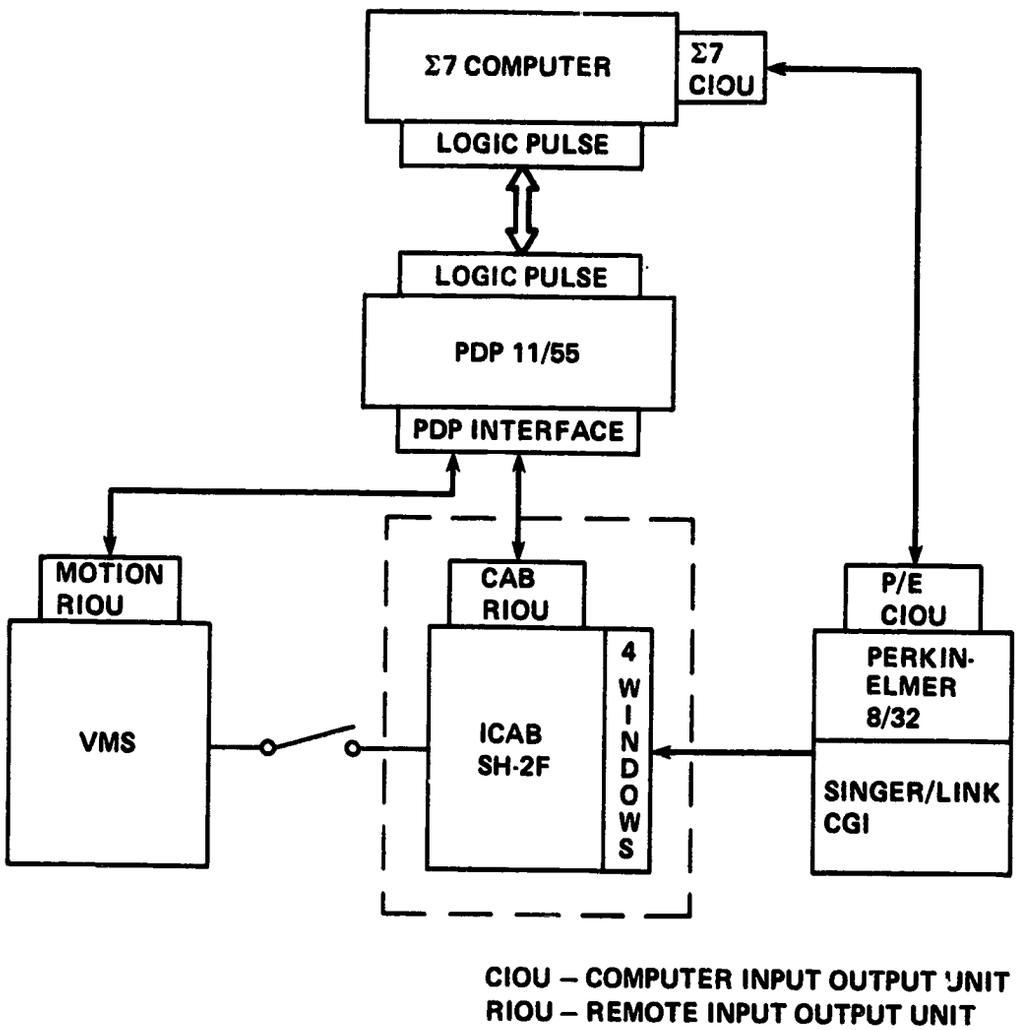

Figure 7.- ICAB system block diagram.

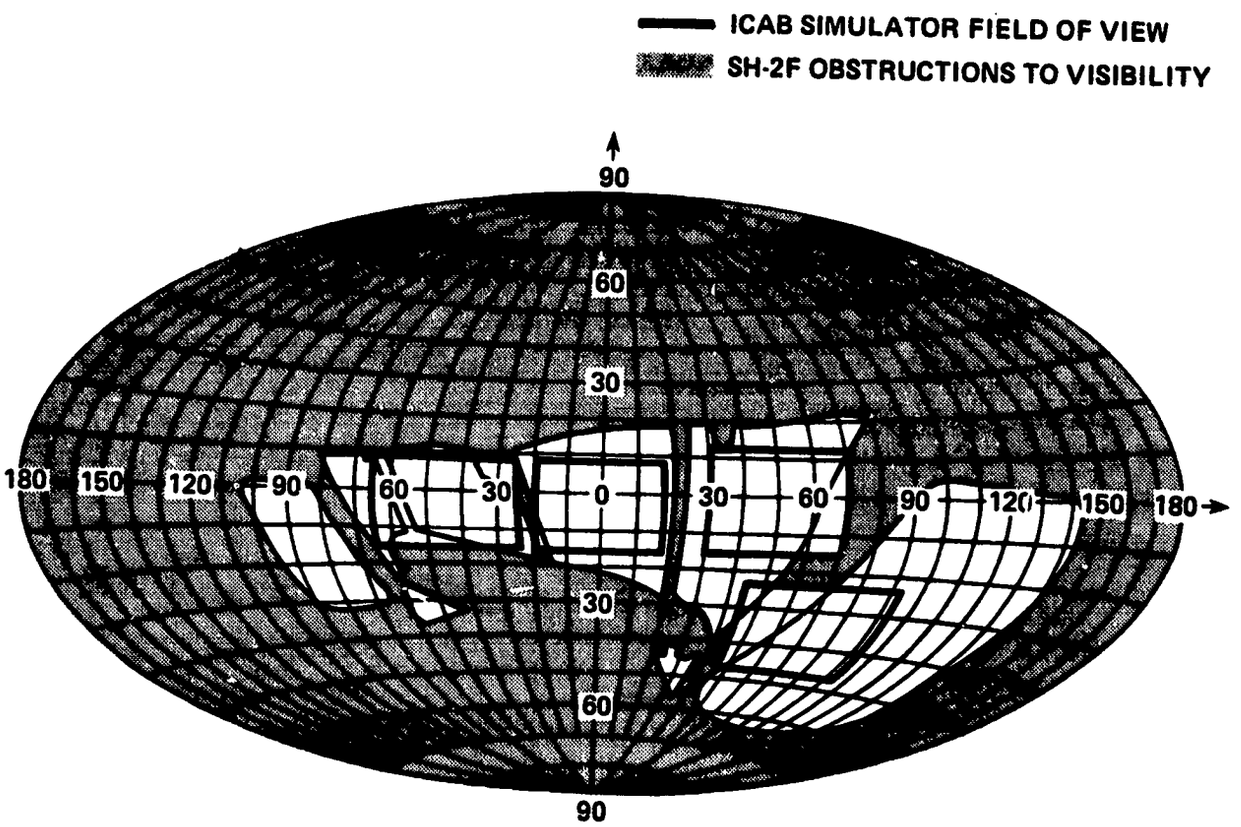

Figure 8.- Comparison of SH-2F helicopter and ICAB field-of-view.

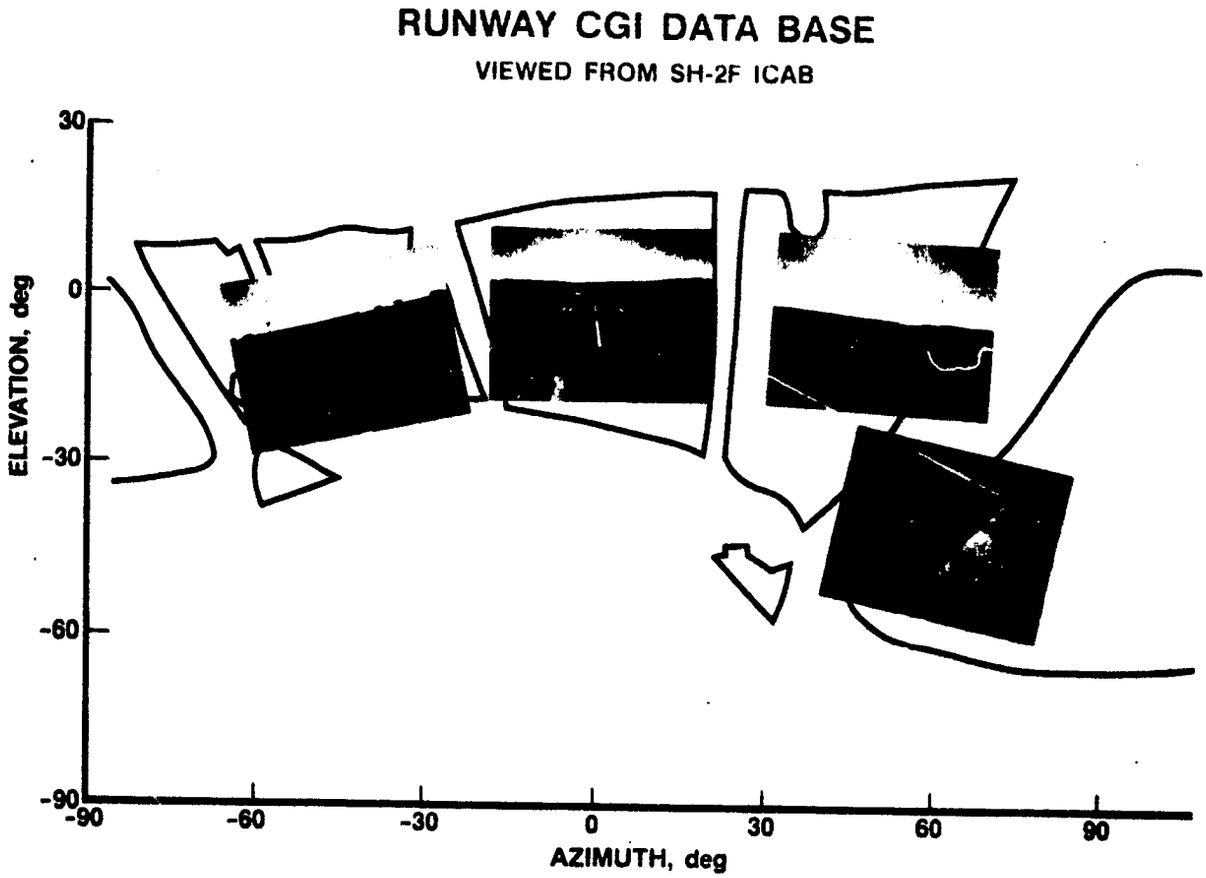

Figure 9.- SH-2F cockpit field of view with four-window CGI scene of runway superimposed.

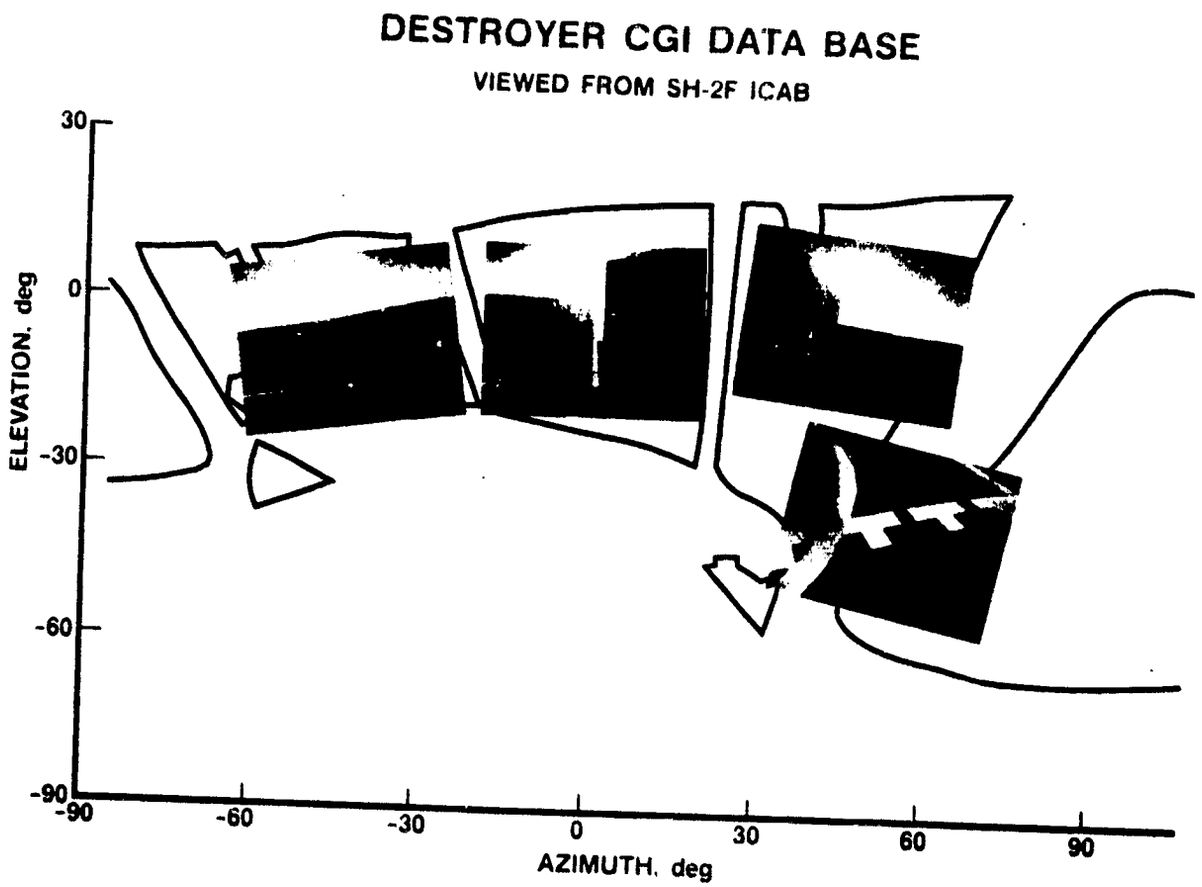

Figure 10.- SH-2F cockpit field of view with four-window CGI scene of destroyer superimposed.

Figure 11.- SH-2F simulator cockpit.

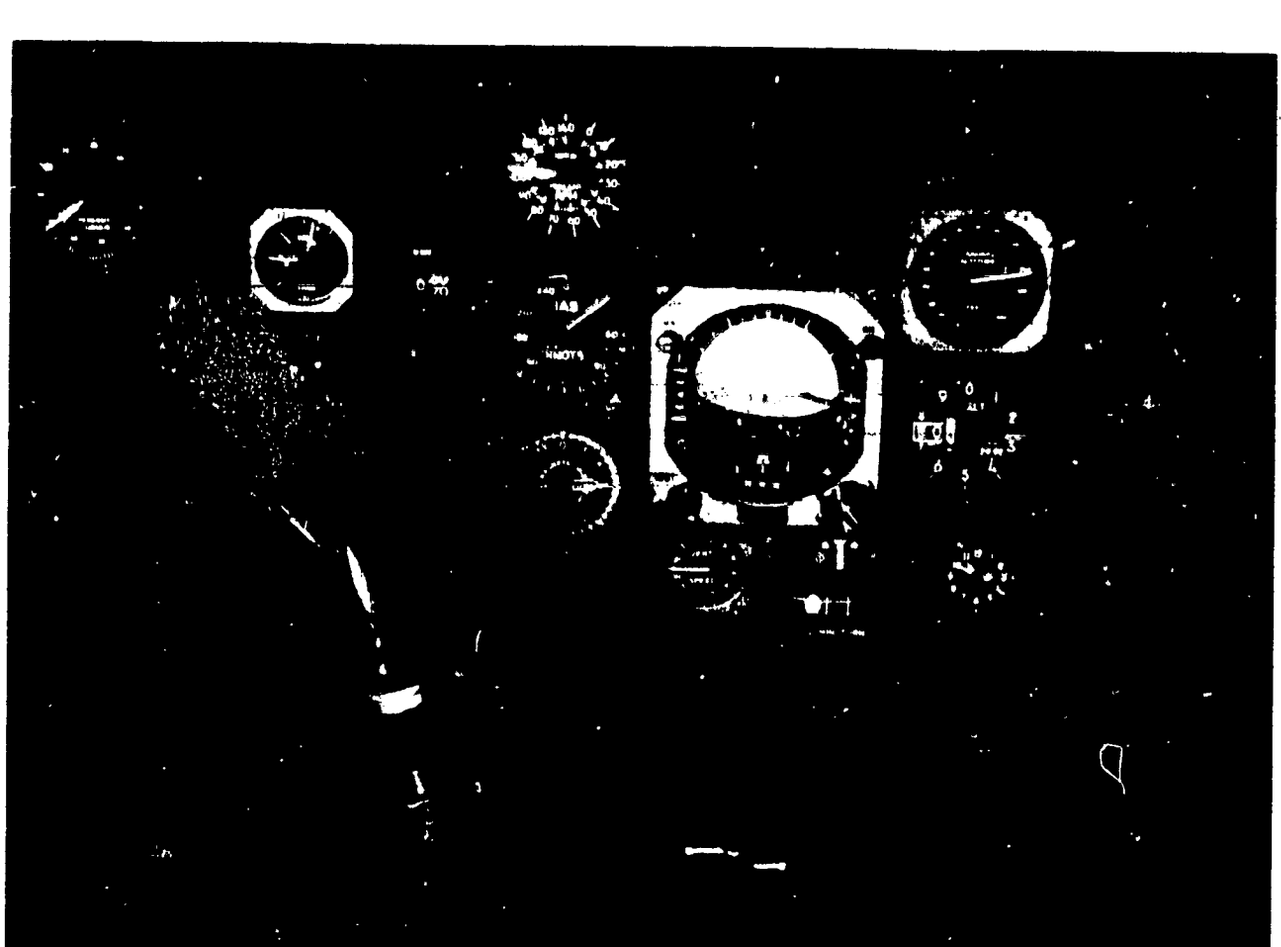

Figure 12.- SH-2F simulator instrument panel.

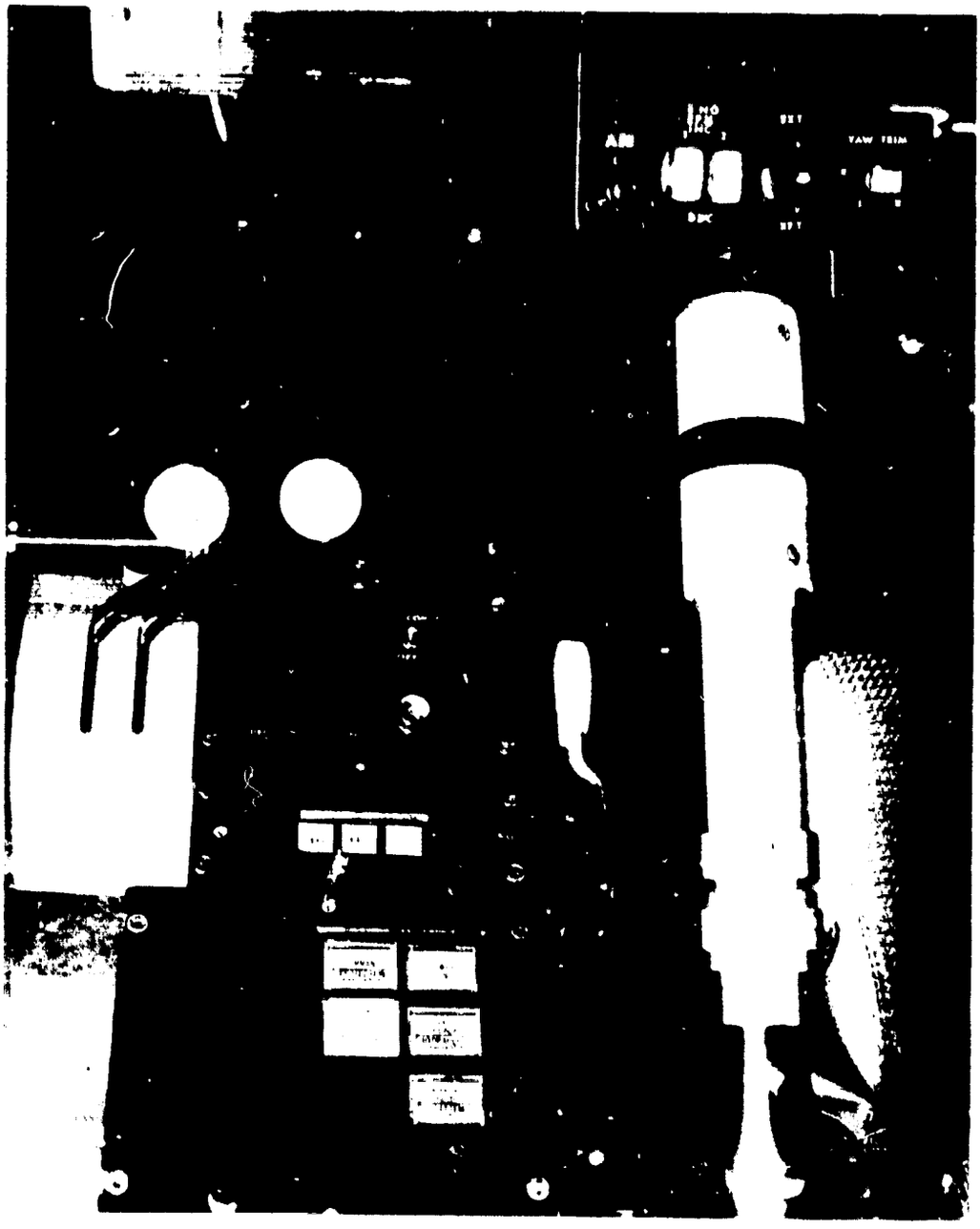

Figure 13.- SH-2F simulator center console.

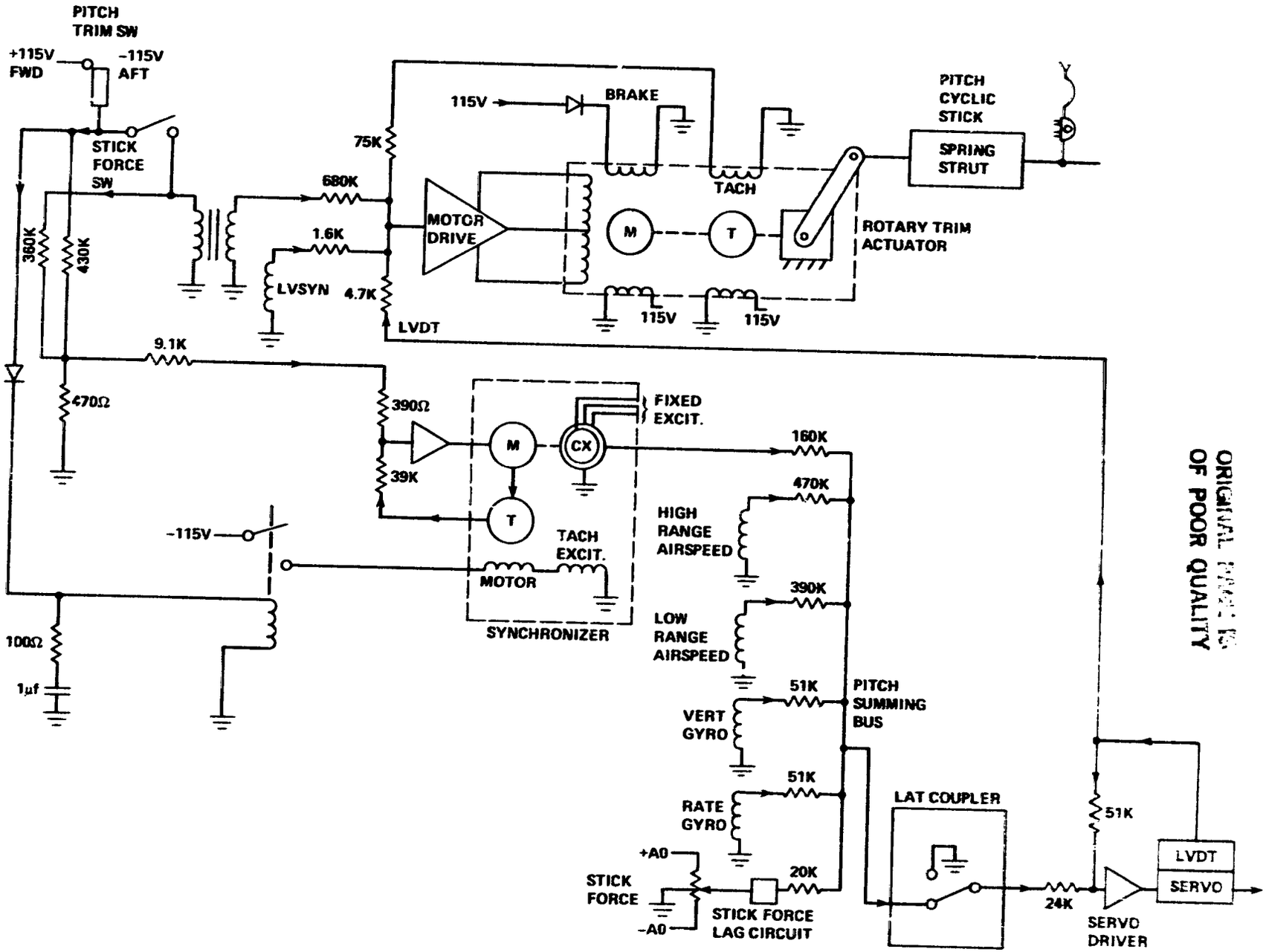

Figure 14.- Pitch ASE channel, ASE engaged with airspeed/attitude hold.

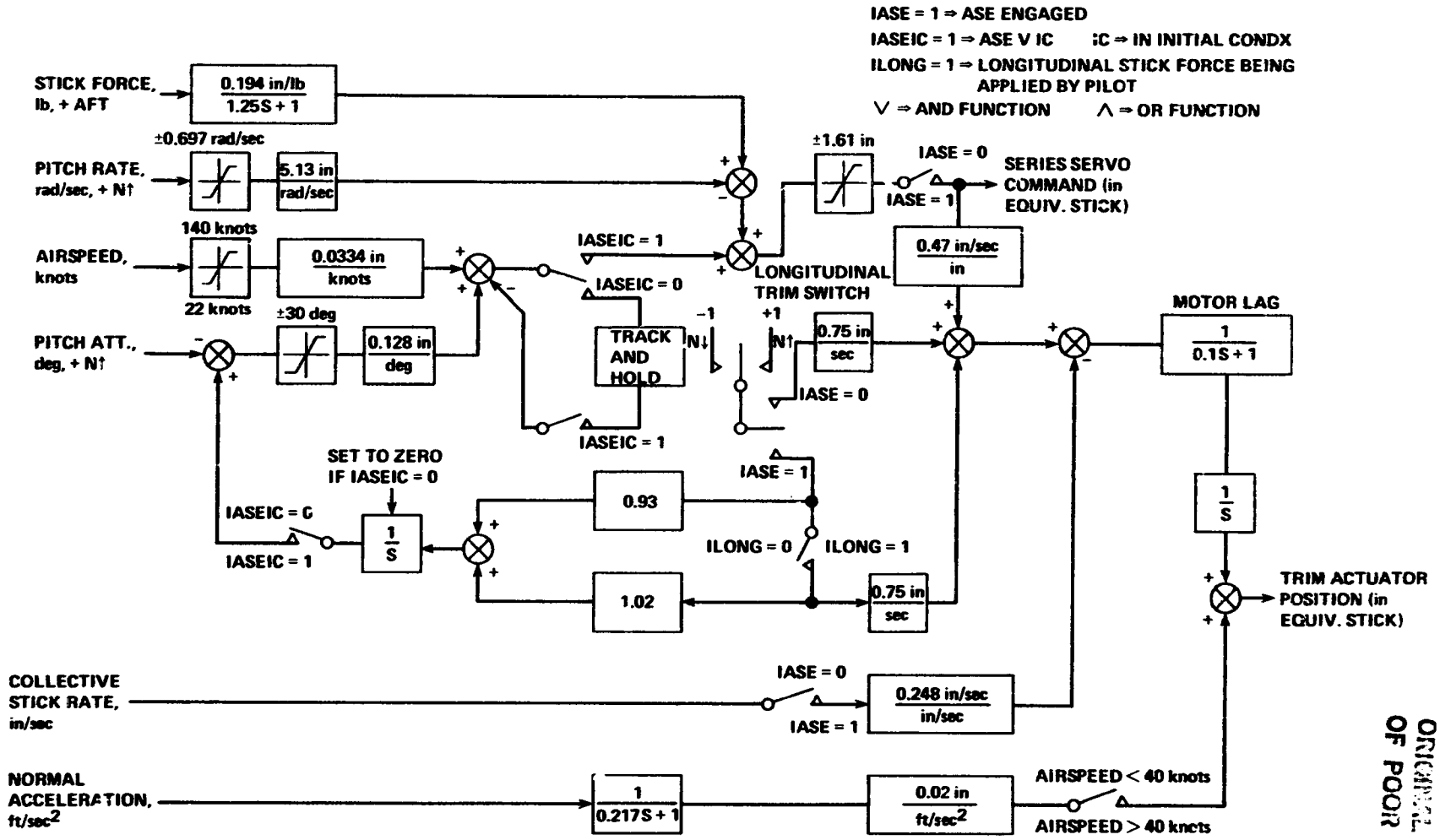

Figure 15.- Pitch ASE channel block diagram.

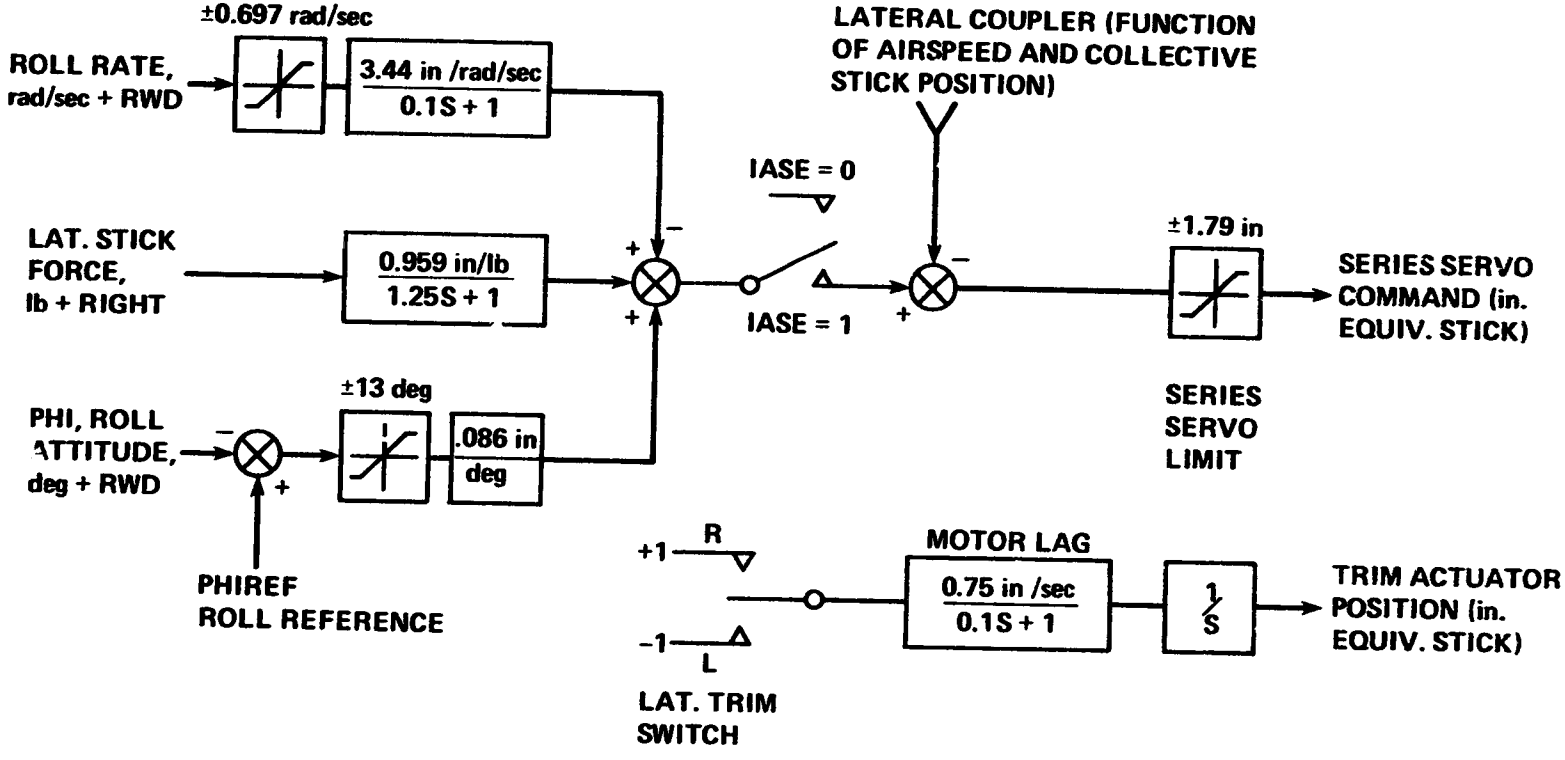

IASE = 1 ⇒ ASE ENGAGED
IF (IASE, EQ. O.) PHIREF = PHI

Figure 16.- Roll ASE channel block diagram.

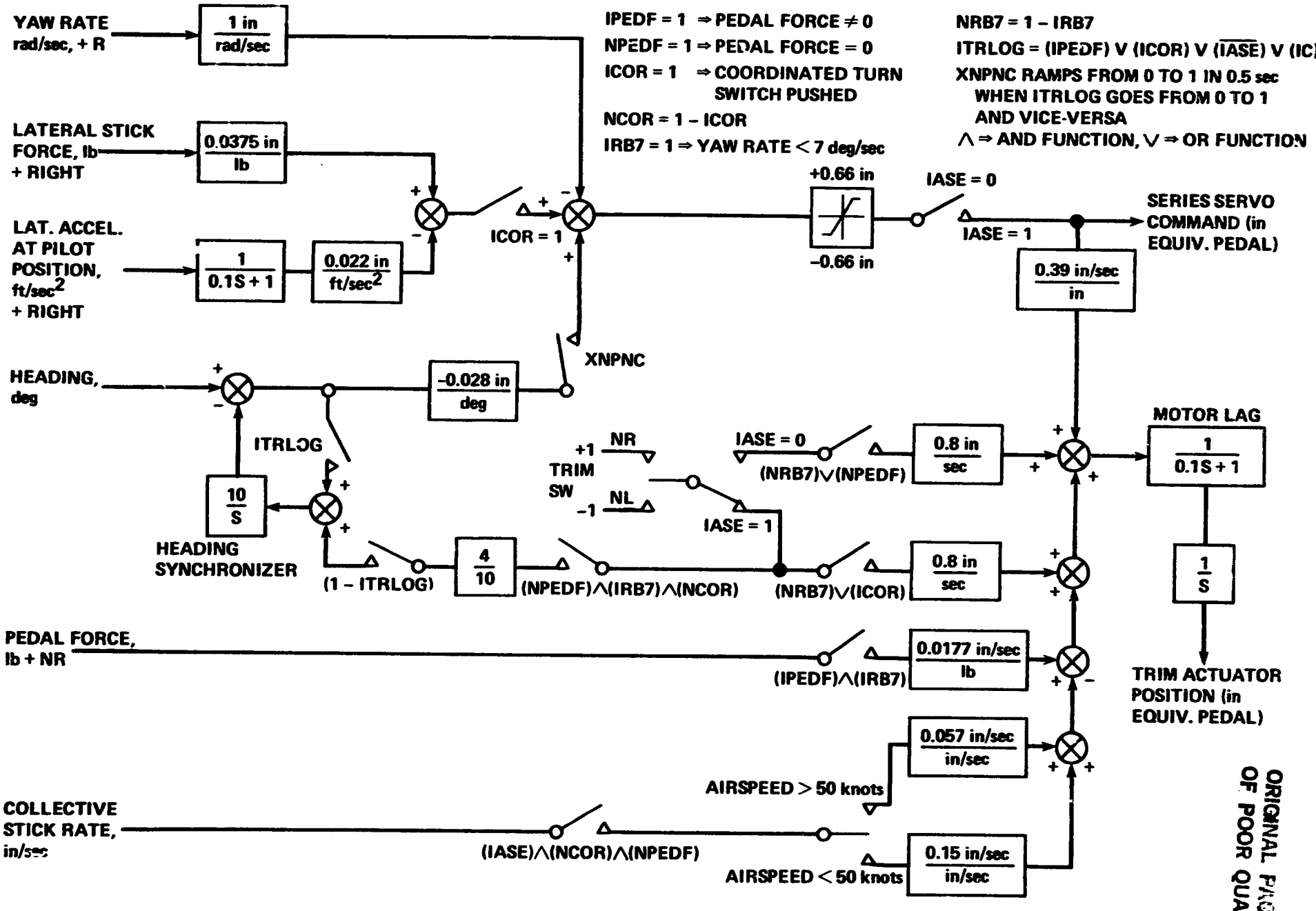

Figure 17.- Yaw ASE channel block diagram.

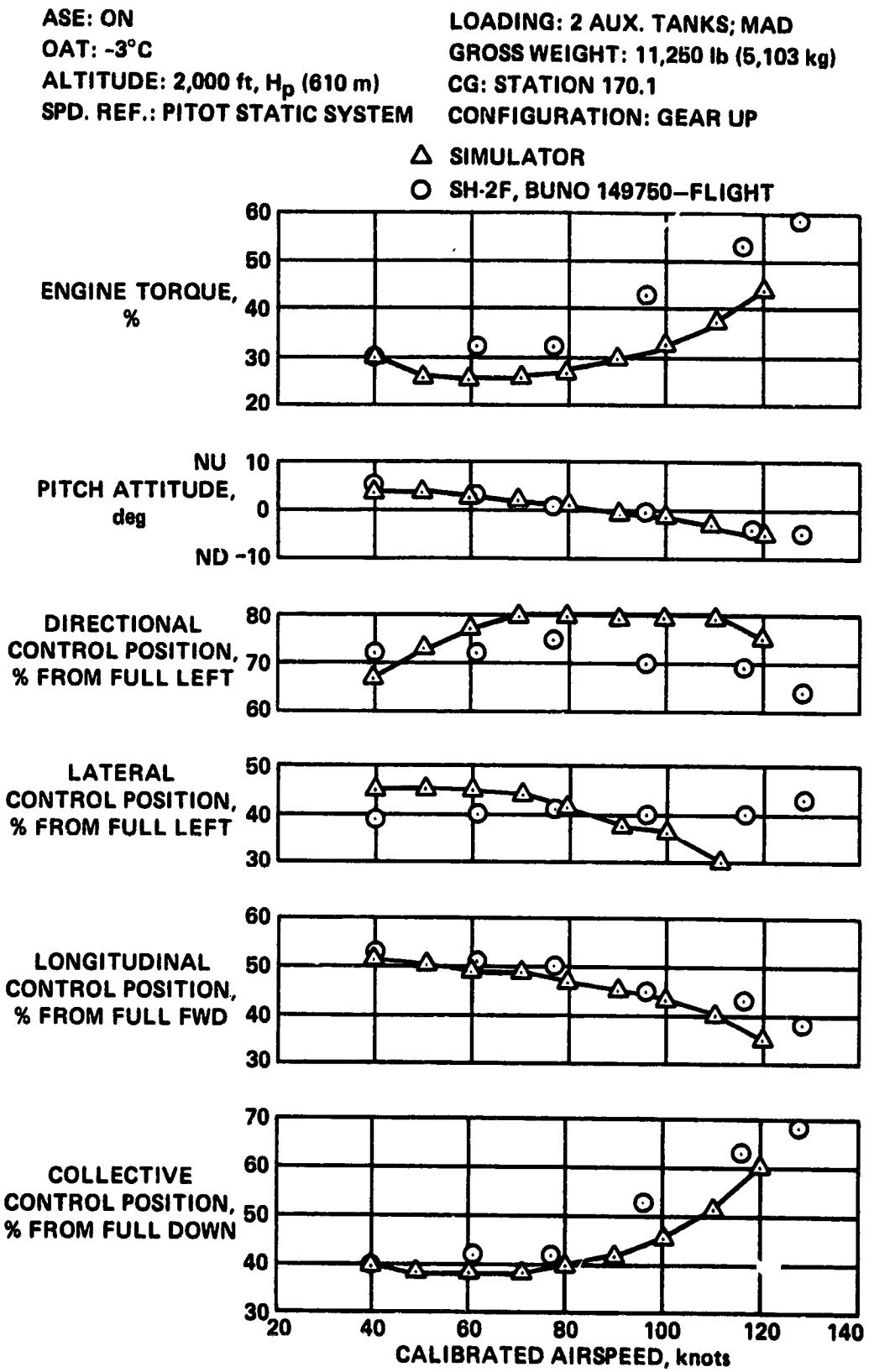

Figure 18.- Forward flight trimmed control position comparison.

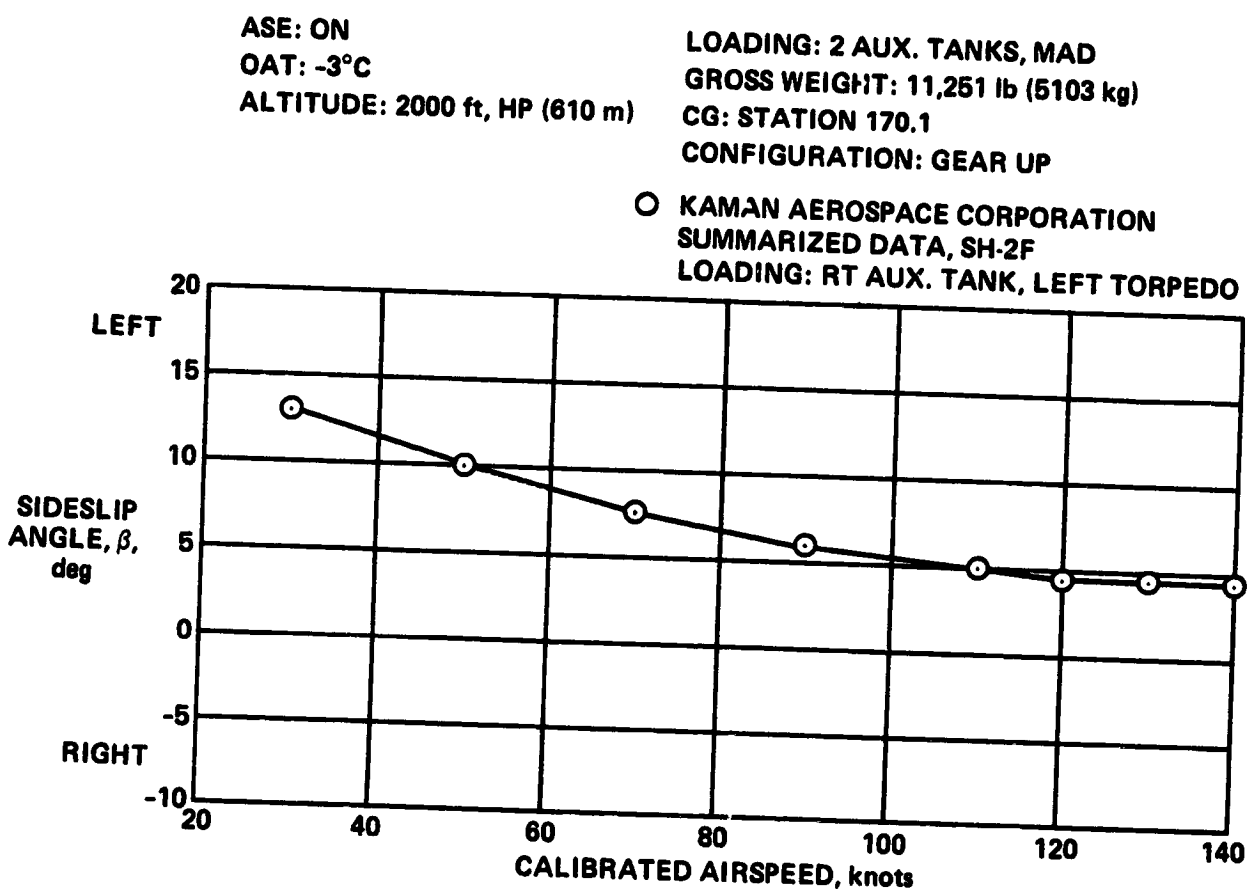

Figure 19.- Inherent sideslip characteristics.

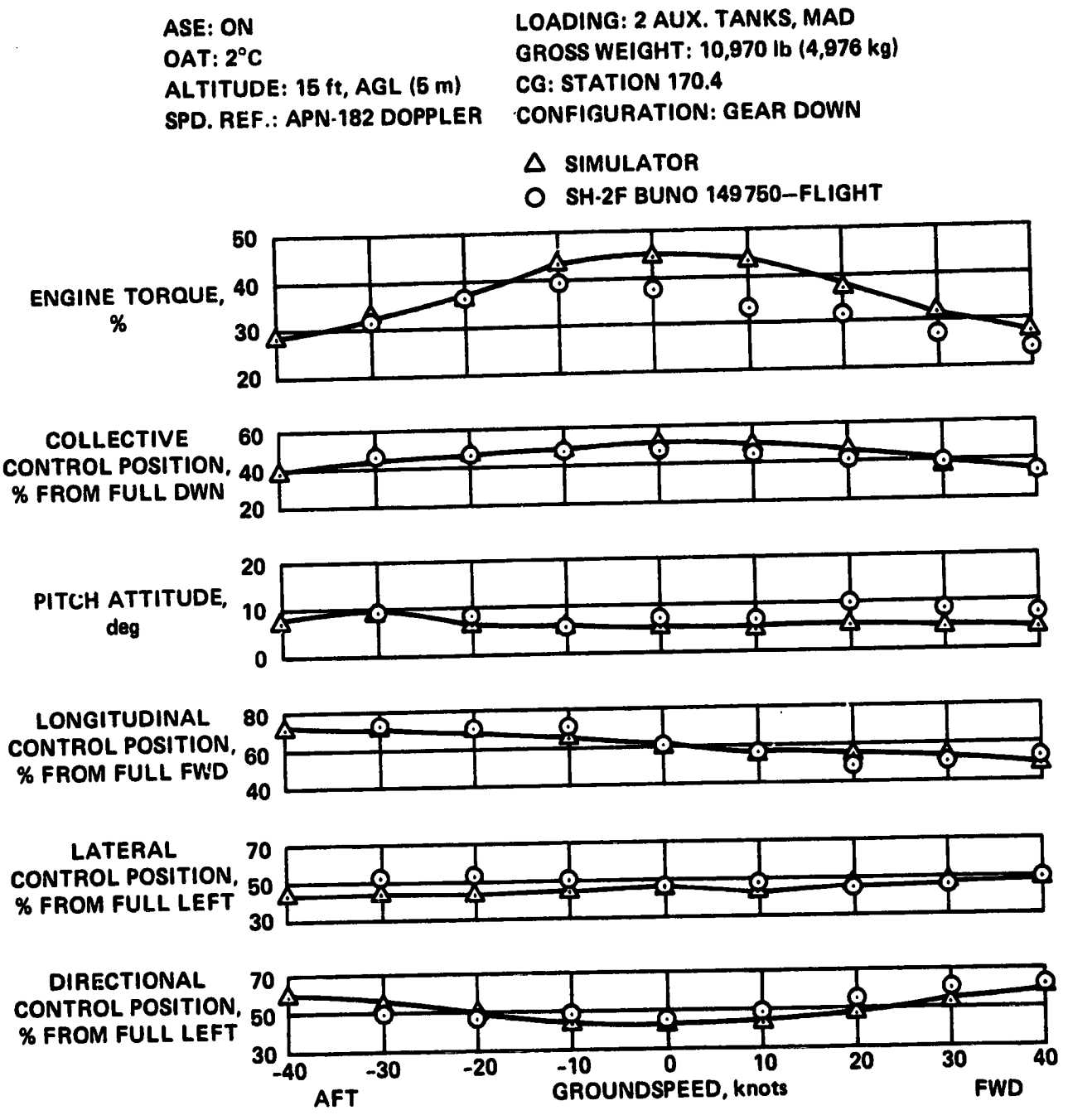

Figure 20.- Low speed trimmed control position comparison.

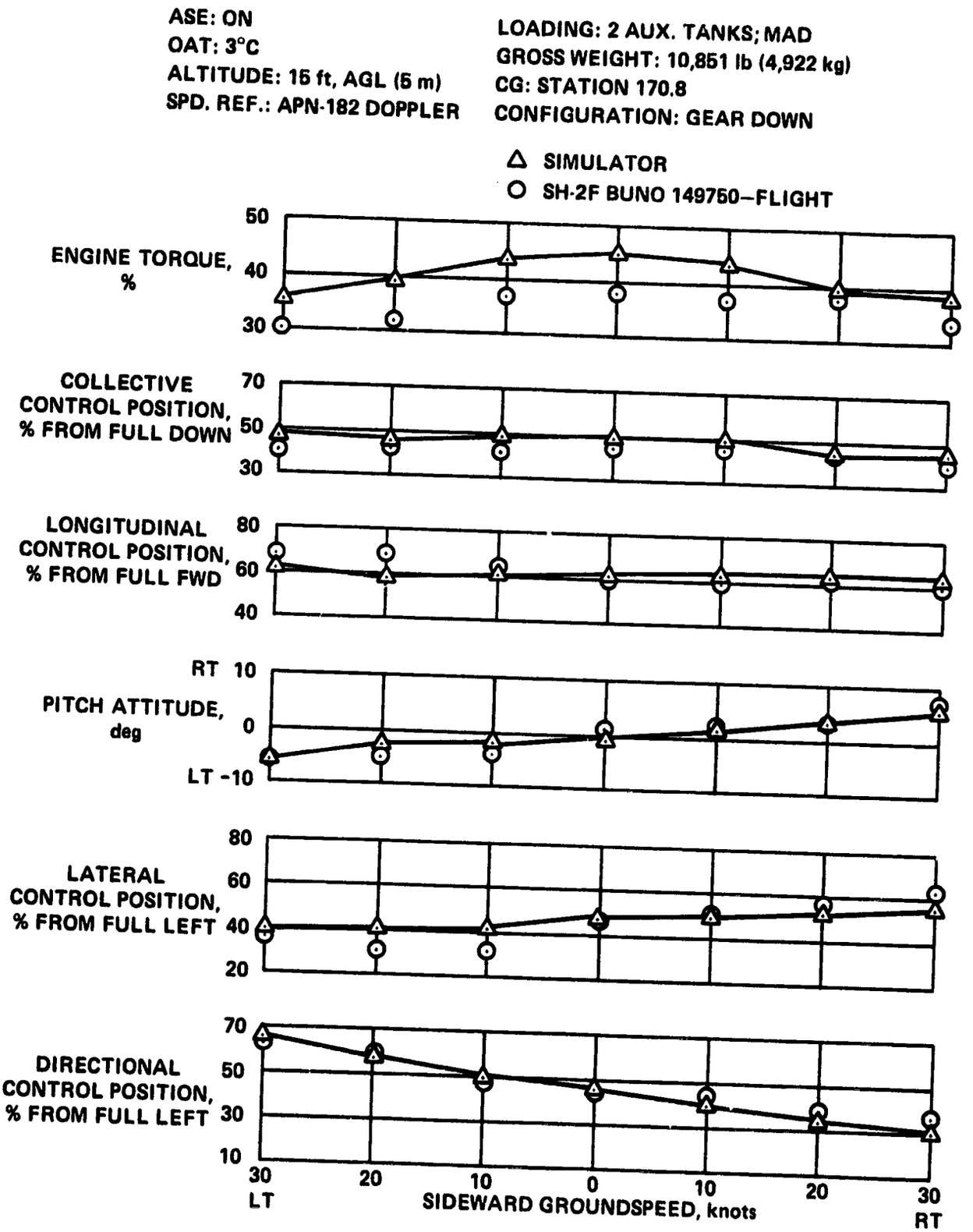

Figure 21.- Lateral flight trimmed control position comparison.

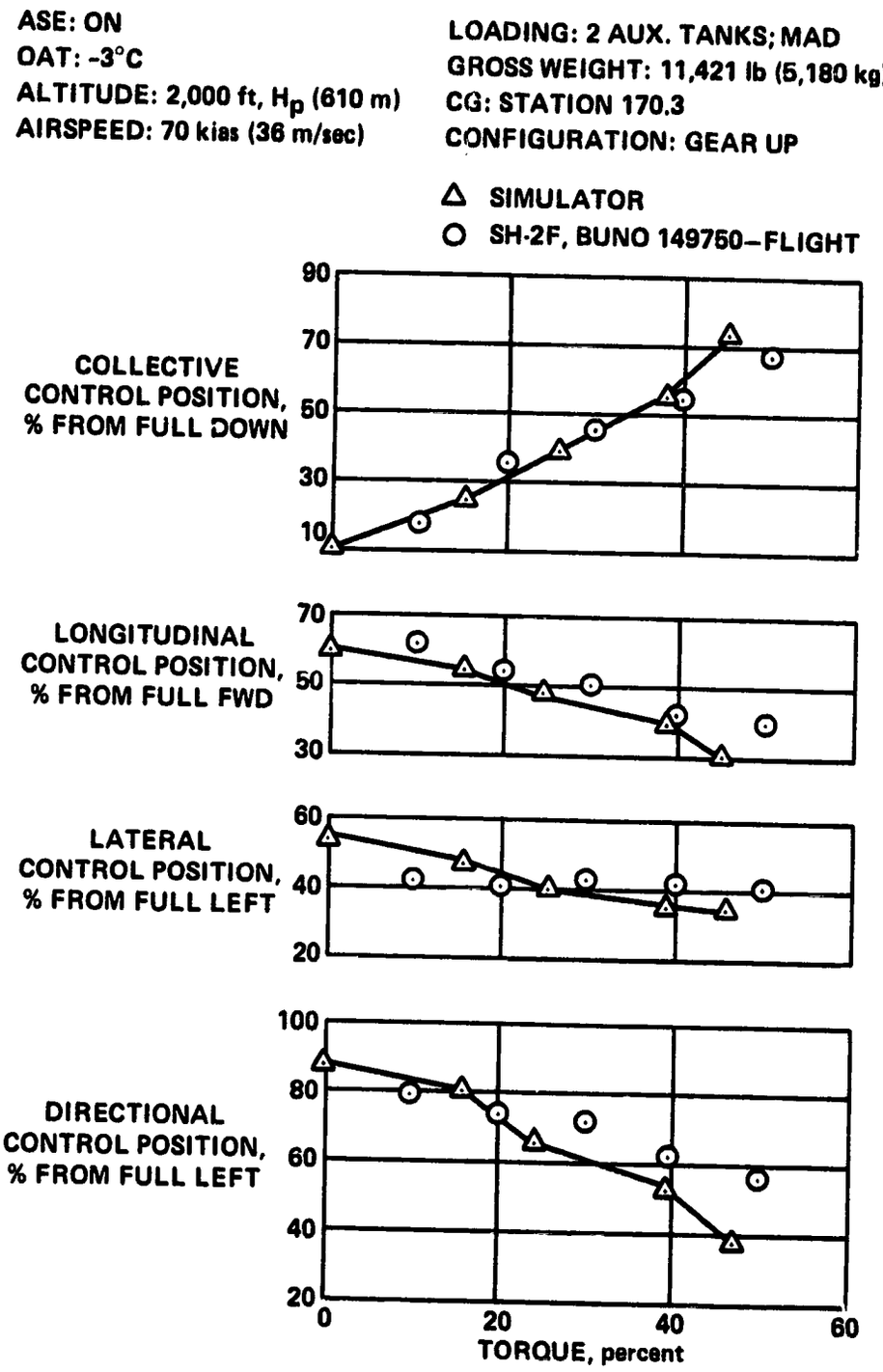

Figure 22.- Power effects on trimmed control positions comparison.

ASE: ON
OAT: -4°C
ALTITUDE: 15 ft, AGL (5 ni)
WIND: 15 knots (7.7 m/sec)

LOADING: 2 AUX. TANKS; MAD
GROSS WEIGHT: 11,207 lb (5,083 kg)
CG: STATION 170.1
CONFIGURATION: GEAR DOWN

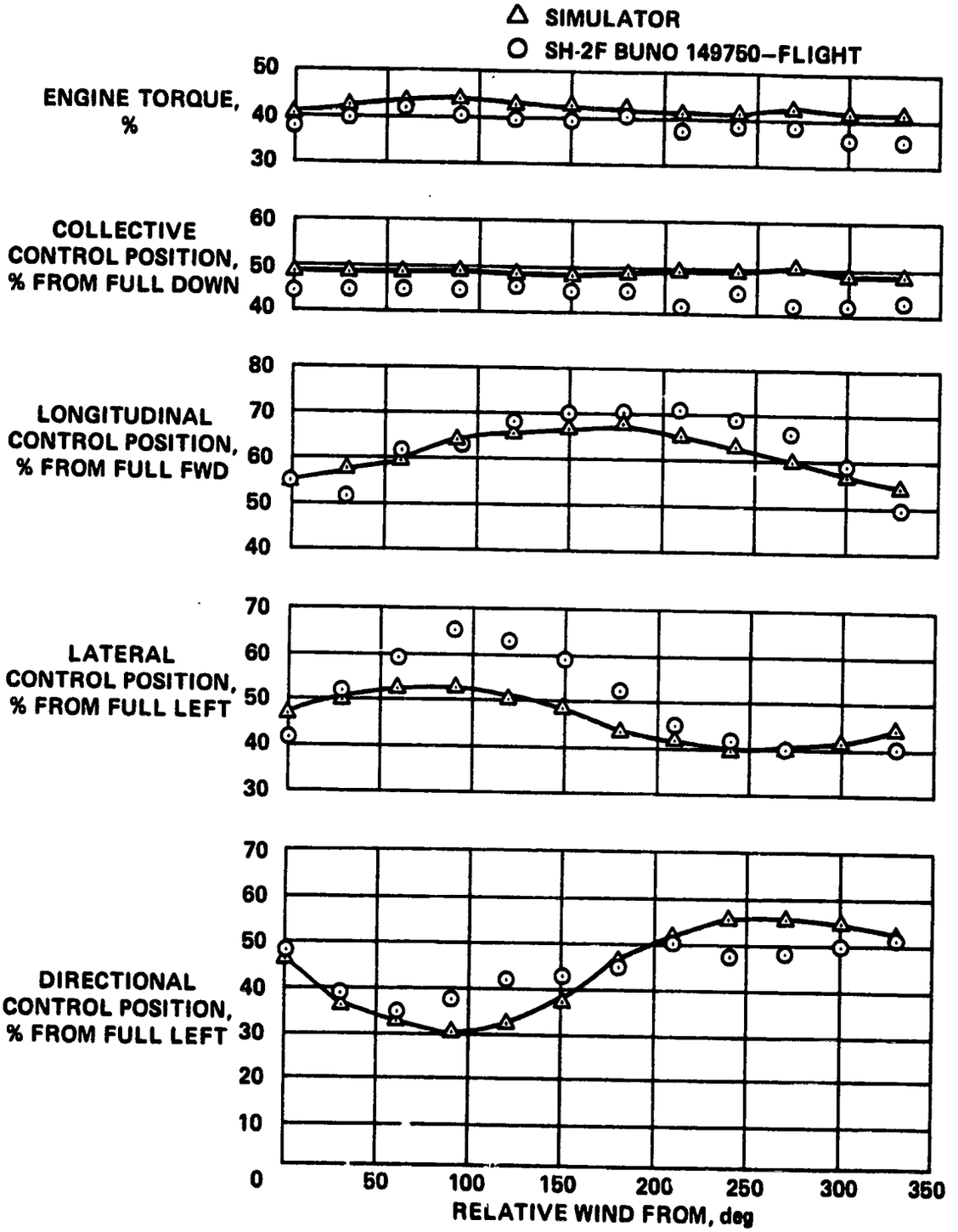

Figure 23.- Critical azimuth comparison.

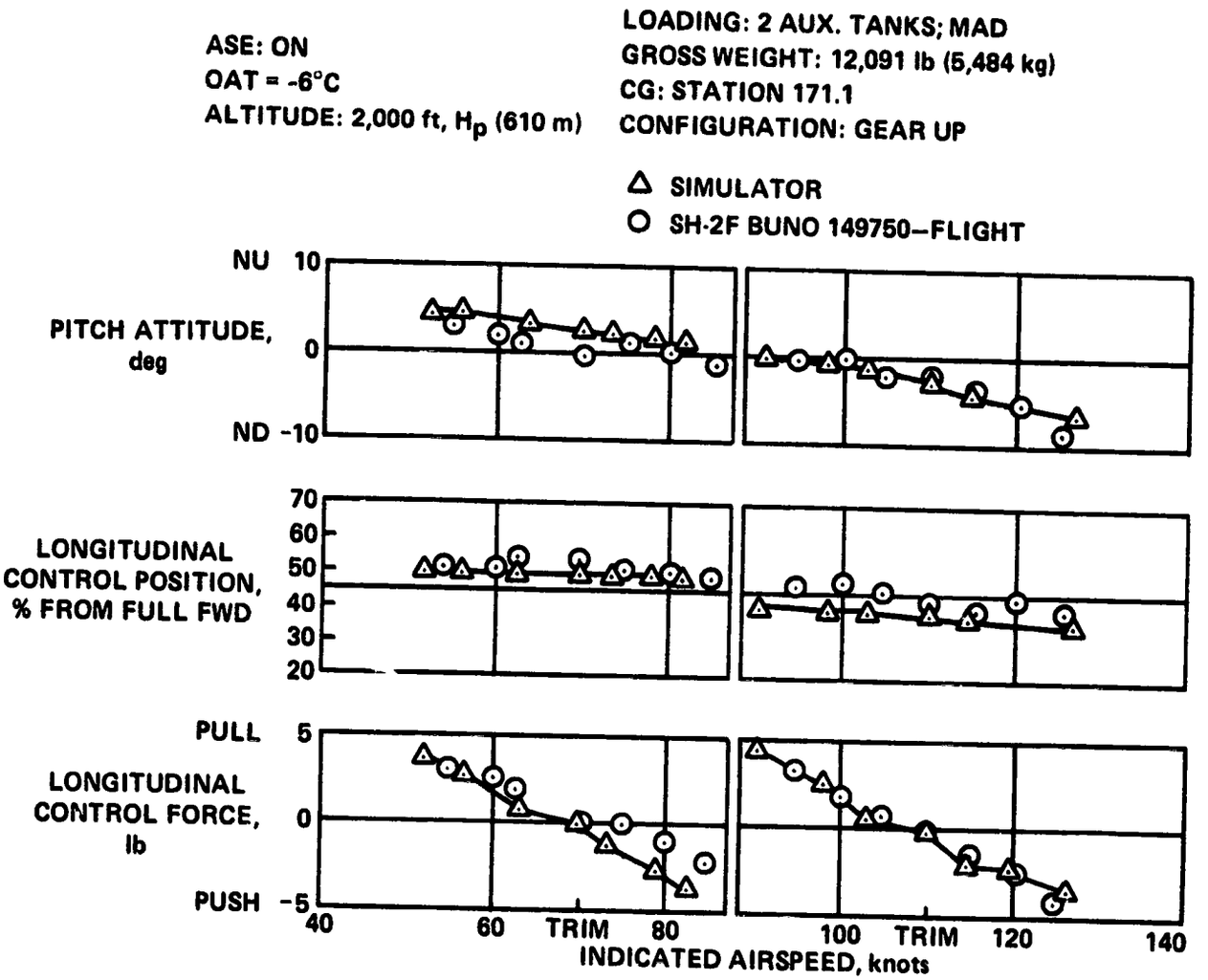

Figure 24.- Static longitudinal stability comparison.

ASE: ON
AIRSPEED: 70 kias (36 m/sec)
OAT: -3°C
ALTITUDE: 2000 ft, H_p (610 m)
SIDESLIP: DIRECT READING IN DIRECTIONAL GYRO TECHNIQUE IN A/C

LOADING: 2 AUX. TANKS, MAD
GROSS WEIGHT: 11,705 lb (5,309 kg)
CG: STATION 170.6
CONFIGURATION: GEAR UP

△ SIMULATOR
○ SH-2F BUNO 149750–FLIGHT

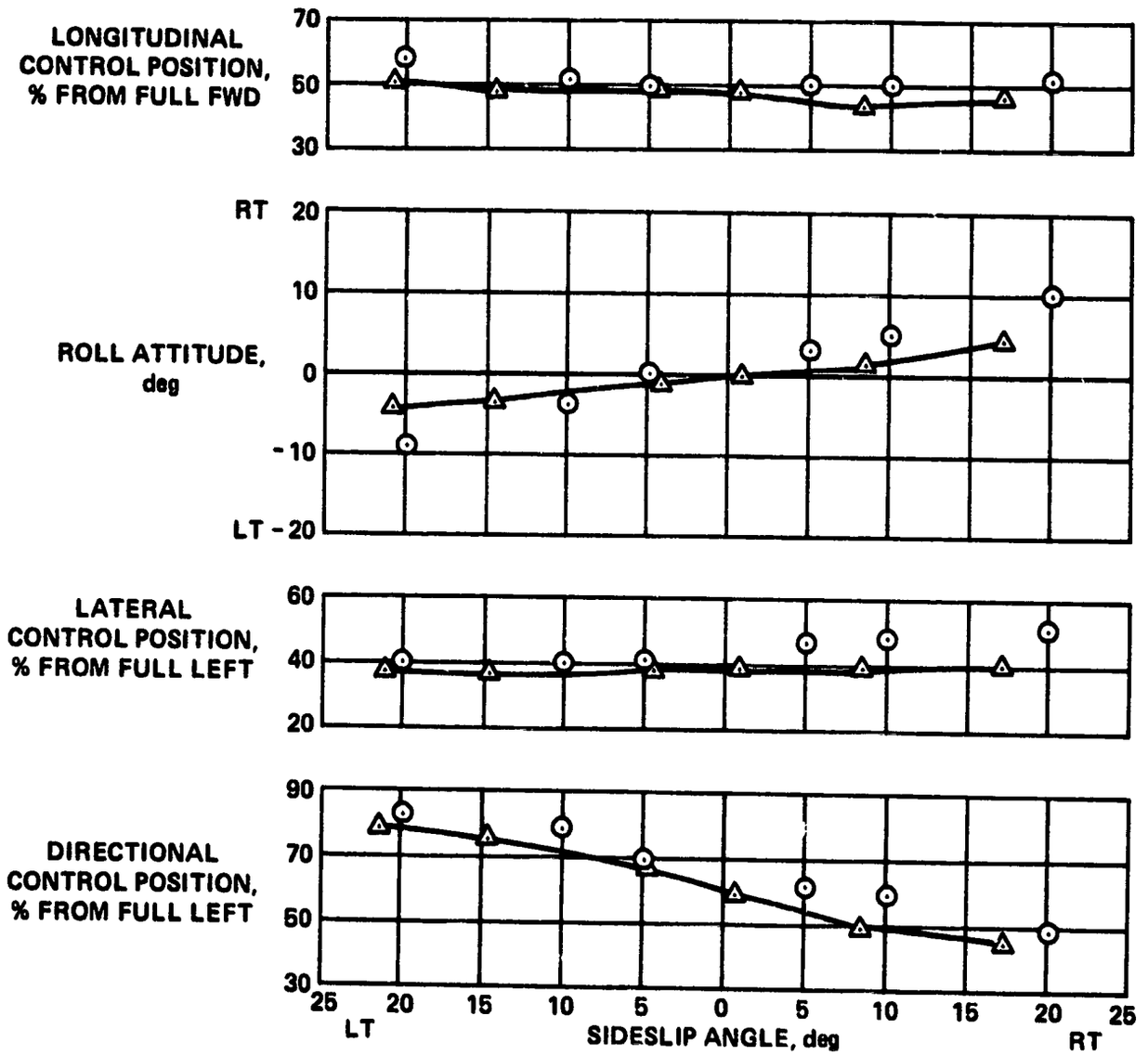

Figure 25.- Static lateral-directional stability comparison.

AIRSPEED = 5.1 m/sec (10 knots)
ASE = OFF
ALTITUDE = 244 m

WEIGHT = 10,291 lb
CG STATION = 169.8
TEMPERATURE = 8°C

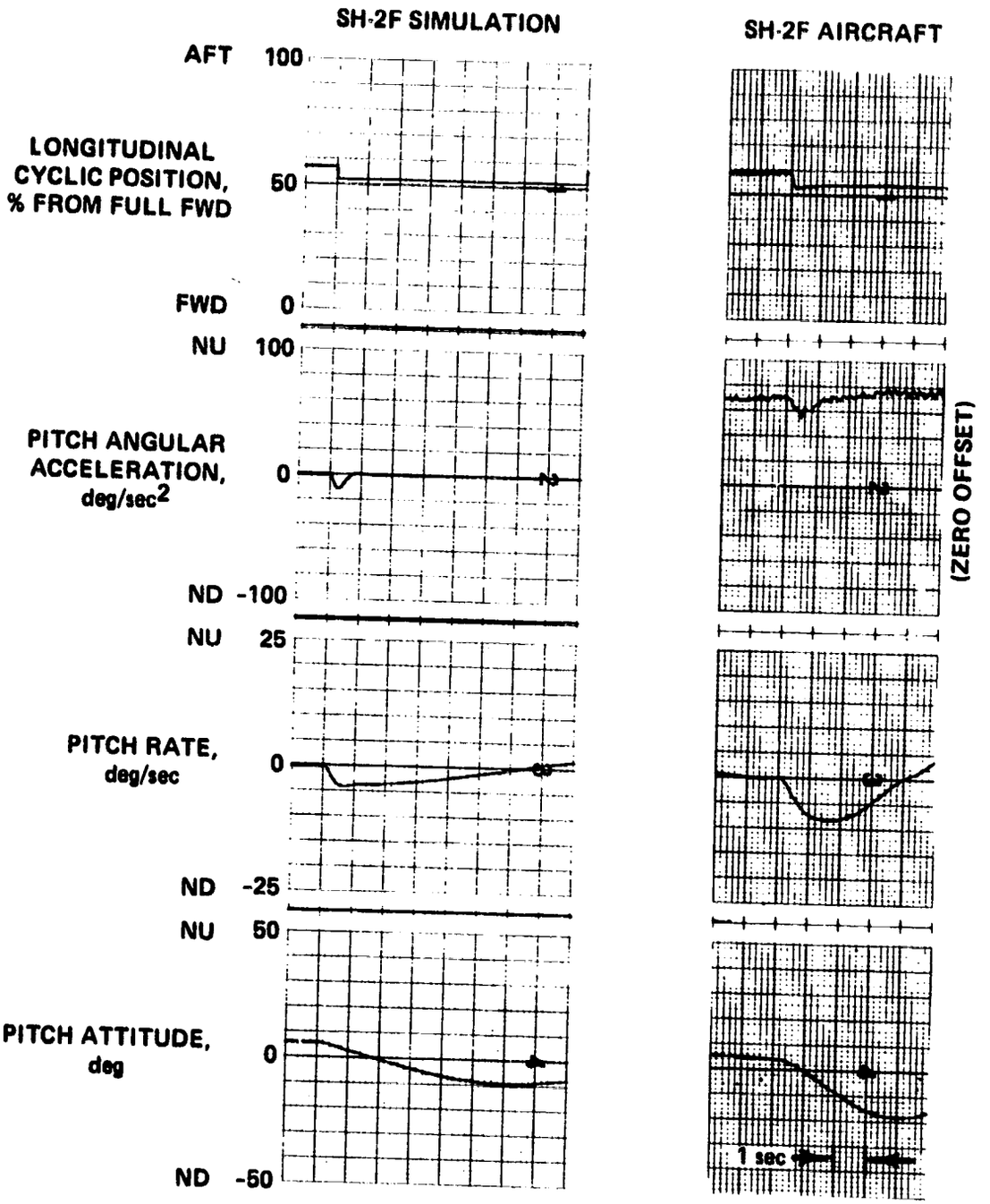

Figure 26.- Pitch axis control response, 10 knots, ASE off.

AIRSPEED = 36.0 m/sec (70 knots)
ASE = OFF
ALTITUDE = 610 m

WEIGHT = 12,120 lb
CG STATION = 171.0
TEMPERATURE = 18°C

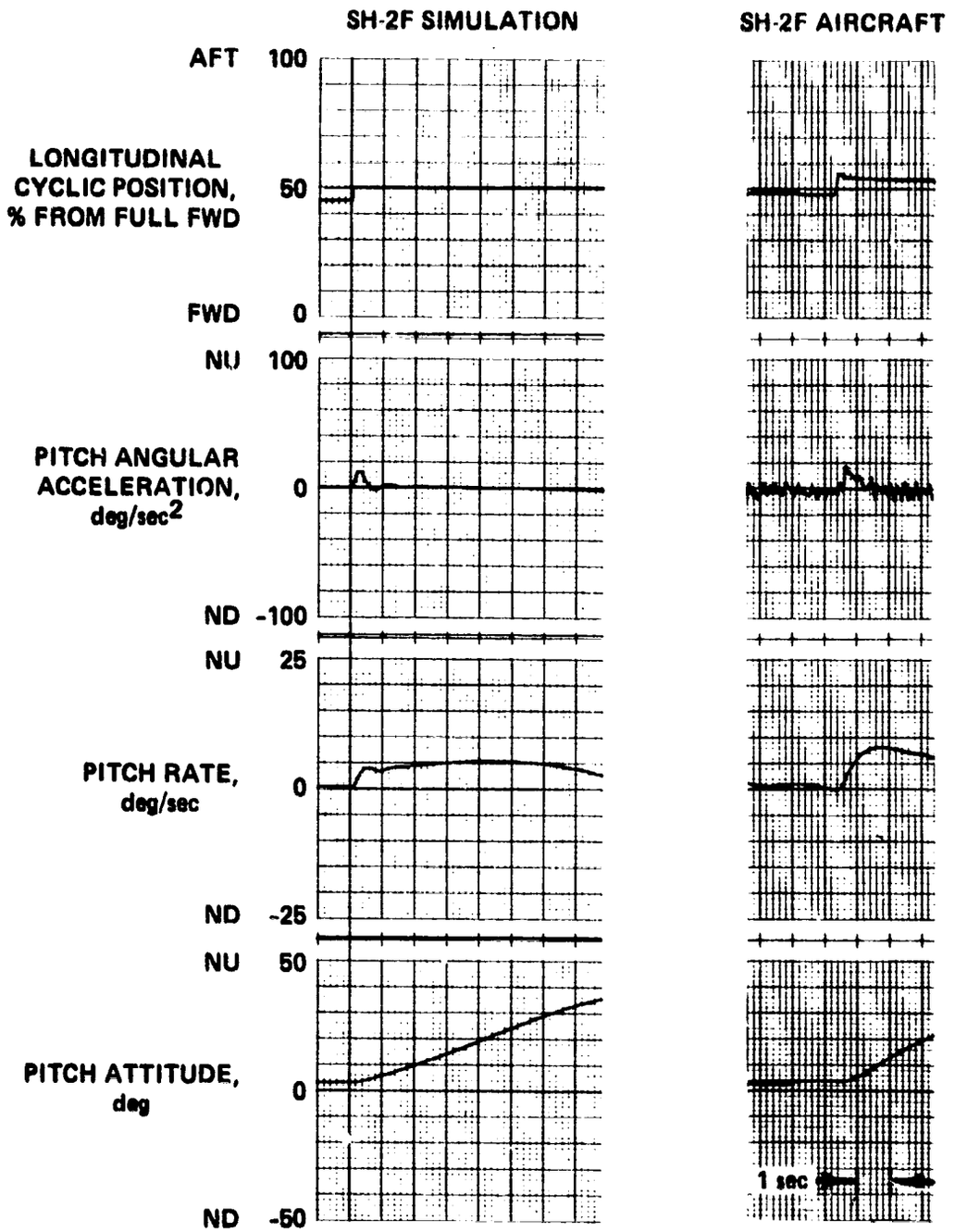

Figure 27.- Pitch axis control response, 70 knots, ASE off.

AIRSPEED = 5.1 m/sec (10 knots)
ASE = ON
ALTITUDE = 244 m

WEIGHT = 11,588 lb
CG STATION = 170.5
TEMPERATURE = 7°C

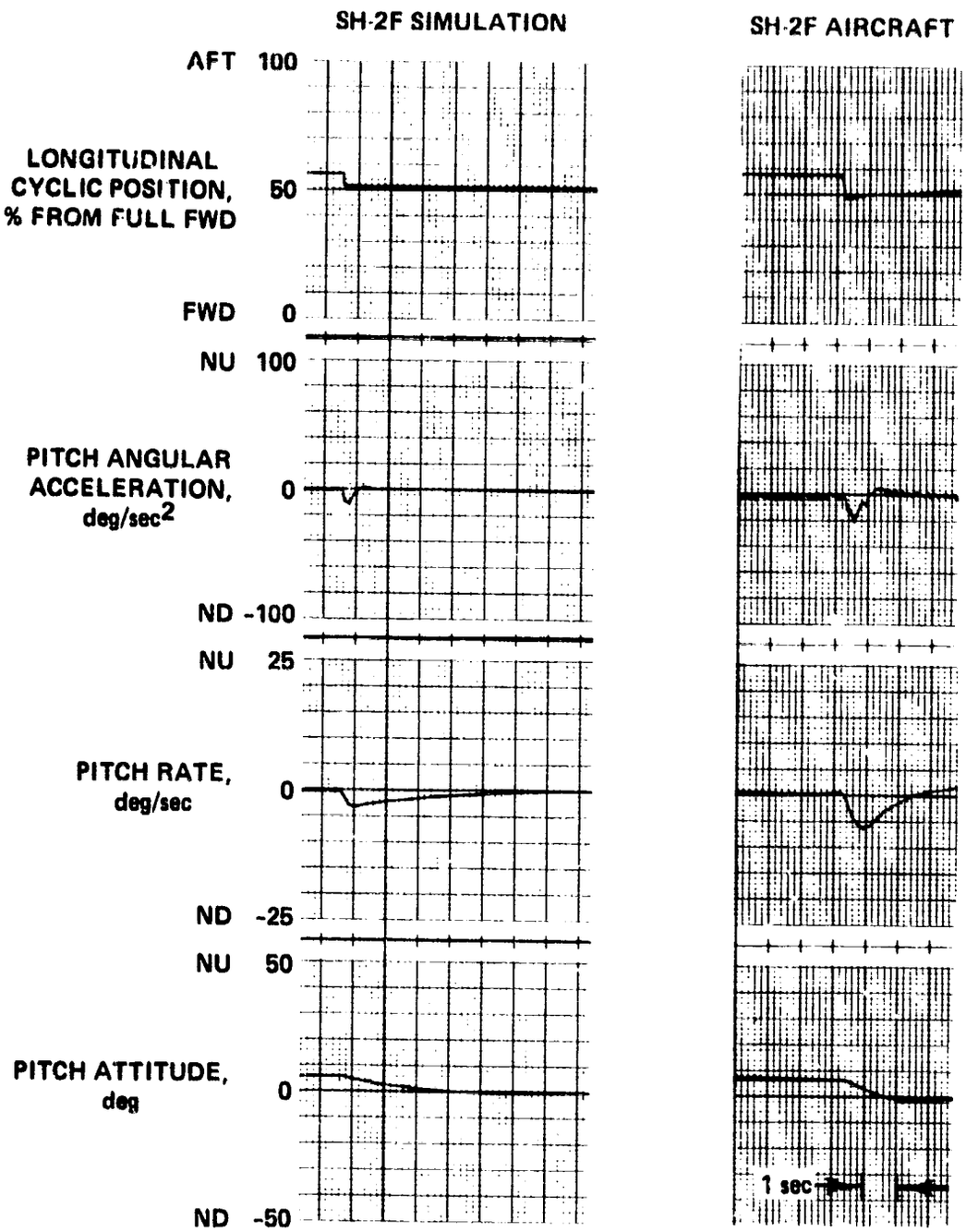

Figure 28.- Pitch axis control response, 10 knots, ASE on.

AIRSPEED = 36 m/sec (70 knots)
ASE = ON
ALTITUDE = 610 m

WEIGHT = 11,632 lb
CG STATION = 170.1
TEMPERATURE = 8°C

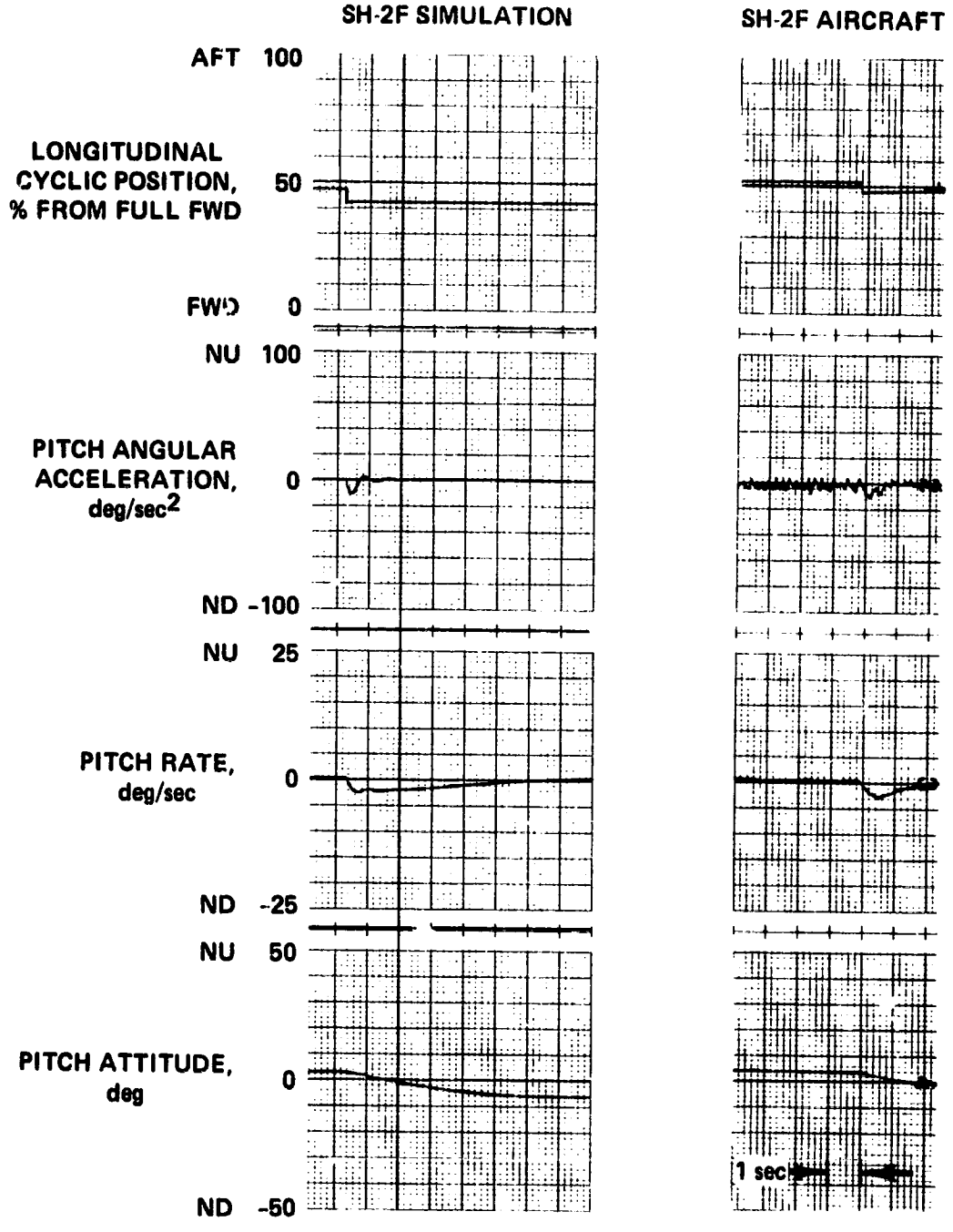

Figure 29.- Pitch axis control response, 70 knots, ASE on.

AIRSPEED = 5.1 m/sec (10 knots)
ASE = OFF
ALTITUDE = 244 m

WEIGHT = 10,721 lb
CG STATION = 170.1
TEMPERATURE = 8°C

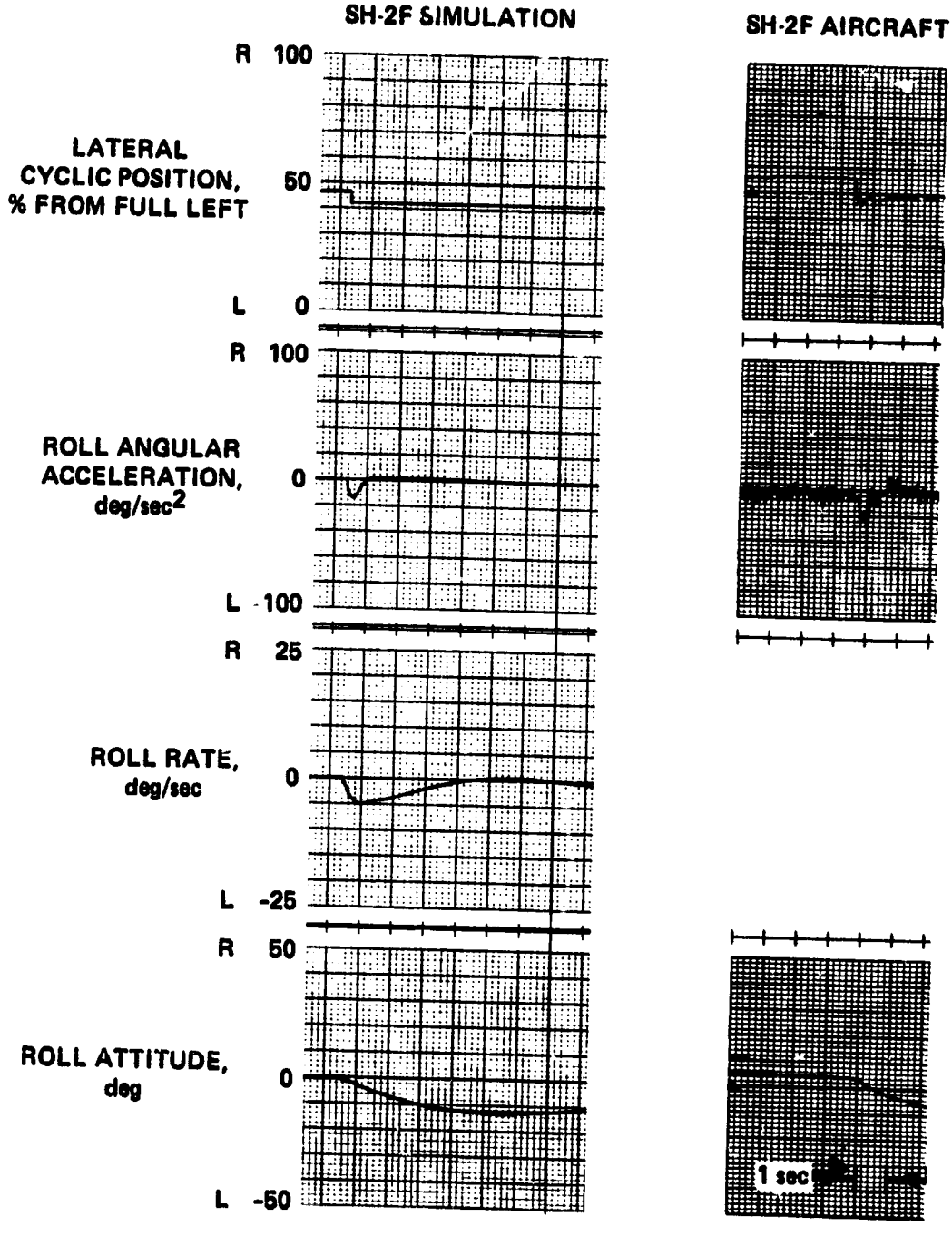

Figure 30.- Roll axis control response, 10 knots, ASE off.

AIRSPEED = 36 m/sec (70 knots)
ASE = OFF
ALTITUDE = 610 m

WEIGHT = 12,012 lb
CG STATION = 170.9
TEMPERATURE = 16°C

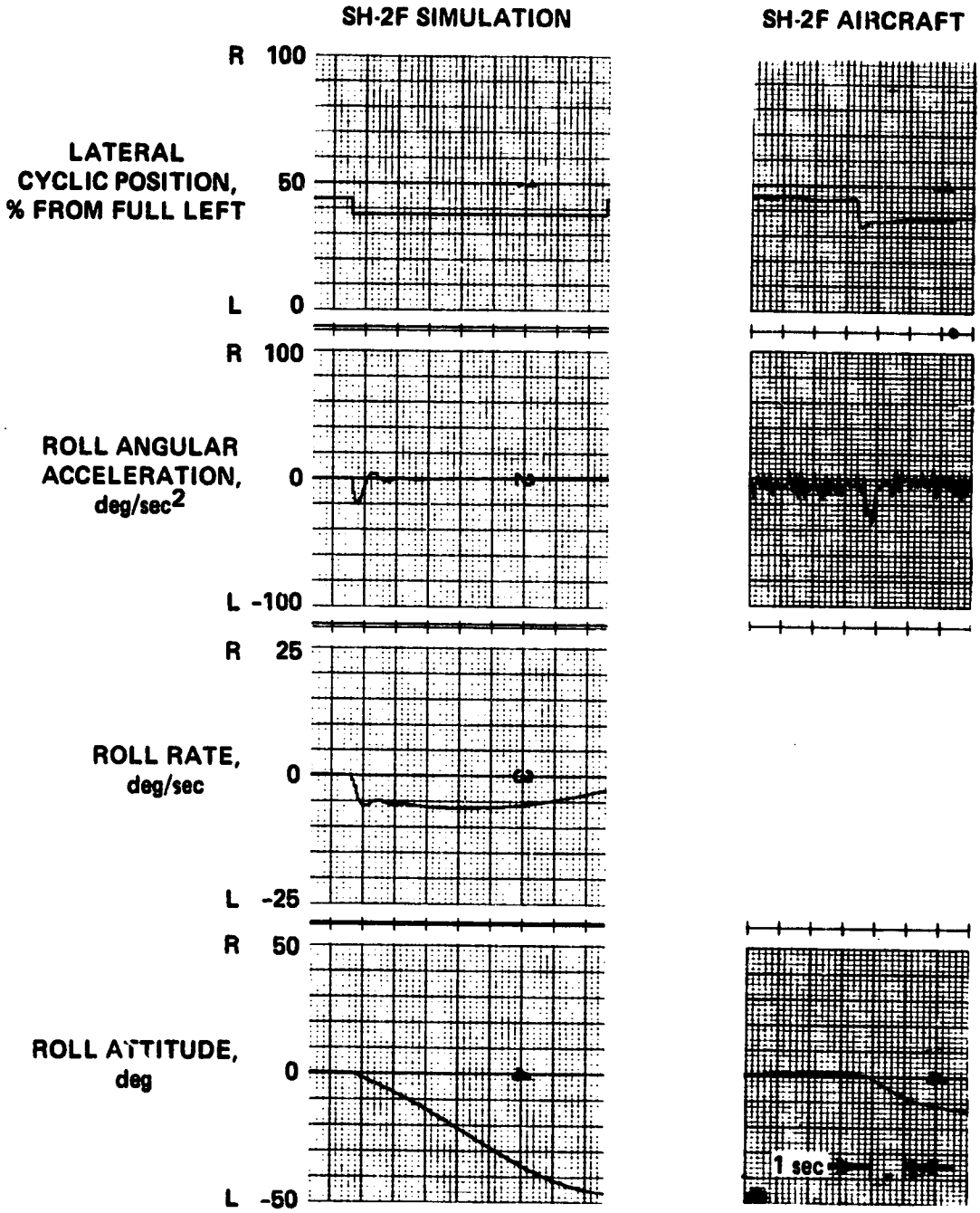

Figure 31.- Roll axis control response, 70 knots, ASE off.

AIRSPEED = 5.1 m/sec (10 knots)
ASE = ON
ALTITUDE = 244 m

WEIGHT = 11,471 lb
CG STATION = 170.4
TEMPERATURE = 7°C

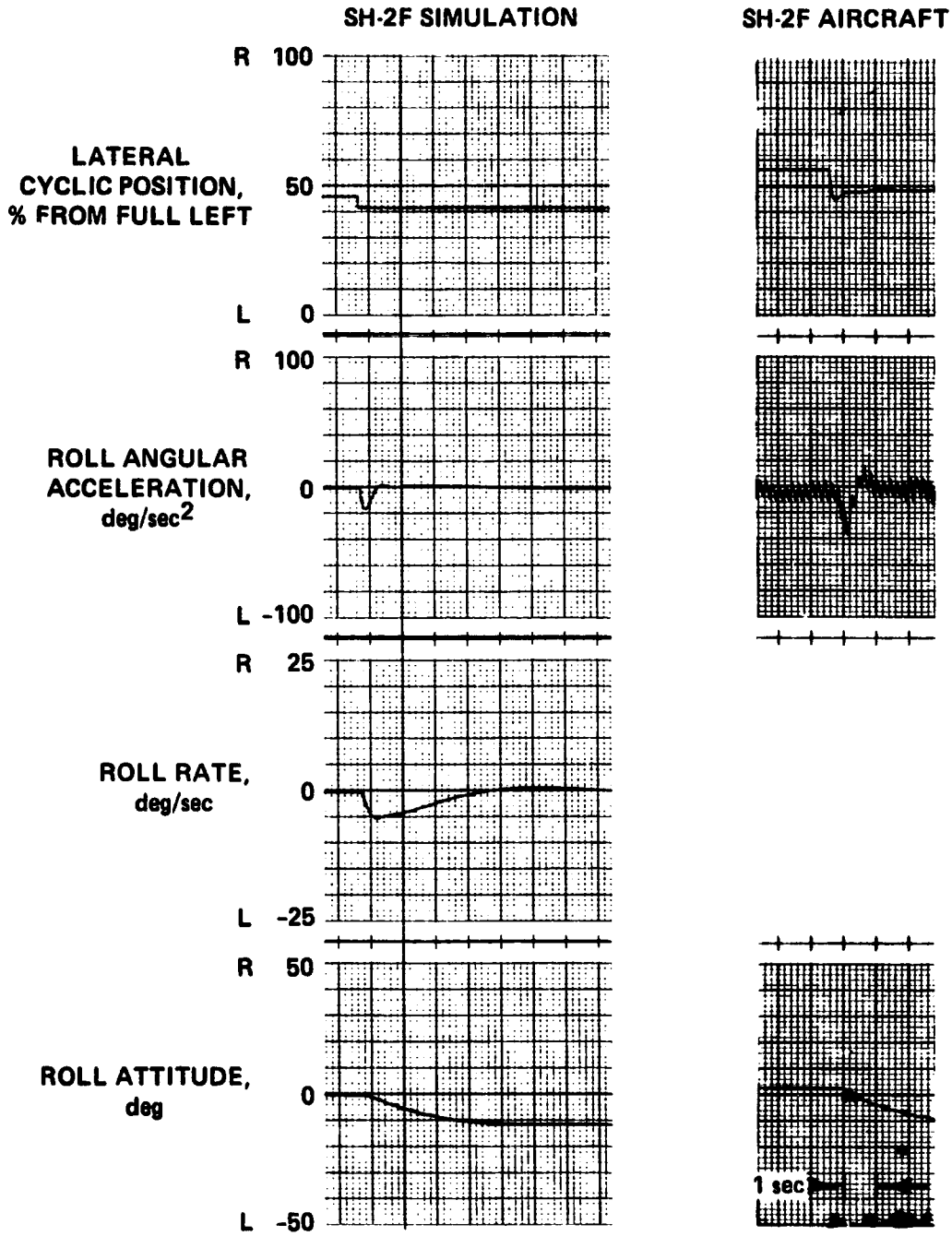

Figure 32.- Roll axis control response, 10 knots, ASE on.

AIRSPEED = 36 m/sec (70 knots)
ASE = ON
ALTITUDE = 610 m

WEIGHT = 11,320 lb
CG STATION = 170.2
TEMPERATURE = 10°C

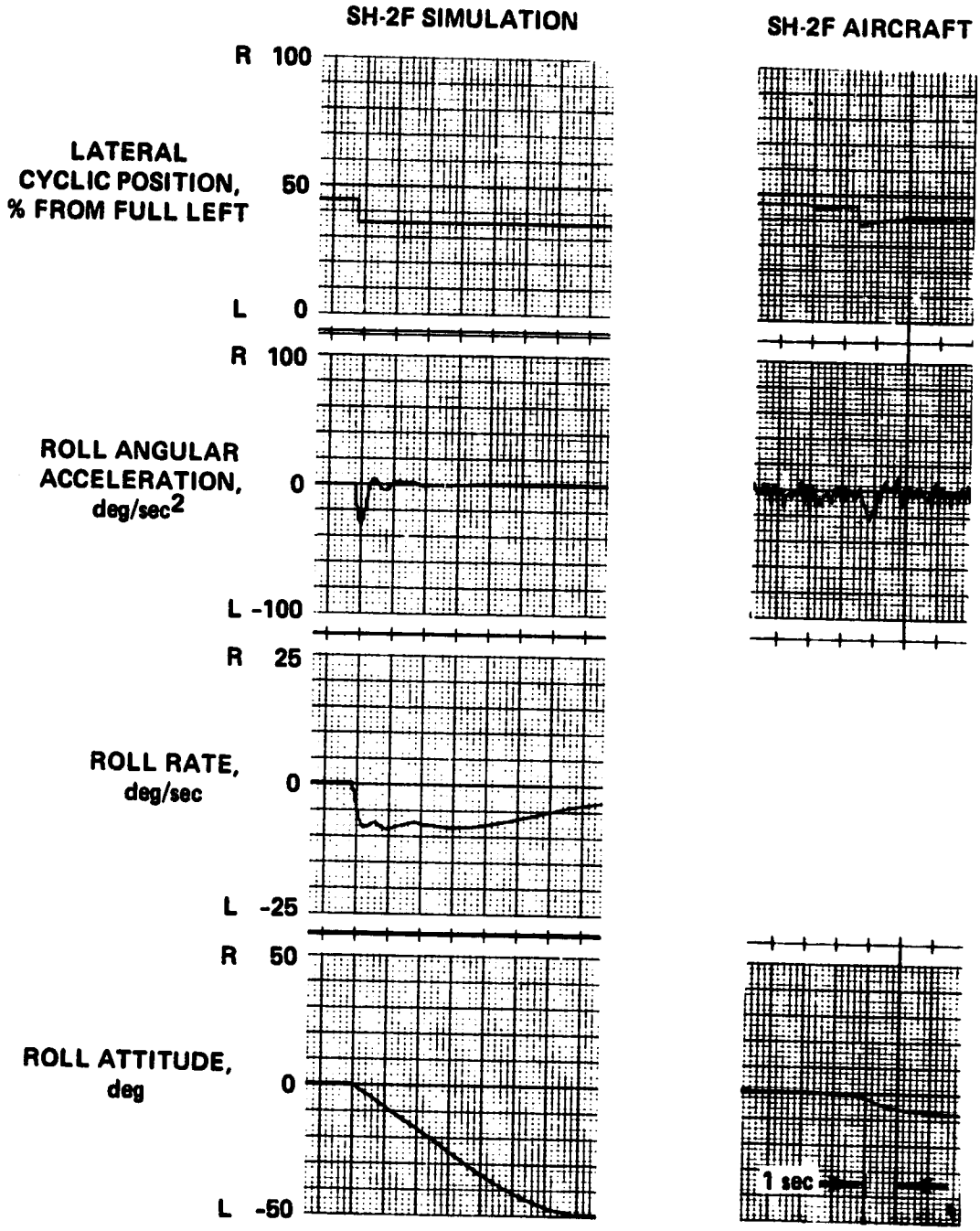

Figure 33.- Roll axis control response, 70 knots, ASE on.

AIRSPEED = 5.1 m/sec (10 knots)
ASE = OFF
ALTITUDE = 61 m

WEIGHT = 10,021 lb
CG STATION = 167.3
TEMPERATURE = 9°C

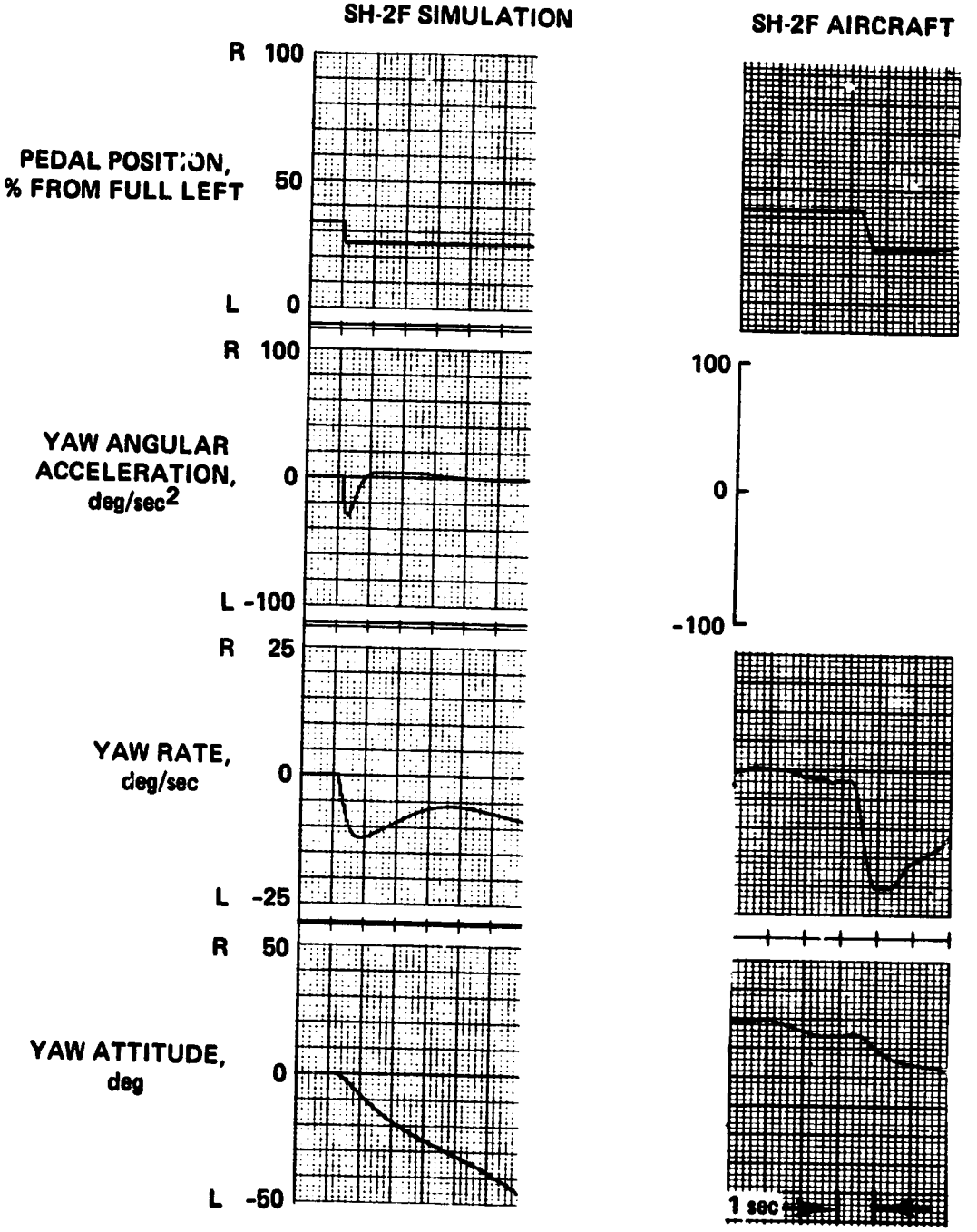

Figure 34.- Yaw axis control response, 10 knots, ASE off.

AIRSPEED = 36 m/sec (70 knots)
ASE = OFF
ALTITUDE = 610 m

WEIGHT = 11,852 lb
CG STATION = 170.4
TEMPERATURE = 14°C

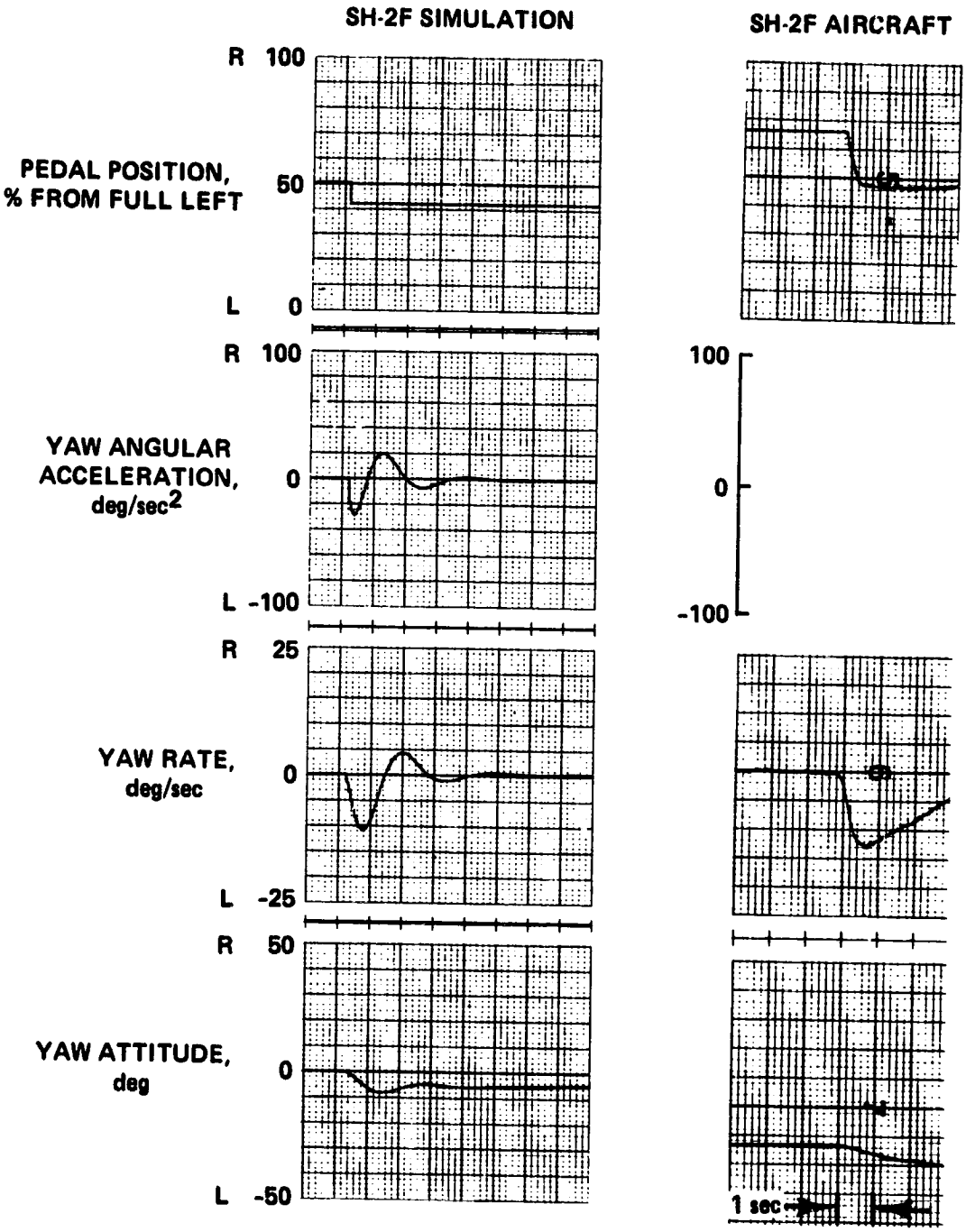

Figure 35.- Yaw axis control response, 70 knots, ASE off.

AIRSPEED = 5.1 m/sec (10 knots)
ASE = ON
ALTITUDE = 61 m

WEIGHT = 10,138 lb
CG STATION = 167.0
TEMPERATURE = 9°C

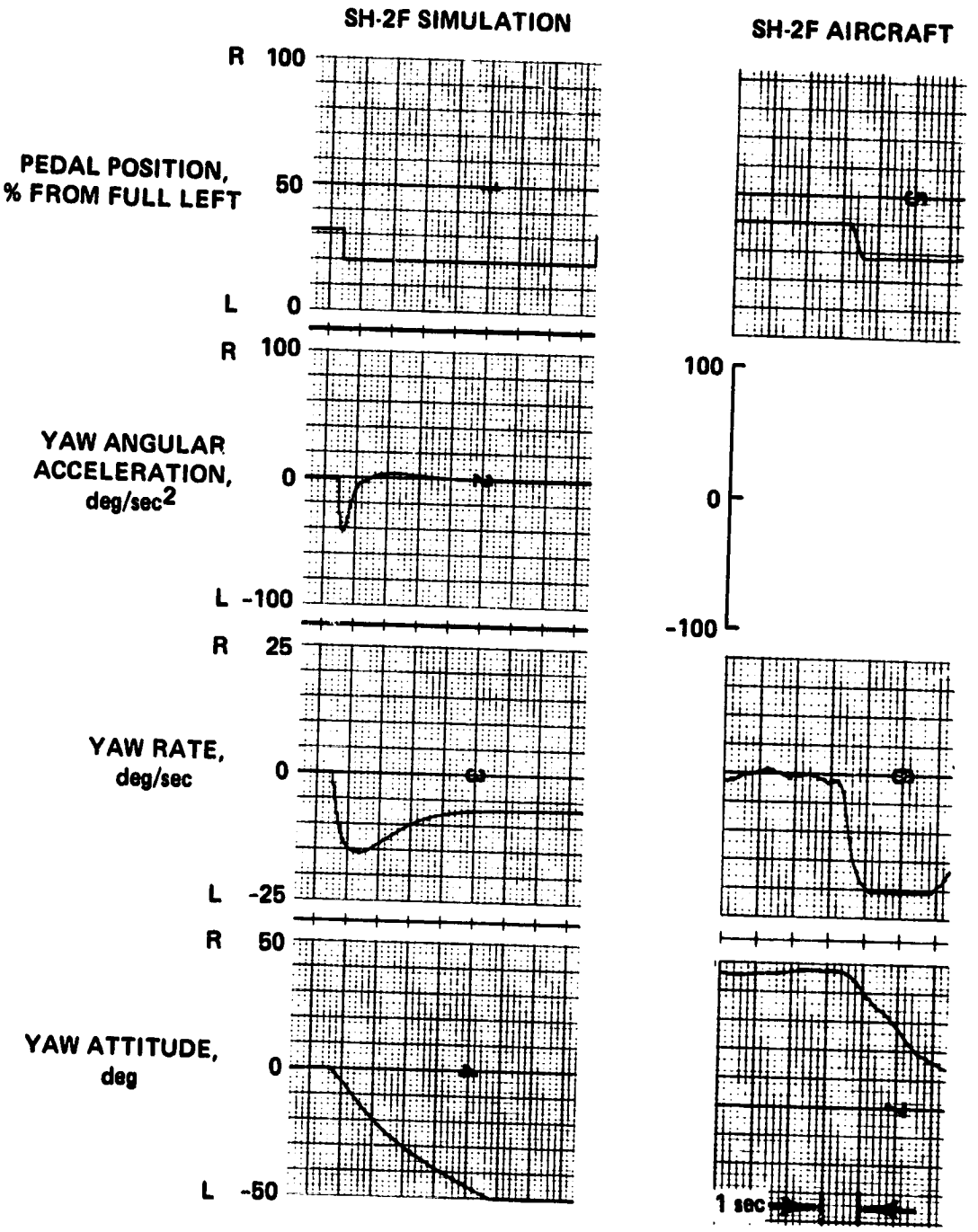

Figure 36.- Yaw axis control response, 10 knots, ASE on.

AIRSPEED = 36 m/sec (70 knots)
ASE = ON
ALTITUDE = 610 m

WEIGHT = 10,972 lb
CG STATION = 170.1
TEMPERATURE = 10°C

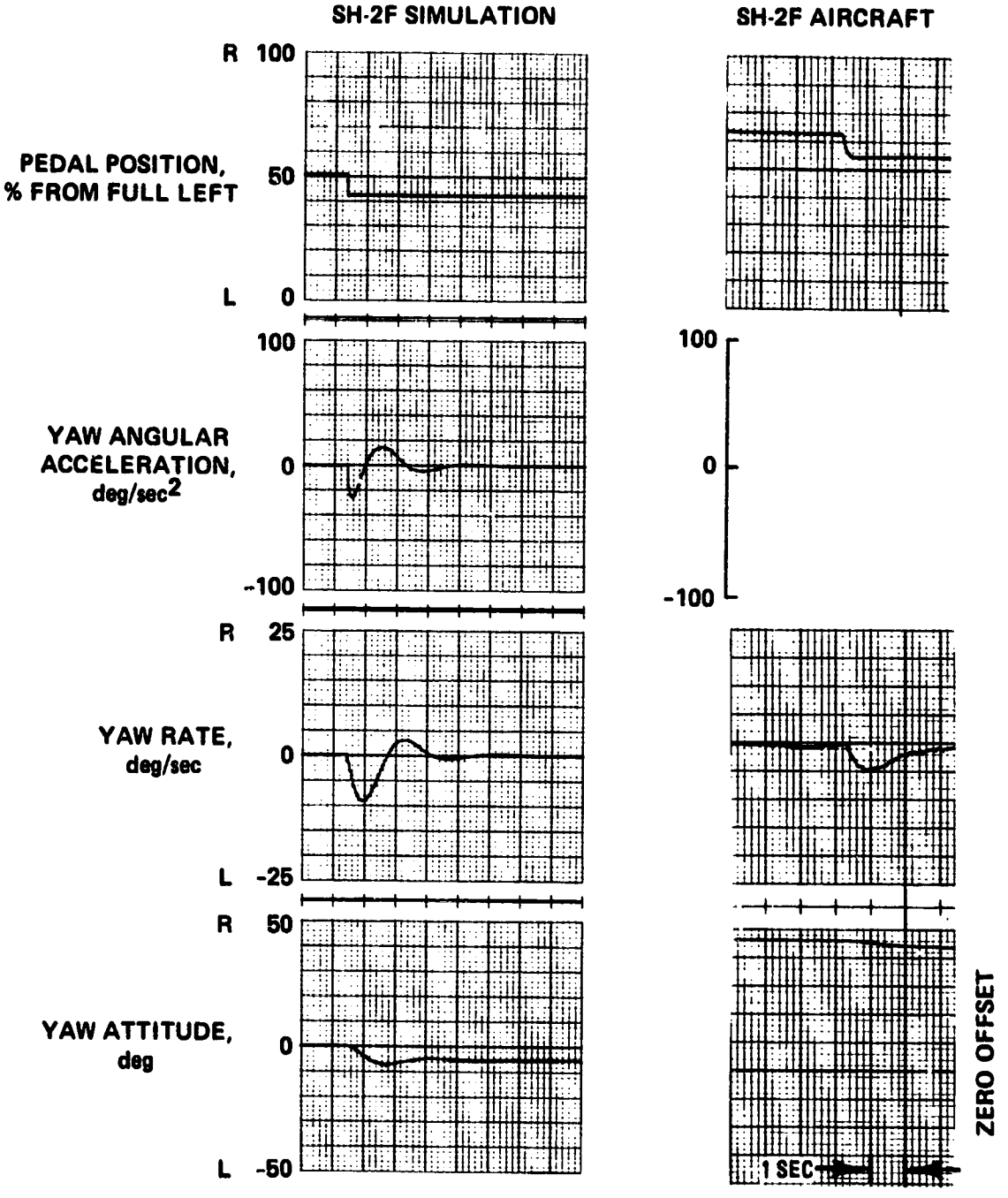

Figure 37.- Yaw axis control response, 70 knots, ASE on.

AIRSPEED = 5.1 m/sec (10 knots)
ASE = OFF
ALTITUDE = 610 m

WEIGHT = 12,120 lb
CG STATION = 170.1
TEMPERATURE = 10°C

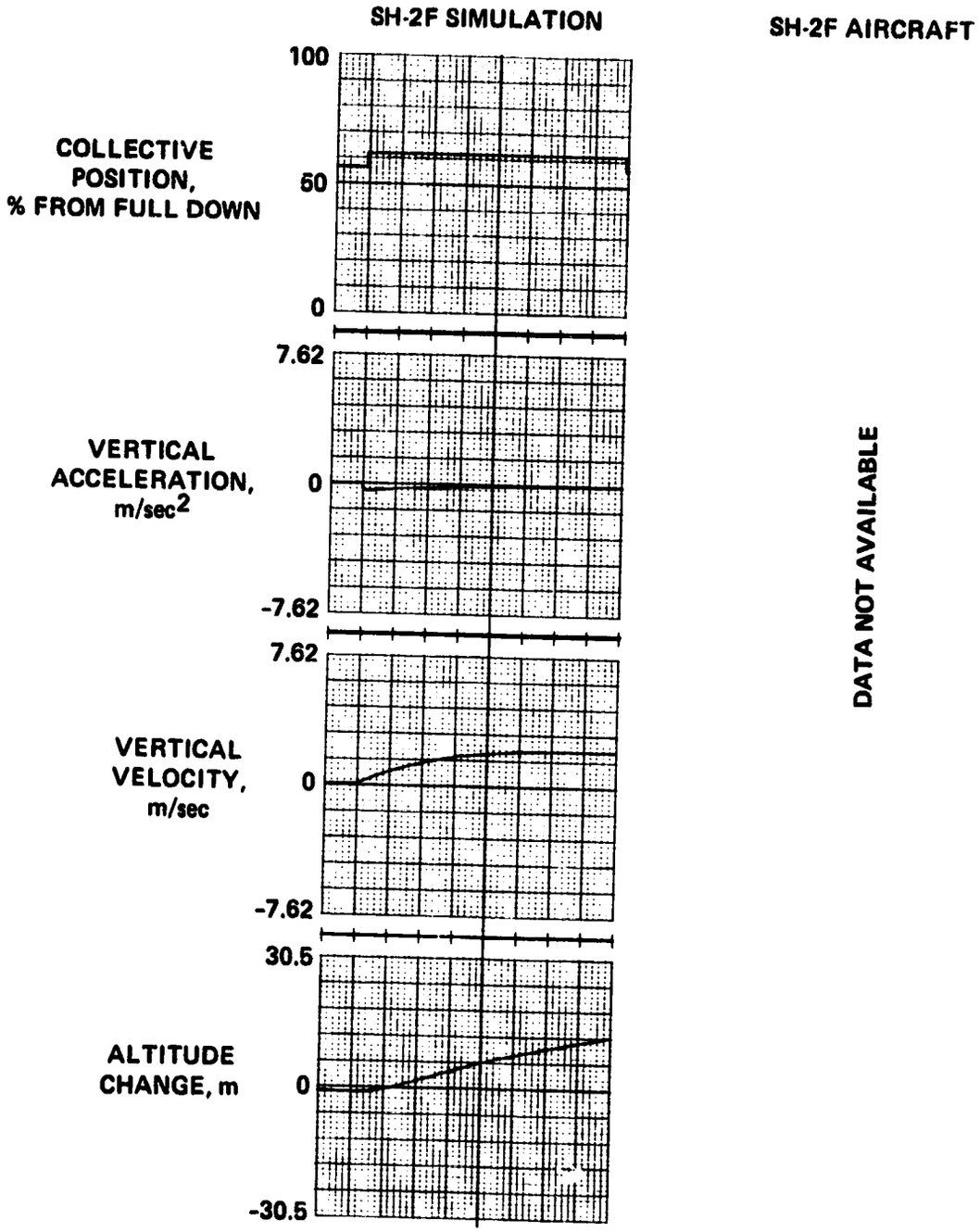

Figure 38.- Height axis control response, 10 knots, ASE off.

AIRSPEED = 36 m/sec (70 knots)
ASE = OFF
ALTITUDE = 610 m

WEIGHT = 12,120 lb
CG STATION = 170.1
TEMPERATURE = 10°C

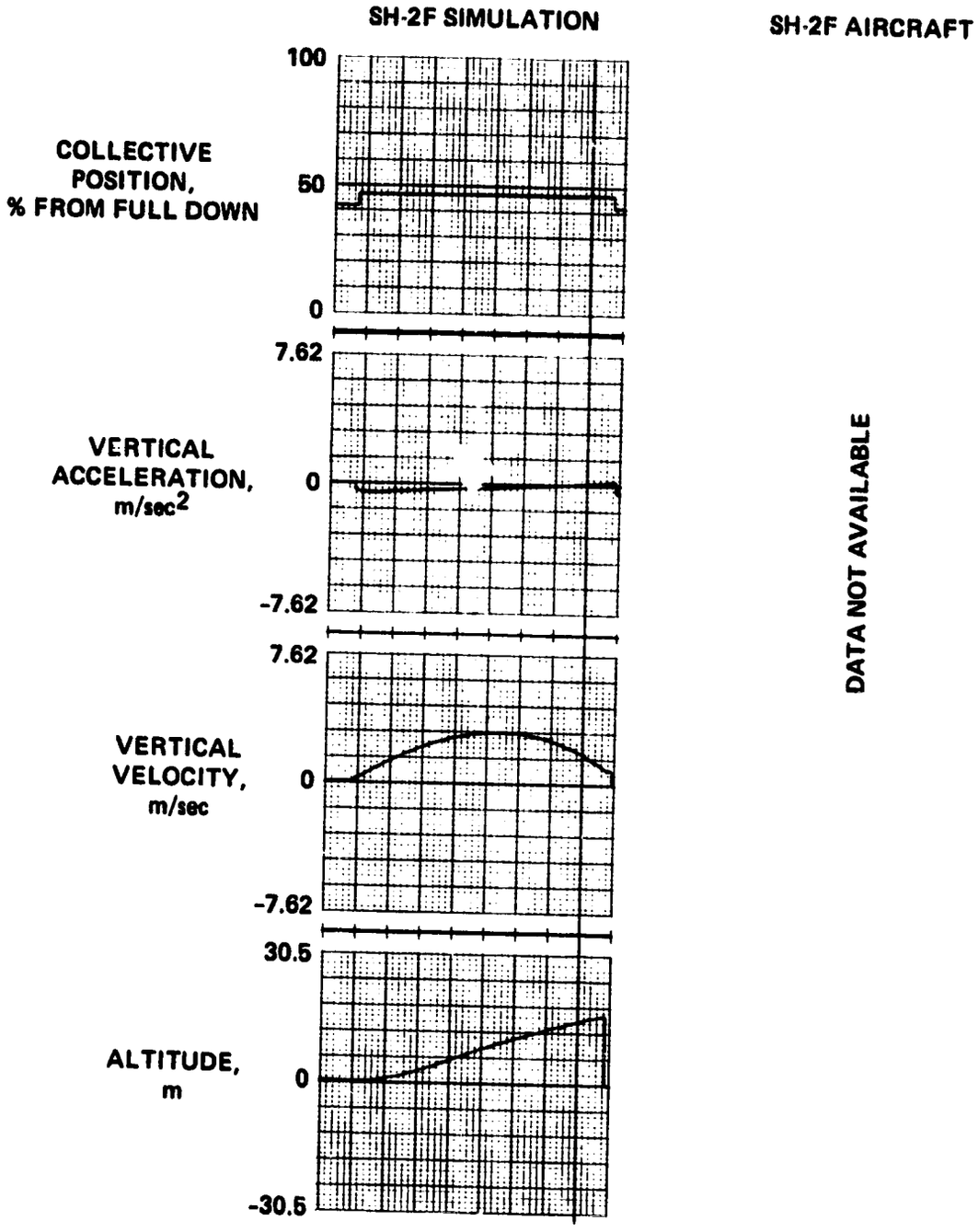

Figure 39.- Height axis control response, 70 knots, ASE off.

AIRSPEED = 5.1 m/sec (10 knots)
ASE = ON
ALTITUDE = 610 m

WEIGHT = 12,120 lb
CG STATION = 170.1
TEMPERATURE = 10°C

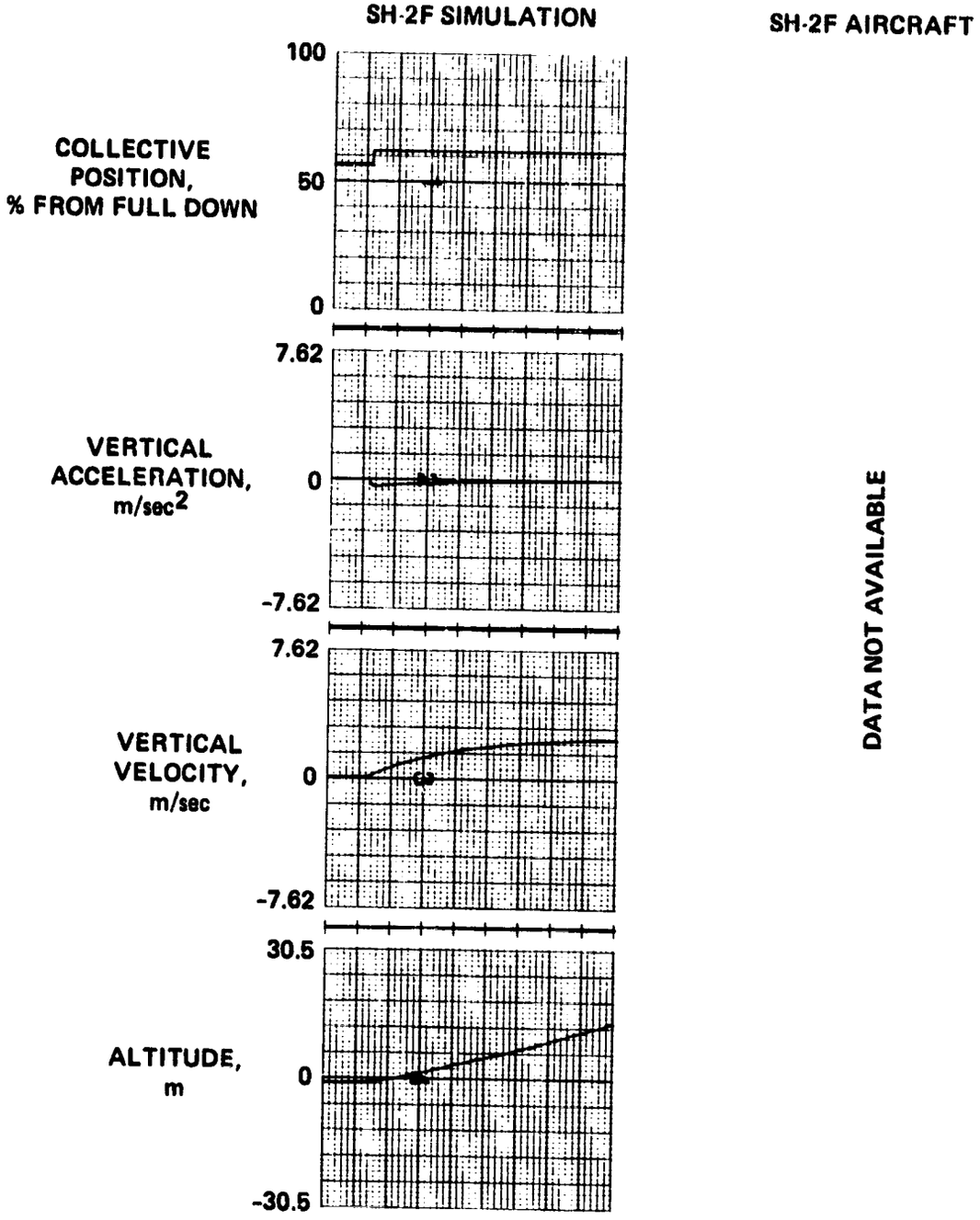

Figure 40.- Height axis control response, 10 knots, ASE on.

AIRSPEED = 36 m/sec (70 knots)
ASE = ON
ALTITUDE = 610 m

WEIGHT = 12,120 lb
CG STATION = 171.0
TEMPERATURE = 7°C

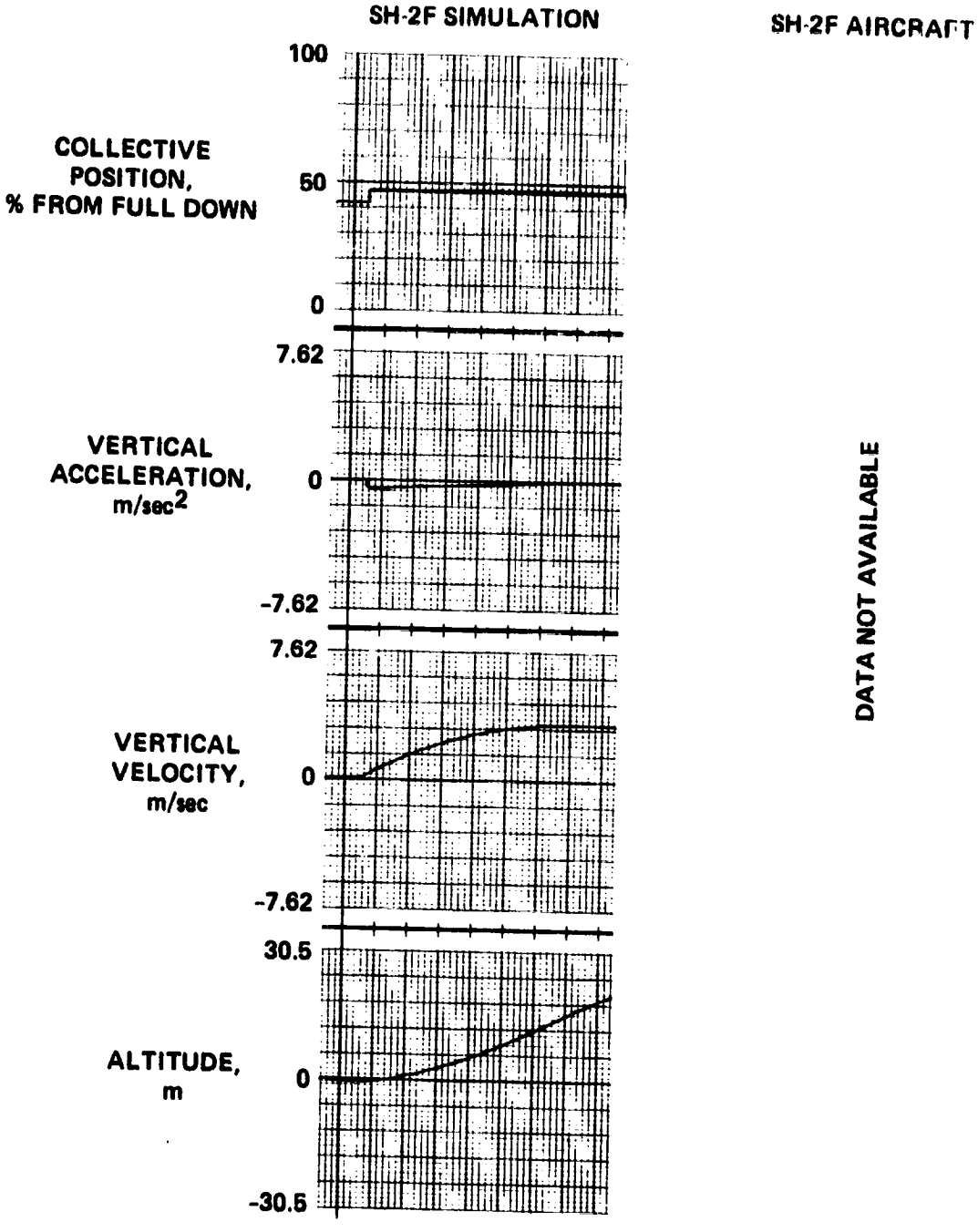

Figure 41.- Height axis control response, 70 knots, ASE on.

AIRSPEED = 5.1 m/sec (10 knots)
ASE = OFF
ALTITUDE = 305 m

WEIGHT = 10,562 lb
CG STATION = 167.3
TEMPERATURE = 19°C

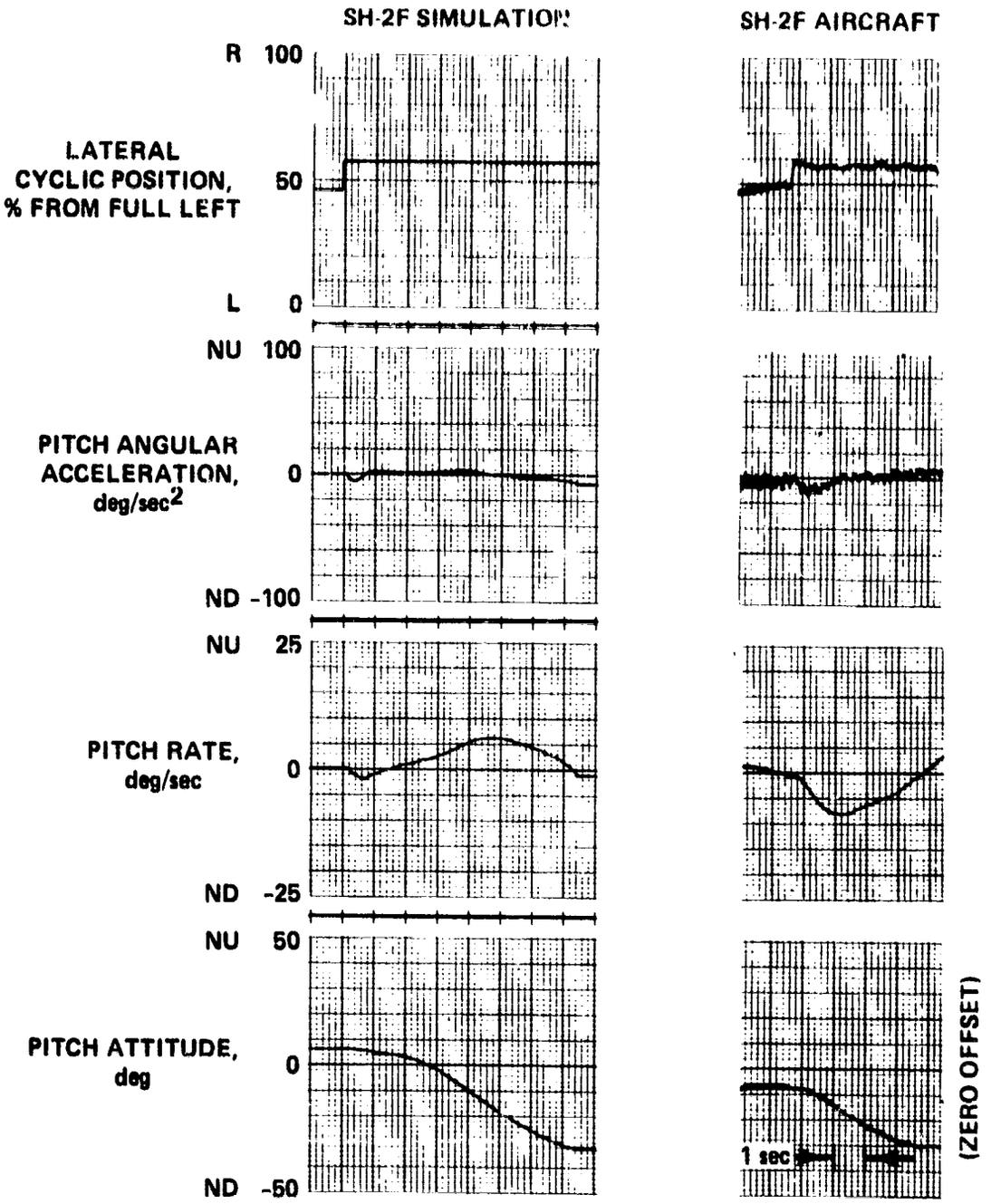

Figure 42.- Pitch due to roll coupling, 10 knots, ASE off.

AIRSPEED = 36 m/sec (70 knots)
ASE = OFF
ALTITUDE = 610 m

WEIGHT = 11,932 lb
CG STATION = 170.6
TEMPERATURE = 14°C

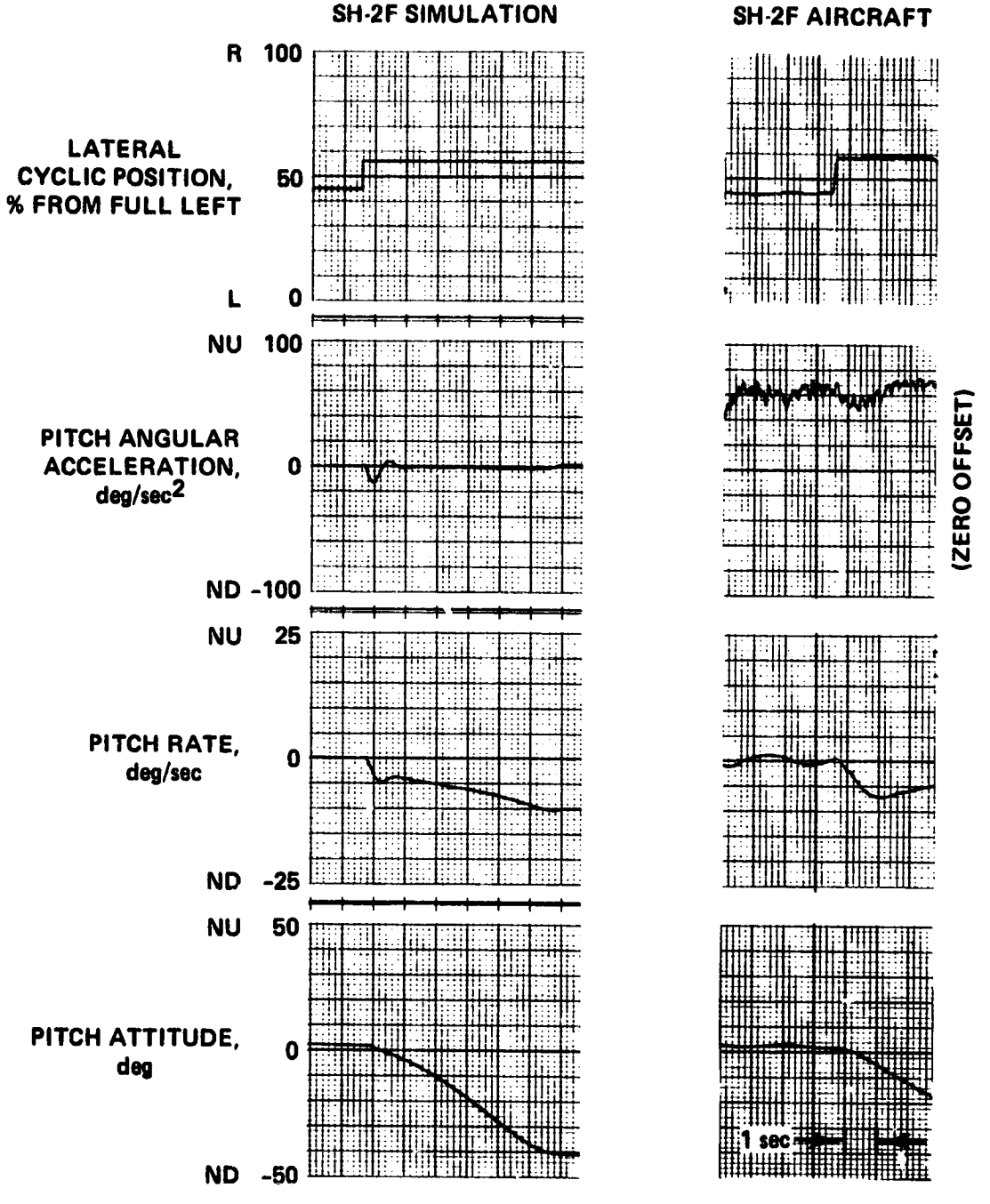

Figure 43.- Pitch due to a '1 coupling, 70 knots, ASE off.

AIRSPEED = 5.1 m/sec (10 knots)
ASE = ON
ALTITUDE = 305 m

WEIGHT = 10,792 lb
CG STATION = 167.6
TEMPERATURE = 19°C

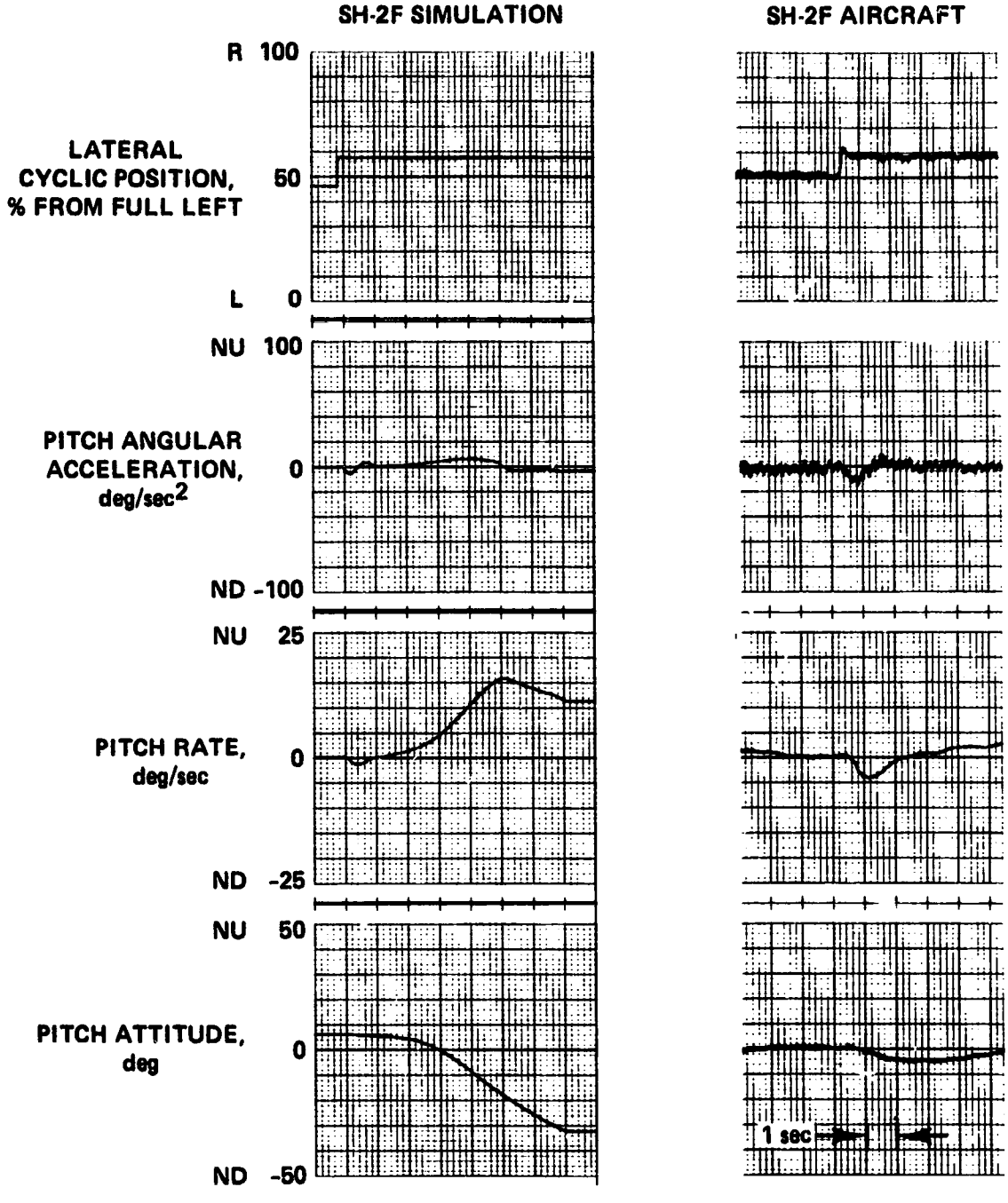

Figure 44.- Pitch due to roll coupling, 10 knots, ASE on.

AIRSPEED = 36 m/sec (70 knots)
ASE = ON
ALTITUDE = 610 m

WEIGHT = 11,222 lb
CG STATION = 170.1
TEMPERATURE = 10°C

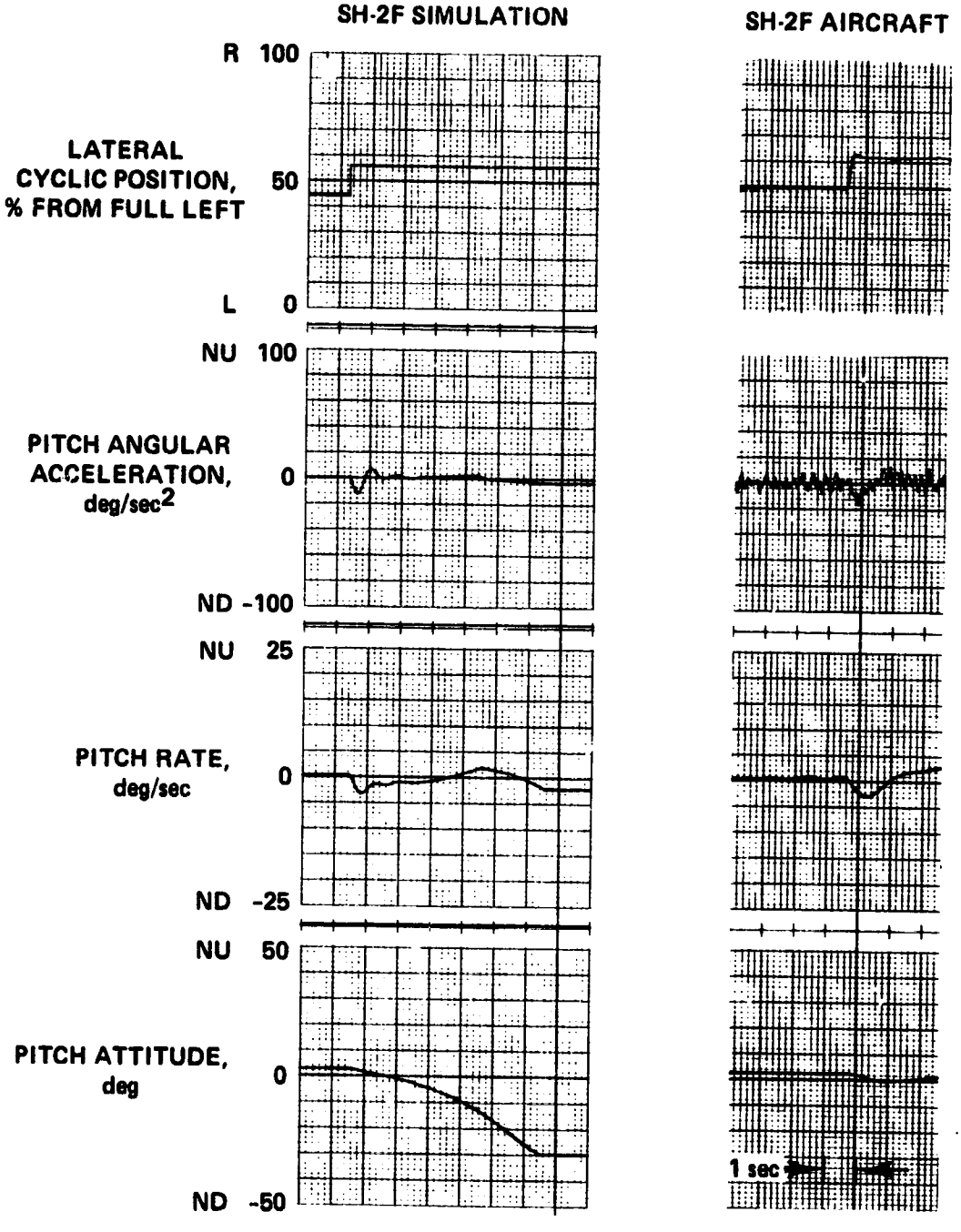

Figure 45.- Pitch due to roll coupling, 70 knots, ASE on.

AIRSPEED = 5.1 m/sec (10 knots)
ASE = OFF
ALTITUDE = 244 m

WEIGHT = 10,871 lb
CG STATION = 169.7
TEMPERATURE = 8°C

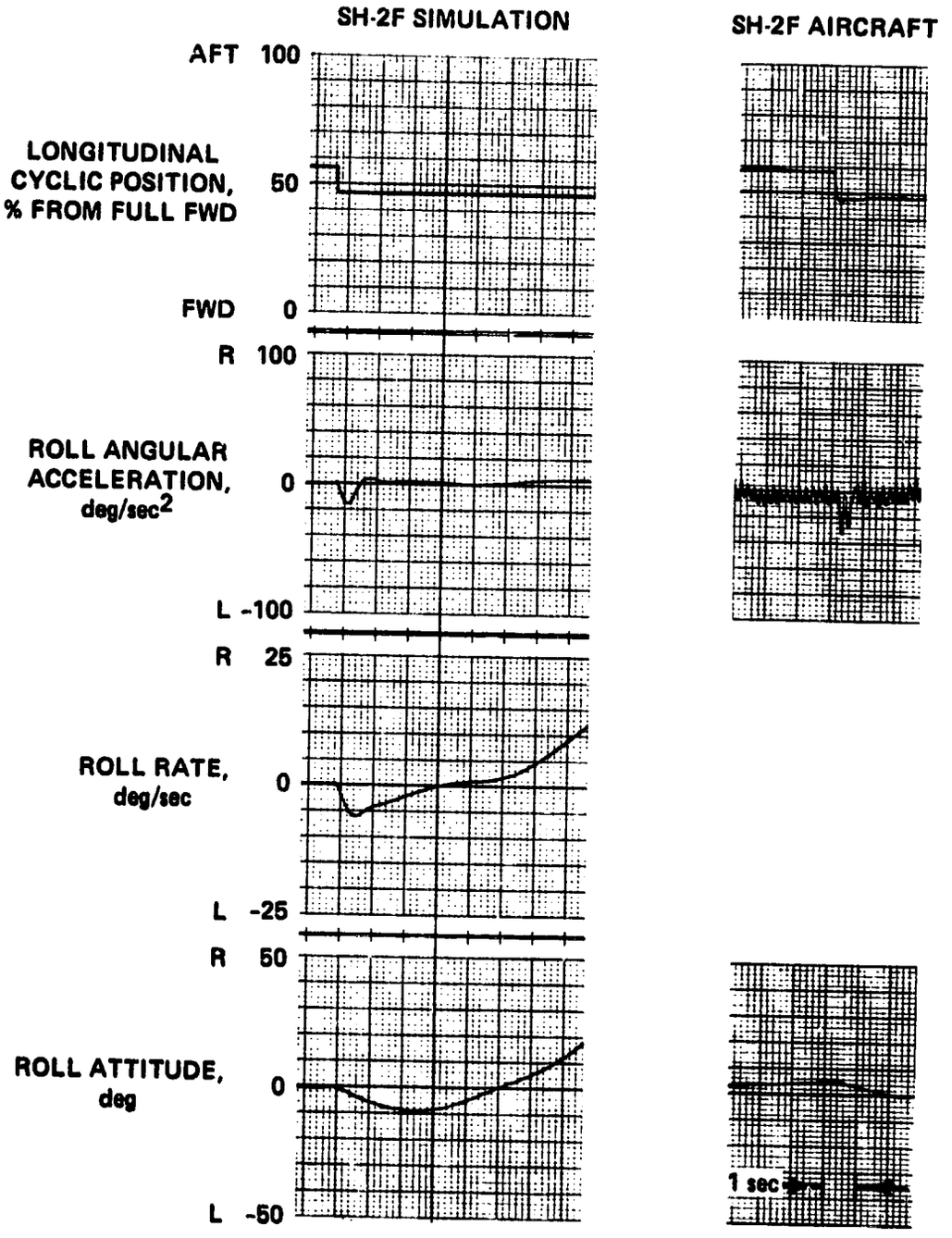

Figure 46.- Roll due to pitch coupling, 10 knots, ASE off.

AIRSPEED = 36 m/sec (70 knots)
ASE = OFF
ALTITUDE = 610 m

WEIGHT = 12,032 lb
CG STATION = 170.9
TEMPERATURE = 16°C

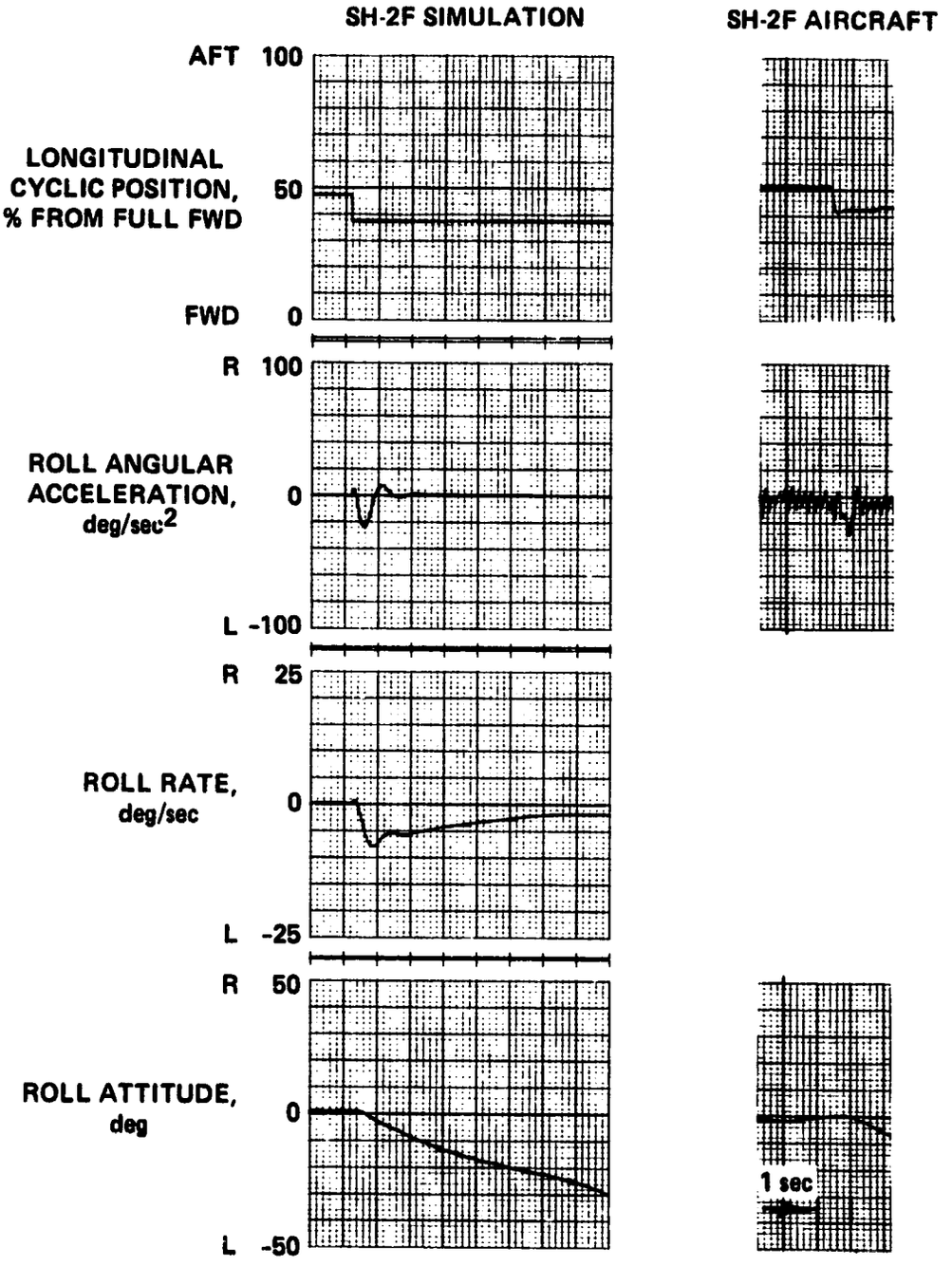

Figure 47.- Roll due to pitch coupling, 70 knots, ASE off.

AIRSPEED = 5.1 m/sec (10 knots)
ASE = ON
ALTITUDE = 244 m

WEIGHT = 11,521 lb
CG STATION = 170.4
TEMPERATURE = 7°C

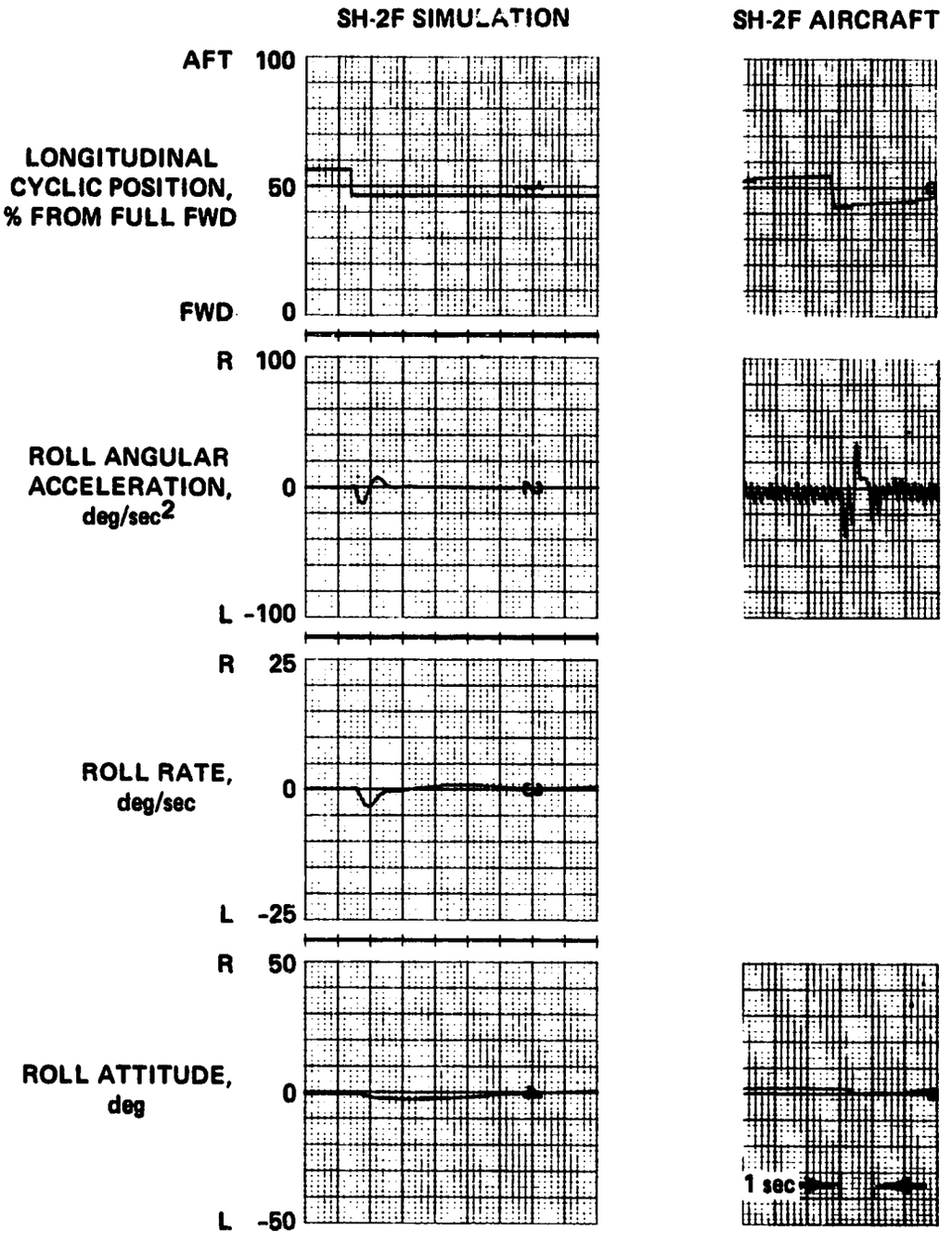

Figure 48.- Roll due to pitch coupling, 10 knots, ASE on.

AIRSPEED = 36 m/sec (70 knots)
ASE = ON
ALTITUDE = 610 m

WEIGHT = 11,540 lb
CG STATION = 170.4
TEMPERATURE = 10°C

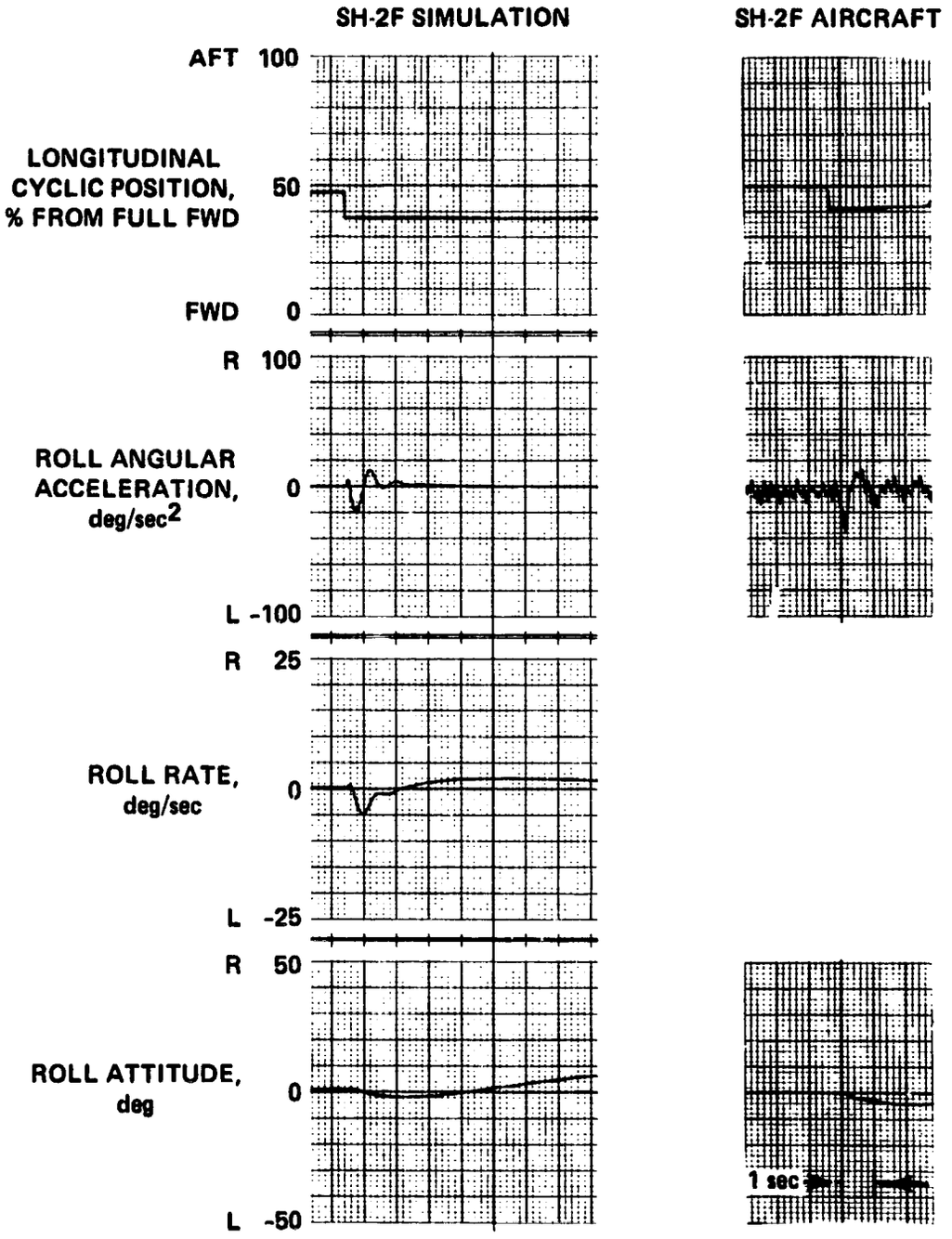

Figure 49.- Roll due to pitch coupling, 70 knots, ASE on.

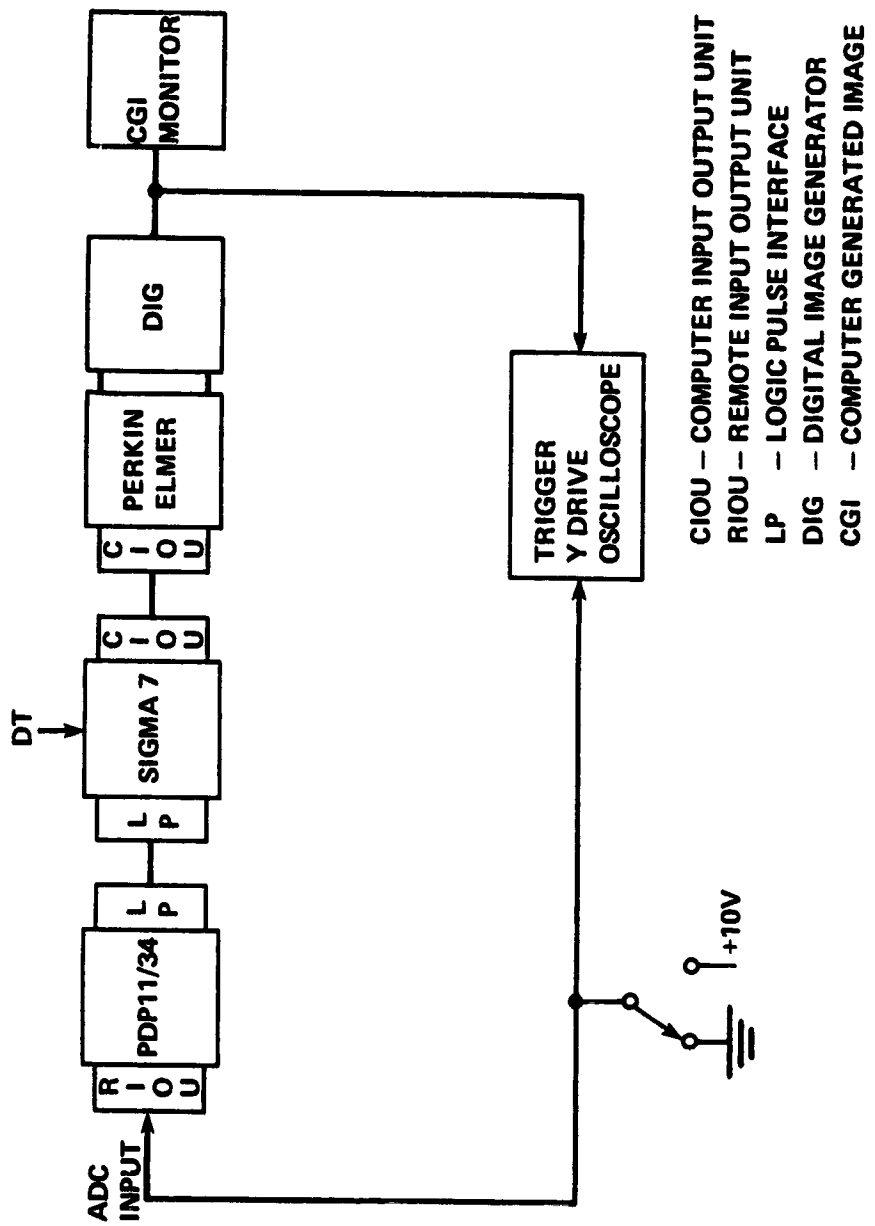

Figure 50.- Visual system time delay measurement test setup.

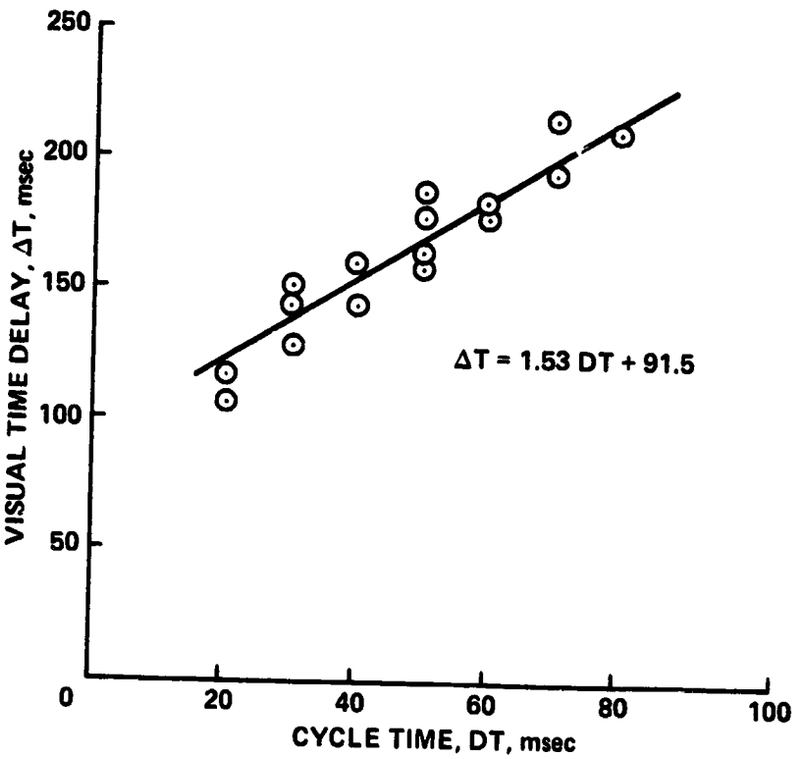

Figure 51.- Effect of cycle time on visual system time delay.

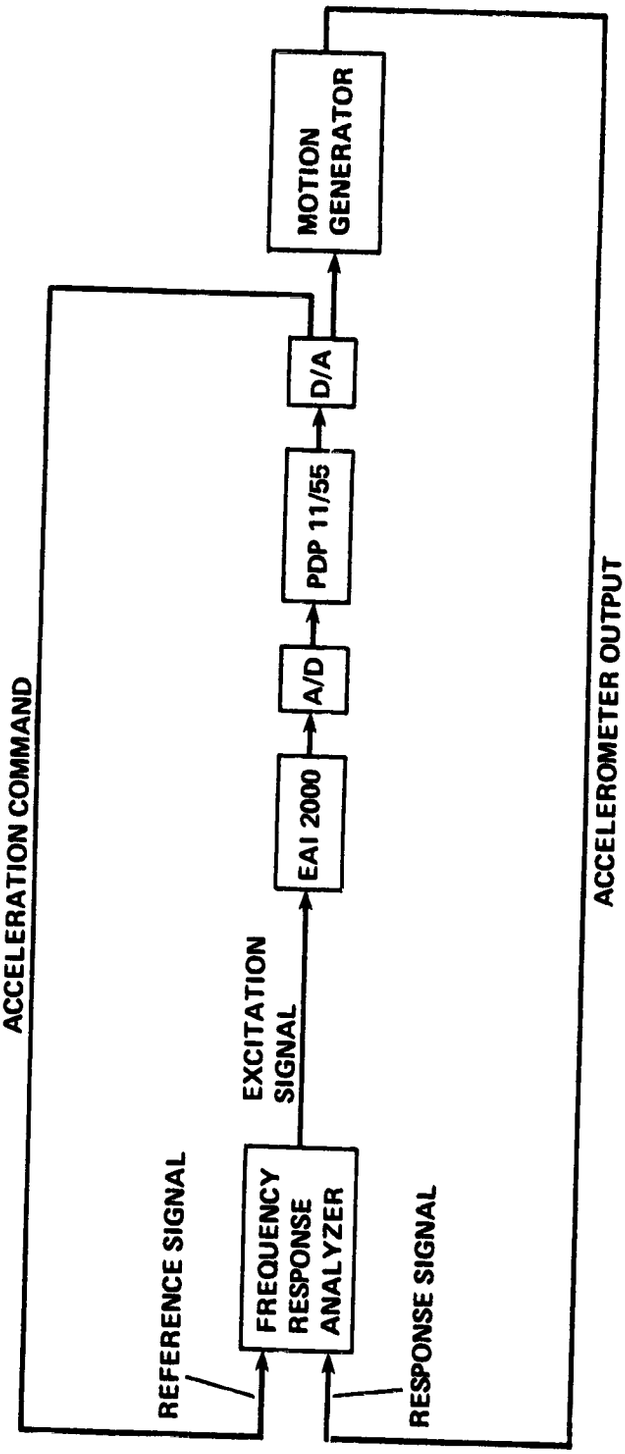

Figure 52.- Motion system frequency response test setup.

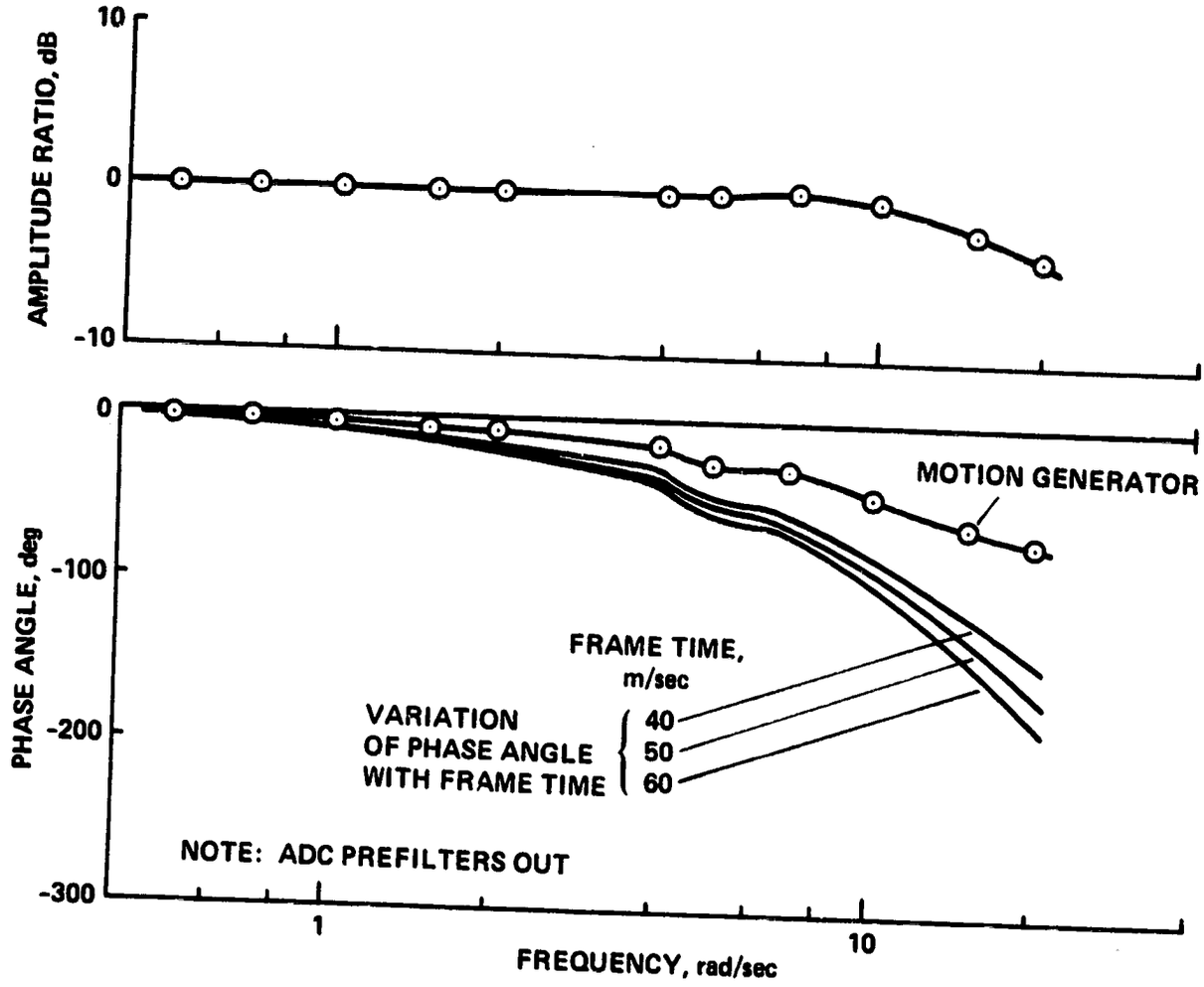

Figure 53.- VMS motion system, roll acceleration frequency response.

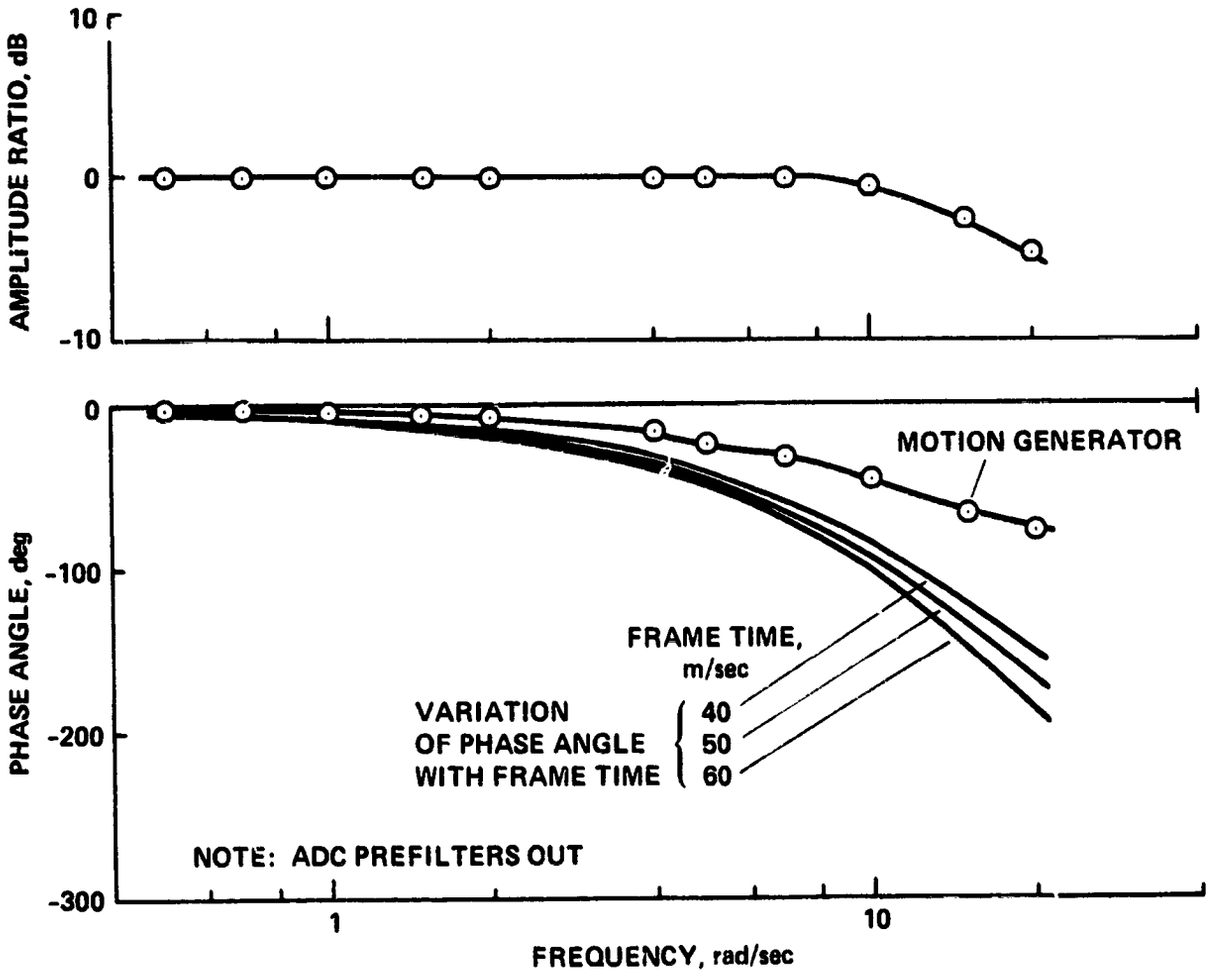

Figure 54.- VMS motion system, pitch acceleration frequency response.

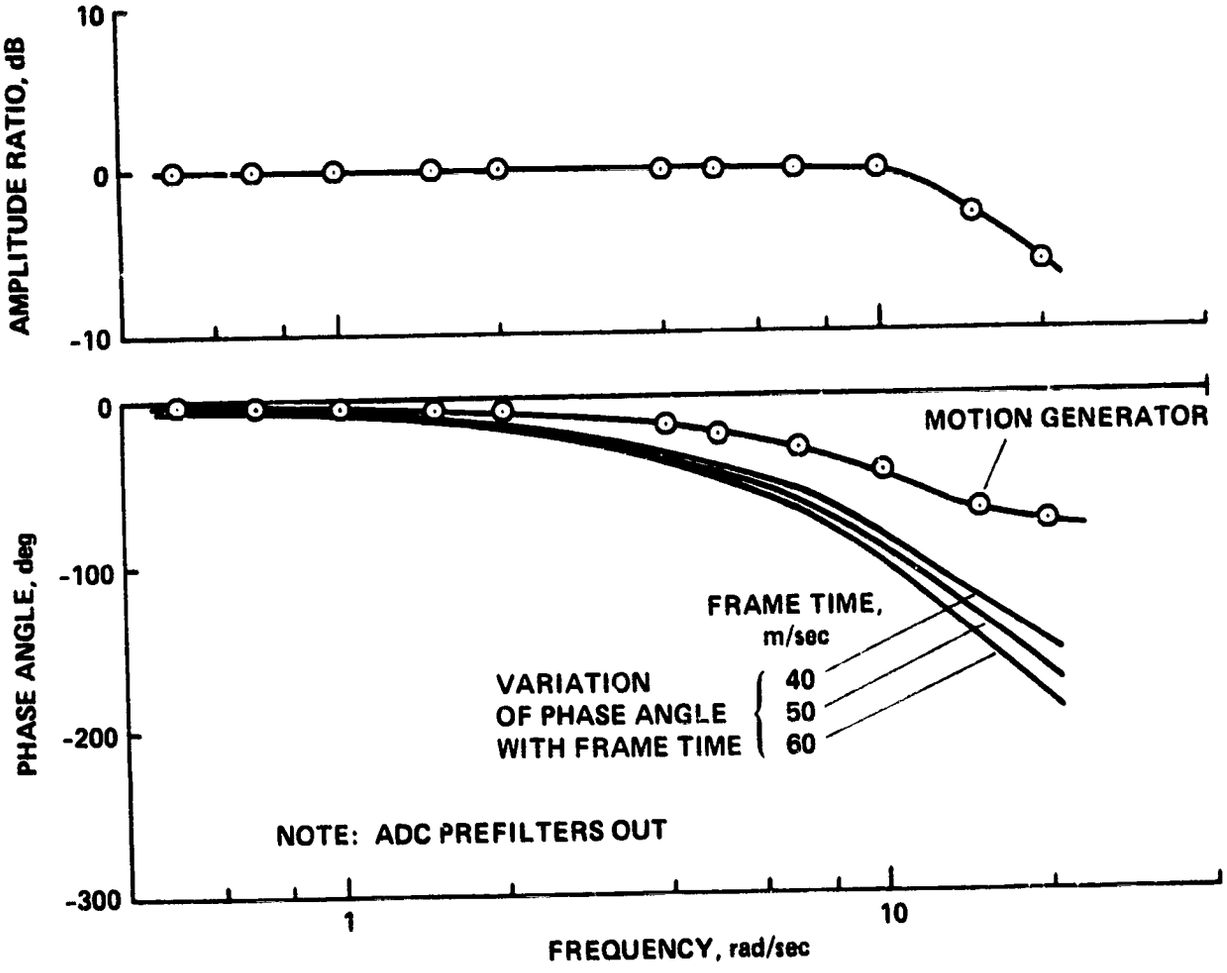

Figure 55.- VMS motion system, yaw acceleration frequency response.

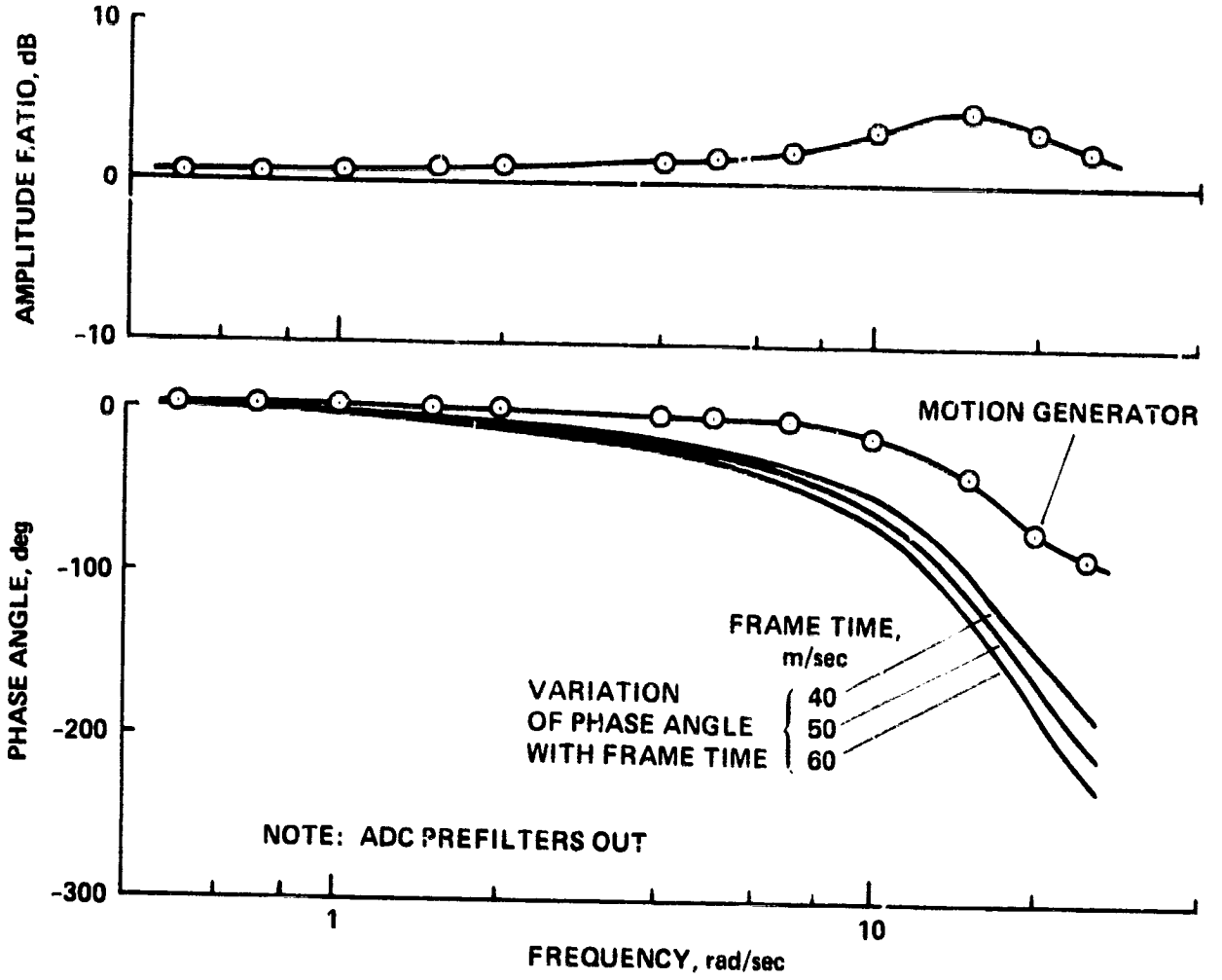

Figure 56.- VMS motion system, lateral acceleration frequency response.

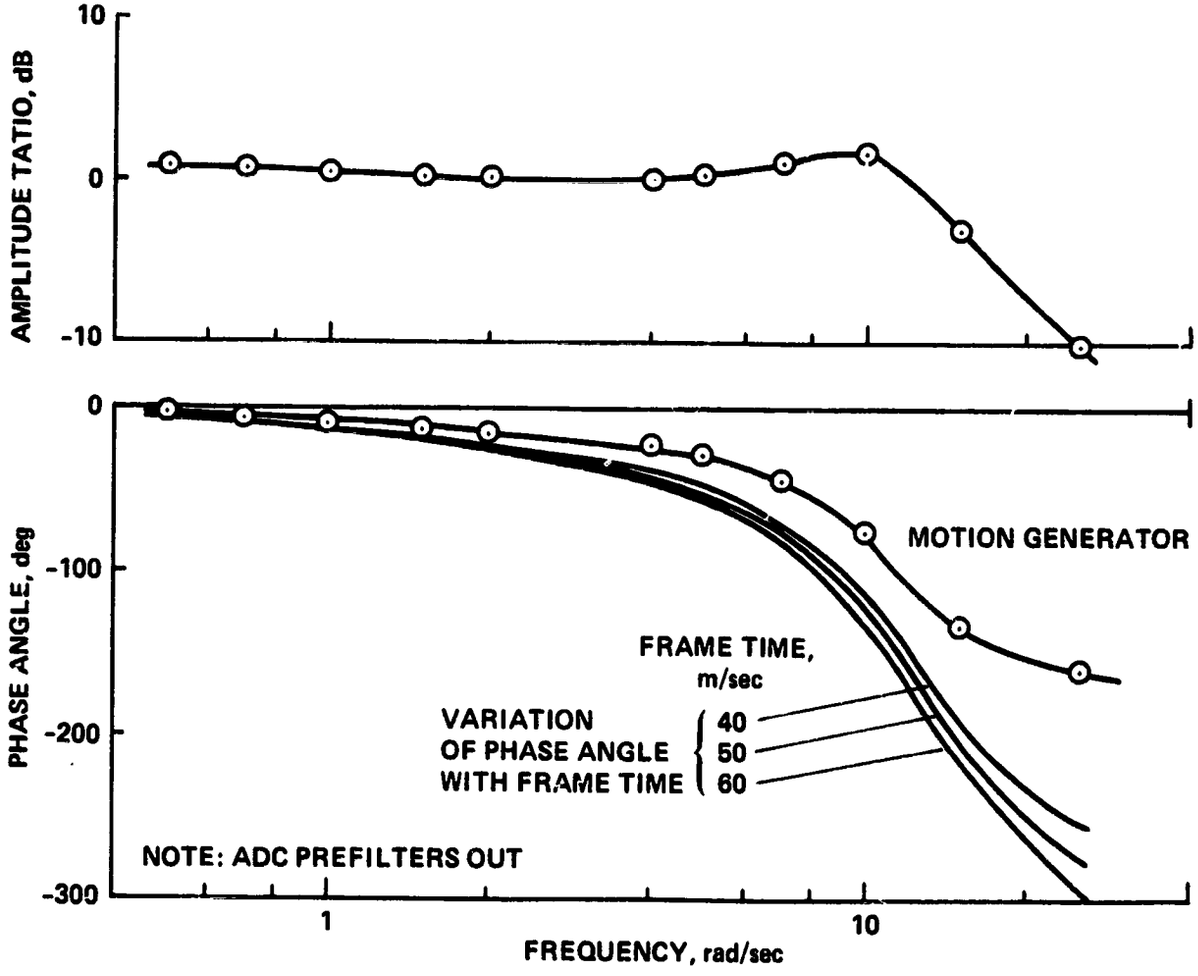

Figure 57.- VMS motion system, longitudinal acceleration frequency response.

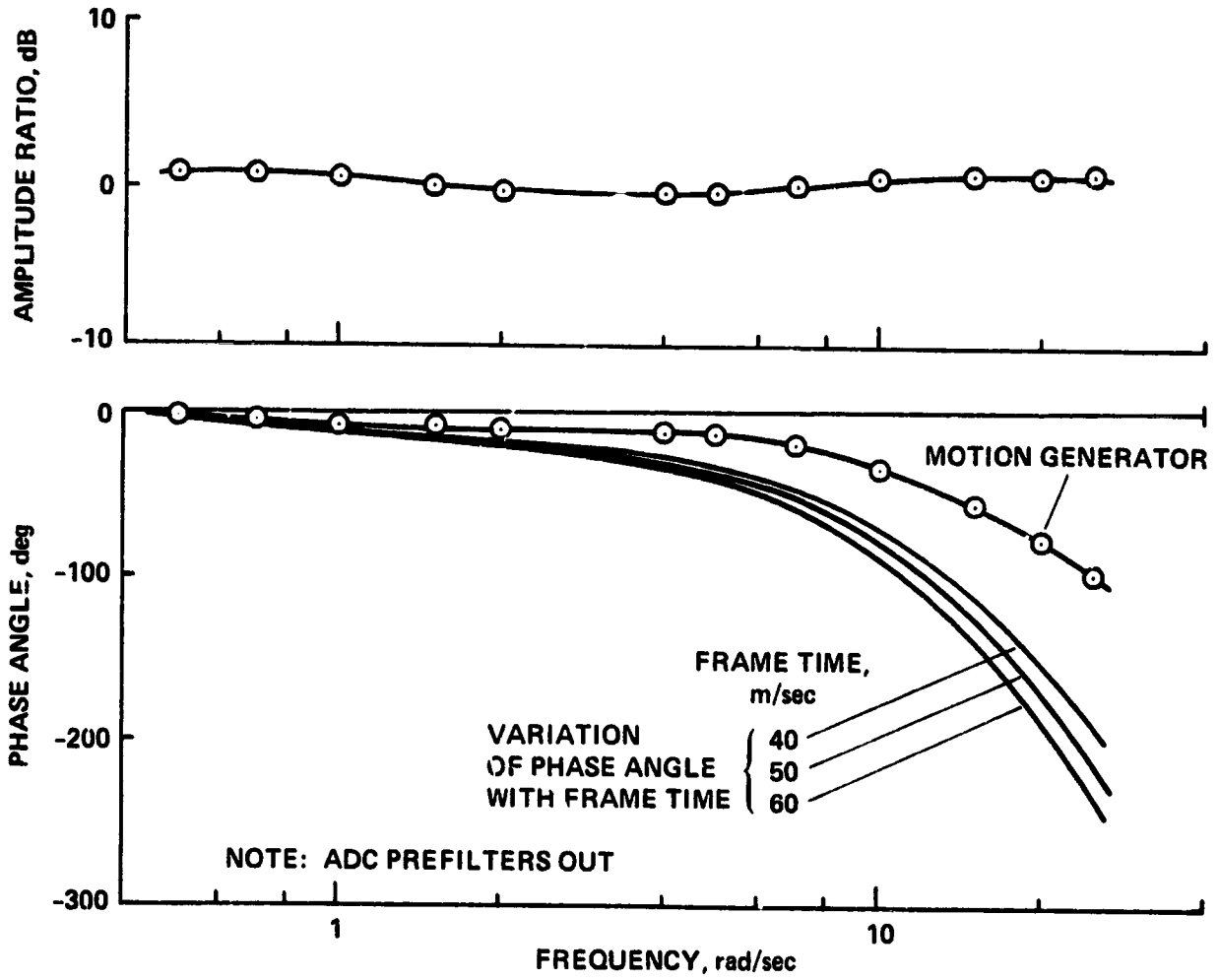

Figure 58.- VMS motion system, vertical acceleration frequency response.

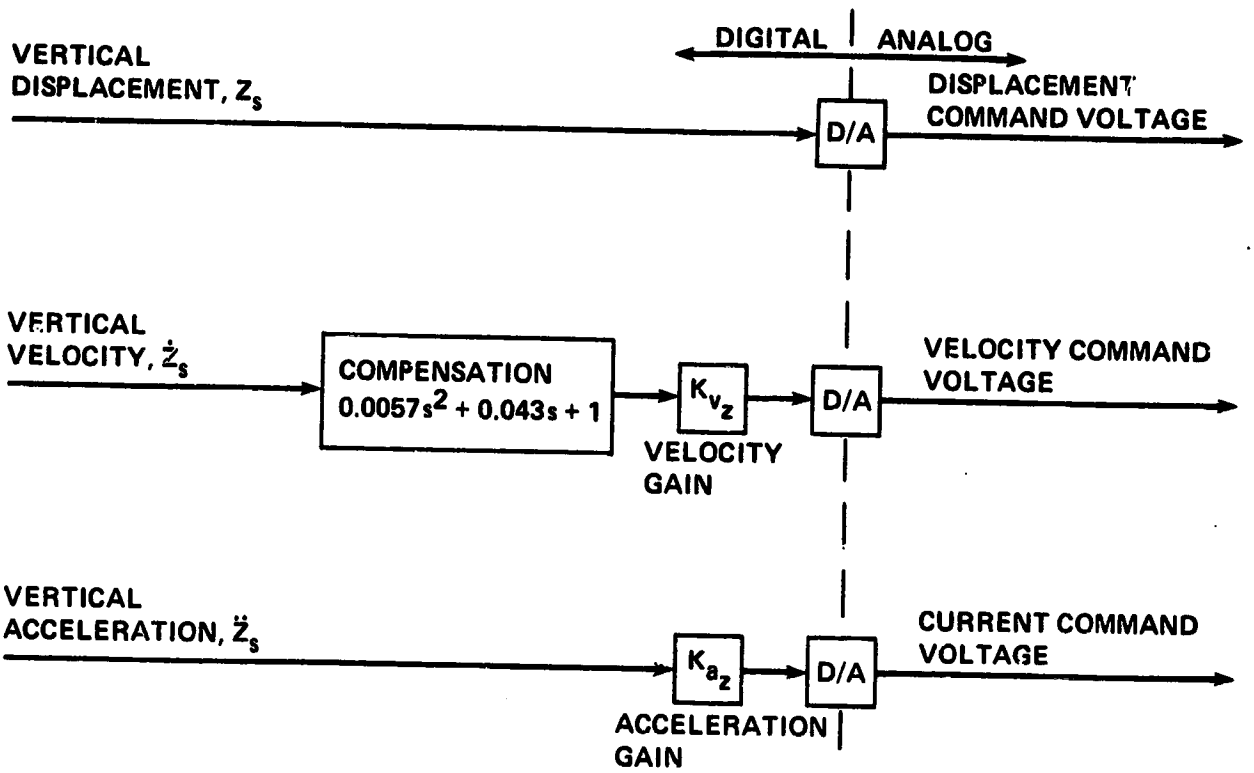

Figure 59.- Compensation for VMS vertical motion drive.